UNIVERSITÀ
DEGLI STUDI
DI PADOVA

DIPARTIMENTO
DI INGEGNERIA
DELL'INFORMAZIONE

DIPARTIMENTO DI INGEGNERIA DELL'INFORMAZIONE

CORSO DI LAUREA MAGISTRALE IN BIOINGEGNERIA

"OPTIMIZATION OF THE 4D CONTRAST-ENHANCED COMPUTED TOMOGRAPHY POSTPROCESSING SETTINGS FOR ACCURATE STRAIN MAPPING OF VASCULAR TISSUES"

Relatore: Dott. Marco Castellaro
Correlatore: Prof.ssa Greet Kerckhofs

Laureanda: Martina Bottos
Matricola: 2057763

ANNO ACCADEMICO 2022 – 2023

Data di laurea 26 ottobre 2023

Abstract

Cardiovascular pathologies represent all around the word an incumbent problem causing every year the death of millions of people. The perfect functioning of the heart and blood vessels is fundamental for the healthy maintenance of the body. The mechanical behaviour of the vessels' tissue is strongly linked to their microstructure, but this can be harmed by the damaging effects of pathologies. Hence, more interest is raised about the cardiovascular anatomy to deepen the relationship occurring between microstructure of the tissues and cardiovascular diseases.

The progress of the technology led to the development of many imaging tools. Microfocus X-rays computed tomography (microCT) is a non-destructive approach able to resolve micrometre scale structure. The combination of this technology with in situ mechanical tests (i.e., 4DmicroCT) allows to describe the mechanical response of the material analysed when loaded or stressed. In material science this field is widely covered, but in biomedical field more studies are required since many difficulties are still not overcome. Hard and mineralized tissues lend themself well to 4DmicroCT analysis; on the contrary soft tissue, such as blood vessels, because of their low X-rays attenuation makes this approach more complex. To overcome this issue, the introduction of contrast agents has been implemented (i.e., contrast-enhanced microCT or CECT) leading to the acquisition of 3D images of the microstructure while the structure in analysis is deformed (i.e., 4D-CECT). The further combination of 4DmicroCT with specific techniques, such as the Digital Image Correlation (DIC) or the Digital Volume Correlation (DVC), bring to the possibility to quantify the displacement and the strain. Despite so, in literature there is the necessity of investigate this field in particular to define the post-processing imaging procedure and the image acquisition parameters setting, balancing the image quality and the tissue damage caused by the X-rays radiation dose and the loading process.

This study aims to explore the postprocessing analysis, focusing on the DVC technique. Two different types of datasets, synthetic sheets originated via Python script aiming to mimic the elastin fibres and porcine aorta specimen microCT scans, are virtually deformed and the displacement field is computed. The first main goal is to understand if the synthetic sheets could be a reliable tool able to faithfully reproduce the behaviour of the synthetic sheets. The second main goal is to understand how to improve the DVC, analysing the different factors that could influence it and how the different acquisition parameters could affect the image quality. Was possible to assess that the virtual deformation, both on synthetic and real datasets, coupled with the DVC analysis work properly. This master thesis work could represent a good starting point for future improvement of this topic, to get acquaintance with the use of the synthetic sheets as tool for the enhancing of the DVC technique.

Italian version

Le patologie cardiovascolari rappresentano una problematica sempre più impellente in tutto il mondo, causando milioni di morti ogni anno. Il corretto funzionamento del cuore e dei vasi sanguigni è fondamentale per il mantenimento in salute dell'organismo. Il comportamento meccanico dei tessuti vascolari è strettamente legato alla loro microstruttura, ma questa può essere compromessa dagli effetti dannosi delle patologie. Negli anni, lo studio dell'apparato cardiovascolare ha suscitato molto interesse anche per approfondire la relazione tra la microstruttura dei tessuti e le malattie cardiovascolari e i progressi della tecnologia hanno portato allo sviluppo di numerose tecniche di imaging utili a questo scopo. MicroCT (micro-tomografia computerizzata) è un approccio non distruttivo in grado di analizzare strutture su scala micrometrica. La combinazione di questa tecnologia i con test meccanici in situ (4DmicroCT) consente di descrivere la risposta meccanica del materiale analizzato quando viene sottoposto a sollecitazioni. I tessuti mineralizzati si prestano bene all'analisi 4DmicroCT; al contrario, i tessuti molli come i tessuti arteriosi, a causa della loro bassa attenuazione dei raggi X rendono questo approccio più complesso. Perciò, è stato implementato l'uso degli agenti di contrasto, migliorando l'acquisizione di immagini 3D anche dei tessuti molli mentre la struttura in analisi viene deformata (4D-CECT). Essa rappresenta uno strumento valido per indagare la microstruttura dei vasi sanguigni, mirando a raggiungere l'obiettivo principale: chiarire la relazione tra microstruttura ed effetti delle patologie. La combinazione con tecniche specifiche, come la correlazione digitale di volumi (DVC), permette poi di quantificare lo spostamento e la deformazione subiti. Questo lavoro di tesi magistrale punta a migliorare la procedura di post-processing concentrandosi sulla tecnica DVC e a definire i parametri di acquisizione delle immagini per ottenere la migliore qualità possibile limitando il danneggiamento dei tessuti e l'alterazione delle loro proprietà meccaniche a causa dell'esposizione ai raggi X. Lo studio si è concentrato su due diversi tipi di dataset che vengono deformati virtualmente, calcolandone poi il campo di spostamento: fibre sintetiche generate tramite uno script in Python che imitino le fibre di elastina della parete arteriosa e campioni di aorta di suino acquisiti tramite microCT. Il primo obiettivo è capire se le fibre sintetiche possano essere uno strumento affidabile in grado di riprodurre fedelmente il comportamento delle fibre di elastina. Il secondo obiettivo è migliorare la procedura di DVC, analizzando i diversi fattori che potrebbero influenzarla. È stato possibile valutare, sia su dataset sintetici che reali, la fattibilità della deformazione virtuale unita all'analisi DVC. Pertanto, in questo lavoro di tesi magistrale vengono discussi diversi aspetti che influenzano la DVC, al fine di acquisirne una migliore comprensione.

Table of contents

Abstract 1
Table of contents 3
List of figures and tables 5
Glossary 8
Personal acknowledgement 9
I. Introduction 10
II. State of the art 13
A. Blood vessels: anatomy, mechanical characterisation and the impact of the cardiovascular pathologies 13
B. Contrast-enhancement techniques 18
C. 4DmicroCT 22
D. 4D-CECT 27
III. Problem statement, aim and objectives 29
IV. Materials and methods 31
A. Synthetic sheets datasets 31
1. Generation of the synthetic sheets and Python code 31
B. Porcine aortic sample 34
1. Harvesting of the sample 34
2. Image acquisition protocol 35
C. Dataset pre-processing analyses 36
1. Signal to noise ratio 36
D. Post processing analyses 37
1. Virtual deformation of porcine aorta specimen 37
2. DVC uncertainty measurement 40
3. DVC protocol 40
V. Result and discussion 44
A. Porcine aorta 44
1. Porcine aorta specimen datasets comparison 44
2. Scaling in Z direction of the VOI 49
3. Scaling in Z direction of VOI centred in global reference system 52
4. Scaling in Z direction of aorta specimen and DVC on VOI 59
5. Conclusion 62
B. Synthetic sheets 65
1. Mesh 65
2. Noise 67
3. Radius parameter 72

4. Scaling in Z direction 75
5. Conclusion 76
VI. Conclusion 79
Bibliography 81
Web references 85
Appendix 86
A. Introduction to micro focus X-rays computed tomography 86
B. Bidirectional scaling on porcine aorta VOI 89
C. Result of DVC analysis on synthetic sheets 90
D. Analysis of the lower VOI after porcine aorta volume deformation 93

List of figures and tables

Figure 1: Artery with cutaway section to reveal deposits of plague narrowing the passagefor blood flow as effect of the atherosclerosis [C], ... 11
Figure 2: Schematic representation of artery wall [C]. 13
Figure 3: Schematic representation of vein wall [C]. 14
Figure 4: Representative transverse and longitudinal VVG-stained images of the descending thoracic aorta (TA, top) and the superficial femoral artery (SFA, bottom) of a 14-year-old and 69-year-old subjects, demonstrating differences in the elastin (black) [7]. 16
Figure 5: Representative transverse and longitudinal MTC-stained images of the descending thoracic aorta (TA, top) and the superficial femoral artery (SFA, bottom) of a 14-year-old and 69-year-old subjects, demonstrating the differences in collagen (blue) [7]. 16
Figure 6: Intracochlear soft tissue visualization in PCCT images (A) and absorption-based micro-CT images (B). In the picture are visible Scala tympani (ST) and Scala vestibuli (SV) by the basilar membrane (BM) in the basal, middle and apical turns, spiral ligament (SL), stria vascularis (StV), cochlear nerve (CN) fibers and the spiral ganglion (SG) [14]. 19
Table 1: Average percentage of volume shrinkage on brain, muscle, bone tissues using PTA, IKI, 12E CECAs. 20
Figure 7: Comparison of the different proposed staining procedures. The voxel size for these observations is 25 mm (cubic voxels). For each sample, a circumferential (left image) and a longitudinal cut (right image) of the vessel are given. (a) Reference sample (unstained). (b) Lugol staining. (c) PMA staining. (d) PTA staining. The scale bars are 2 mm [20]. 21
Figure 8: Comparison between images acquisition methods. 23
Equation 1: Equation for the resolution of DVC global approach 24
Equation 2: Correlation residual equation 24
Figure 9: Schematic functioning of local ang global approaches used jointly. 25
Figure 10: Different voxel edge length for subvolume (red square) compared to trabecular bone features [33]. 26
Figure 11: Cross sectional views of the carotid specimen at a stretch of 1.5 and at different pressure steps [36]. 28
Figure 12: Schematic representation of elastin sheets (blue) and collagen (red) fibers in artery wall during workload [5]. 31
Figure 13: (A) Lateral view and (B) top view of the synthetic sheets by Python script, (C) the resulting 3D volume displayed in Avizo. 32
Figure 14: Different synthetic sheets configuration changing the amplitude parameter, in (A) is 1, in (B) is 3 in (C) upper part is 1 and lower part is 3. 32
Figure 15: Different synthetic sheets configuration changing the amplitude parameter; (A) is 1, (B) is 3; (C) is 5. 33
Figure 16: (A) Histogram synthetic sheets radius 1, (B) histogram synthetic sheets radius 3. 33
Figure 17: (A) Porcine aorta sample, small incision in the corner to distinguish the longitudinal to the radial direction, (B) specimen wrapped in parafilm and positioned on the left part of the plastic support. 34
Table 2: Acquisition parameters 35
Table 3: Acquisition parameters of porcine aorta specimen 35
Table 4: CT reconstruction settings 36
Equation 3: Signal to noise ratio 36
Figure 18: (A) Selected path on VOI in Porcine_Aorta_0, (B) path statistics provided by Dragonfly software. 37

Figure 19: (A) Original porcine aorta, (B) segmented volume (physical size: 5247.5, 21225.5, 4622.5 µm), (C) 2D slice of the VOI (physical size: 1312.5, 530, 1155 µm). 38
Figure 20: Comparison between reference VOI (blue) and deformed VOI (grey). (A) scaling in positive and negative Z direction, (B) scaling in positive Z direction..... 39
Figure 21: Example of autocorrelation plot, the red circle highlights the asymptote point. 41
Figure 22: Edge collapsing for mesh simplification [Avizo helper]. 42
Figure 23: (A) cubic mesh generate via generate surface tool, (B) sheets-shaped mesh, (C) cubic mesh generated via DVC tool. 43
Figure 24:Datasets of porcine aorta specimen at different acquisition parameters (A) Porcine_aorta_0, (B) Porcine_aorta_1, (C) Porcine_aorta_2, (D) Porcine_aorta_3, (E) Porcine_aorta_4, (F) Porcine_aorta_5, (G) Porcine_aorta_6, (H) Porcine_aorta_7, (I) Porcine_aorta_8, (L) Porcine_aorta_9, (M) Porcine_aorta_10, (N) Porcine_aorta_11, (O) Porcine_aorta_12, ... 46
Figure 25: VOI extracted from datasets of porcine aorta specimen at different acquisition parameters (A) Porcine_aorta_0, (B) Porcine_aorta_1, (C) Porcine_aorta_2, (D) Porcine_aorta_3, (E) Porcine_aorta_4, (F) Porcine_aorta_5, (G) Porcine_aorta_6, (H) Porcine_aorta_7, (I) Porcine_aorta_8, (L) Porcine_aorta_9, (M) Porcine_aorta_10, (N) Porcine_aorta_11, (O) Porcine_aorta_12. 47
Table 5: SNR porcine aorta specimen dataset acquired 48
Figure 26: Comparison between (A) scaling, (B) resampling, (C) registration of porcine aorta. In gray the reference volume, in blue the deformed one. 50
Figure 27: Subtract images between reference and deformed volume after the registration. 51
Figure 28: (A) Vector field and (B) Uz of porcine specimen VOI scaled in Z direction [µm]. 51
Table 6: DVC Uncertainty measurement results for VOI extracted from Porcine_aorta_0 dataset 53
Figure 29: (A) displacement vector field, (B) Uz of the VOI centred in global reference system before the scaling of Porcine_aorta_0 dataset. 54
Figure 30: (A) Uz uncertainties in function of Cell size, (B) SD of Uz in function of Cell size. 55
Figure 31: Displacement vector field (A) and Uz (B) of Porcine_aorta_2 (range values normalized [µm]). 56
Table 7: Displacement ranges computed for the porcine dataset 57
Figure 32: Result of Porcine_aorta_6 (A) displacement vector field, (B) residual image. 58
Figure 33: VOI of porcine aorta analysed. 59
Figure 34: (A) displacement vector field, (B) Uz of VOI of specimen aorta deformed [µm]. 60
Figure 35: Subtract images between reference and deformed configuration of the VOI extracted from the upper part of the aorta specimen. 61
Figure 36: Comparison different mesh generated via surface generator tool. 66
Figure 37:(A) Automatic cubic generated mesh showing homogeneous faces, (B) manually cubic generated mesh showing nonhomogeneous faces. 67
Figure 38: (A) synthetic sheets no-noise configuration, (B) 3D volume no-noise configuration, (C) synthetic sheets noisy configuration, (D) 3D volume noisy configuration. 68
Figure 39: (A) histogram of no-noise configuration, (B) histogram of noisy configuration, (C) typical histogram of aorta; ImageJ software. 69
Table 8: SNR of porcine aorta and no-noise and noisy configuration of synthetic sheets. 70
Table 9: statistic of the metric map and residual correlation (mean average, dimensionless) 71
Figure 40: Residual image of noise configuration; low correlation areas are in correspondence of brighter and darker strings. 71
Figure 41: schematic representation of elastin fibres behaviour during deformation in synthetic sheets (A) and in reality (B). In orange the relaxed condition, in black the stretched condition. 72
Figure 42: Comparison between synthetic sheets (A) radius 1 and (B) radius 3. 73
Figure 43: Comparison between histogram of (A) noise configuration and (B) brighter configuration. 73

Table 10: Comparison between displacement range of brighter and noisy configuration 74
Figure 44: (A) Displacement vector field and (B) Uz computed after scaling the synthetic sheets [µm]. 75
Figure 45: Schematic set up for MicroCT scan. 86
Figure 46: Displacement vector field of VOI bidirectional scaling. 89
Table 11: Displacement ranges for no-noise and noisy configuration of the synthetic sheets 90
Figure 47: Manual measurement of Uy using Measurement tool 91
Figure 48: (A,B,C) Vector field, Uz, Uy no-noise configuration and (D,E,F) noise configuration [µm] 92
Figure 49: Comparison between displacement vector field and Uz for lower (A,B) VOI and upper (C,D) VOI [µm] 93

Glossary

CVD: cardiovascular diseases

CAD: coronary artery diseases

CCD: charge-coupled device

MicroCT: micro focus X-rays computed tomography

SEM: scanning electron microscopy

LM : conventional light microscopy

CLSM : confocal laser scanning microscopy

CA: contrast agents

SRN: signal-to-noise ratio

DVC: digital volume correlation

CCA: casting contrast agent

CESA: contrast-enhancing staining agents

CECT: contrast enhanced microfocus X-rays computer tomography

PCCT: phase contrast microfocus X-rays computer tomography

4D-CECT: 4D contrast-enhanced computer tomography

Personal acknowledgement

I would like to express my sincere gratitude to all those who have helped me throughout this challenging experience. First and foremost, I am deeply thankful to my thesis supervisor, Professor Greet Kerckhofs, for providing me the opportunity of working on this project. The precious advice and constructive criticism throughout this research have been crucial to the success of this work. The knowledge that I have acquired is priceless.
I want to thank also Professor Marco Castellaro, for following me through this project by showing interest in my work and guiding me toward the end of my academic journey.

I extend my thanks to Lara Mazy for her invaluable support and patience day after day. Her feedback and suggestions have been fundamental in shaping the direction of my work and write this thesis.

I would also like to thank Grzegorz Pyka and Victor Joos for their assistance and support in the most technical part of this work, helping me overcoming any difficulties.

Lastly, I want to thank my family and friends for being close to me despite the distance in these months. Your love and support came to Belgium from Italy, inspiring me every day to do better.

In conclusion, I am grateful to have the chance to work on this project, improving my knowledge and pushing myself beyond the difficulties.

I. Introduction

The circulatory system is fundamental for the proper functioning of the human organism; the heart and the blood vessels network work in synergy to remove waste products and carbon dioxide, as well as to deliver oxygen and nutrients to every organ and tissue of the body. The arteries transport oxygen-rich blood via arteriole to the capillaries, where oxygen is released to the surrounding tissues via passive diffusion. Veins and venules have the role of bring deoxygenated blood from the periphery of the body back to the heart; this circuit is known as systemic. Pulmonary circuit is the group of blood vessels that bring the carbon dioxide-rich blood to the lungs; here the carbon dioxide is released, oxygen captured and brought back to the heart to be sent again in the systemic circuit.

Given its important role in keeping the body healthy, several illnesses that can affect the circulatory system are the focus of the attention of the modern medicine.

Cardiovascular diseases (CVD) have a major impact worldwide. It has been estimated by the World Health Organisation that, in 2019, 17.9 million people died because of CVDs [A]. Referring in particular to the arteries, among other pathologies examples are aortic aneurysm, coronary artery diseases (CAD) and atherosclerosis. An aneurysm is an abnormal and permanent pathologic dilatation of the arterial wall caused by trauma or an alteration that weakens it: when the dilatation of the wall reaches critical levels, the vessel can rupture causing internal bleeding that can lead to death [1]. Atherosclerosis is one of the most common cardiovascular pathologies and it is responsible for almost 30% of all mortalities worldwide [2]; it is a condition involving mostly arteries and is characterised by the creation of plaques made of fatty substances such as cholesterol in the lumen of the vessel (Figure 1). Initially macrophages try to remove the lipid particles, but as the fat deposition continues to grow continuously the white blood cells are not able to stop the fat-deposition process leading to the creation of atherosclerotic plaques of different thickness, narrowing the lumen, until forming a blood clot or travel in the circulatory system causing possible heart attack or stroke [B].

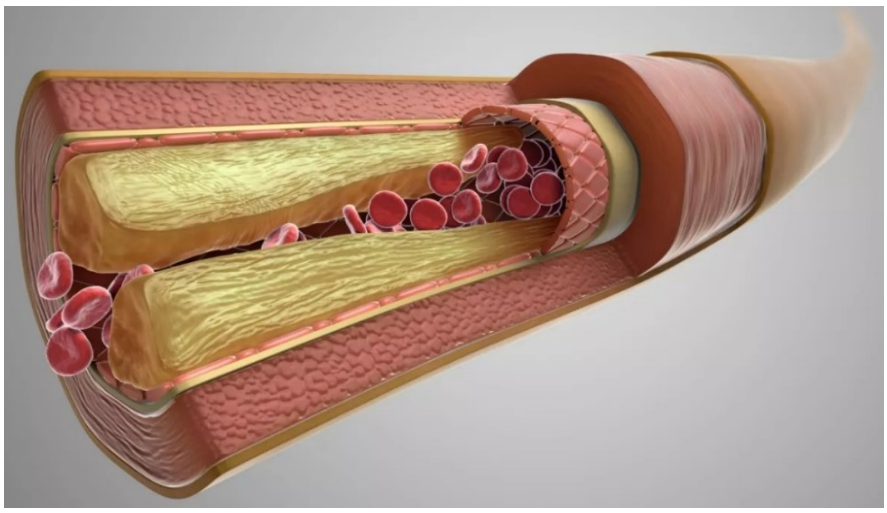

Figure 1: Artery with cutaway section to reveal deposits of plague narrowing the passagefor blood flow as effect of the atherosclerosis [C],

In the medical and biology field, in the recent decades, the development of imaging techniques became necessary to have a 2D and 3D visualisation of the biological structures. Since the first attempt of investigation in medicine and biology fields, histology represents the gold standard for the analysis of tissue sample. It gives the opportunity to appreciate on a microscale the structure of a great variety of biological structure. As downside it provides a 2D static visualisation of the specimen and it is a time-consuming technique requiring many steps.

The progress in the medical field requires in parallel an advancement of the imaging analysis in order to step into the 3D digital visualisation of the tissues. Thanks to the technology development, many techniques are nowadays available: micro focus X-rays computed tomography (microCT), scanning electron microscopy (SEM), conventional light microscopy (LM), and confocal laser scanning microscopy (CLSM) [3]. Each of them shows advantages and disadvantages that can be overcome by the use of a combination of the different techniques. More and more important is becoming the complete understanding of the anatomy of the body, both in macro and micro scale, to better characterise the pathologies and comprehends the relationship between native structure, their physiological functioning and the harmful impact of the pathologies. In particular, the attention has been focused on the cardiovascular system. The use of adequate imaging tools can provide a complete overview of the complex microstructure of the blood vessels and help to define the relation occurring with cardiovascular pathologies.

Among all, this master thesis will focus on the microCT technique for the investigation of the microstructure of blood vessels, focusing more on 4DmicroCT and 4D-CECT. The combination with Digital Volume Correlation technique allows first to perform mechanical test while the scan images are acquired, second to quantify the resulting strain and displacement.

Will be presented the current knowledge in this field, highlighting the reasons why is important to pursue its development and, further, will be discussed the work performed. The first goal was to take acquaintances with the post processing analysis of the image acquired via microCT, in particular with the Digital Volume Correlation technique. The second goal was to better understand its functioning and try to figure out which strategies to adopt to make it work better with the aim of reach the main research purpose: the investigation of the blood vessel microstructure.

II. State of the art

A. Blood vessels: anatomy, mechanical characterisation and the impact of the cardiovascular pathologies

Arteries and veins are the main blood vessels involved in the transportation of the blood to all the compartments of the organism; their walls show the same fundamental structure but have different peculiarities to make them more appropriate to the specific location and purpose.

Generally, an artery presents three main layers (Figure 2): the inner one, the *tunica intima*, is made of endothelial cells composing the *endothelium* which is the layer directly in contact with the blood. The *intima* is separated to the outer layer by fenestrated elastin fibres of the internal elastic lamina. The second layer, the *tunica media*, is made up of smooth muscle cells, collagen and elastin fibres and is able to constrict and dilate and so control the calibre of the artery. The outer layer, the *tunica adventitia* or *tunica externa*, consist of collagen and elastin fibres surrounded by loose connective tissue and connect the artery to other tissues holding it in place [4]. Generally, the *adventitia* shows higher collagen density compared to the *media* layer. Each of these constitutive layers play an important role when the artery experiences higher pressure: the medial layer bears 60% of the load during circumferential tension and the adventitia bears 75% of the load during longitudinal tension. In particular the *adventitia*, according to Chang *et al.* [5], thanks to its high collagen content is the stiffest layer in the artery and shows different micromechanical and viscoelasticity response in different arteries, based on their physiological environment. During high pressure loading it becomes the most responsible layer for the mechanical response and it is involved in pathological processes such as atherosclerosis and hypertension.

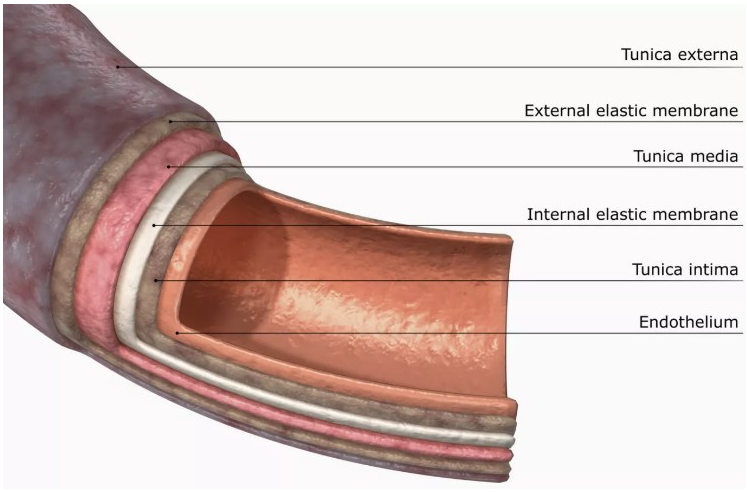

Figure 2: Schematic representation of artery wall [C].

In the human body is possible to identify two types of arteries [D]:

- Elastic arteries: involved mainly in the blood circulation closest to heart, experience higher pressure smoothing it, to bring blood to smaller arteries. Examples of elastic arteries are the aorta and the pulmonary arteries. Compared to muscular arteries, they are characterized by higher density of collagen fibres and elastin primarily organized in form of concentric lamellae in the *tunica media*, improving the resistance of the wall and the ability of stretch. This type of arteries is able to smooth the blood pressure originated by the left ventricles and maintain a constant pressure gradient. The presence of fibroblasts in the *tunica intima,* with aging, cause the accumulation of lipid increasing its thickness, a marker for the atherosclerosis.
- Muscular arteries: are responsible for transporting blood from major elastic arteries to minor calibre arterioles and finally to the organs; examples are the femoral and coronary arteries. The *tunica media* is characterised by a greater number of smooth muscles cells organised in concentric layers. They exhibit higher vasoconstriction capability than elastic arteries, changing their diameter and controlling the blood flow based on the moment-to-moment needs. The average diameter is from 0.1 mm to 10 mm, where elastic arteries show diameter greater than 10 mm since they have to deliver high amount of blood from the left ventricle.

Veins show the same layering as the arteries except for the elastic membranes (Figure 3). In general, veins walls are thinner, less elastic and not designed to undergo high blood pressure. They have to be compressed to push back the blood to the heart against the gravity, in fact, they show internal valves able to block the backward flowing of the blood, maintaining the unique direction. On the contrary this phenomenon in arteries in guaranteed by their capacity to contract [E].

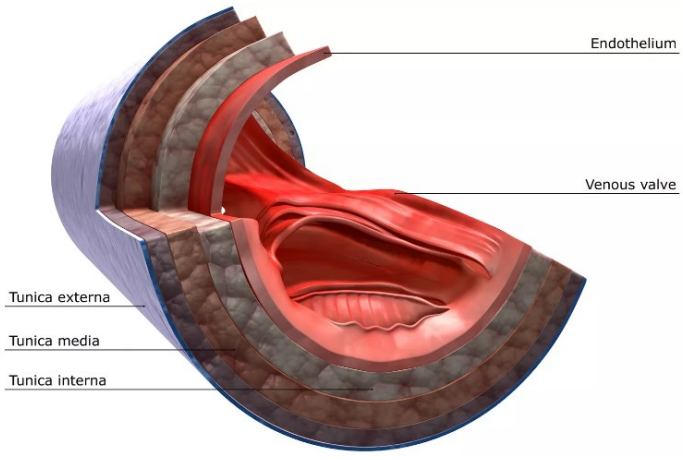

Figure 3: Schematic representation of vein wall [C].

The necessity of know the mechanical properties of blood vessels, is a challenge that originated back in the past century. In 1881, Charles Rot was the first one that conducted mechanical experimentation on human arteries in order to establish their mechanical behaviour and was able to establish that the elastic property of the aorta decreases as age advances [6].

The non-homogeneous structure of the arteries is the cause of its elastic non-linear behaviour when is distended; as consequence, the elastic stiffness increases when the load applied increase. In 1957, Roach and Burton were able to demonstrate the individual role of the elastin and of the collagen and to explain the increasing stiffness during the elongation of the artery. At initial strain the artery's wall shows an elastic behaviour due to the intervention of the elastin but, as the strain value increase, higher stiffness is registered because the collagen fibres are tensioned progressively until they are fully stretched, transferring the load from the elastin to collagen.

Recently, Jadidi *et al.* [7], performing planar biaxal testing and bidirectional classical 2D histology, were able to assess the microstructural and mechanical differences between muscular and elastic arteries proving the aging effect observed before. They focused on thoracic aorta (TA) and superficial femoral artery (SFA) to evaluate the elastin (Figure 4) and collagen (Figure 5) changes in the wall's layers. Vessels' tissue was stained with Masson's Trichrome (MTC) and Verhoeff-Van Gieson (VVG) to quantify respectively collagen and elastin. As expected, the tunica media of TA was 2.2-fold thicker than the SFA. Additionally, the first one showed elastic lamellae with the sandwiched collagen, primarily circumferential smooth muscle cells, GAGs, and radial elastic fibres that formed interlamellar units; the latter showed lack of GAGs and circumferentially oriented smooth muscles cells surrounded by collagen while the elastin was sparse. Because of the aging, in both arteries smooth muscle cell density decreased, elastic fibres and lamellae degraded showing an accumulation of collagen and GAGs. This leads to the thickening of the walls and the decrease of elastin density, so the element responsible for the elastic character of the vessels fails

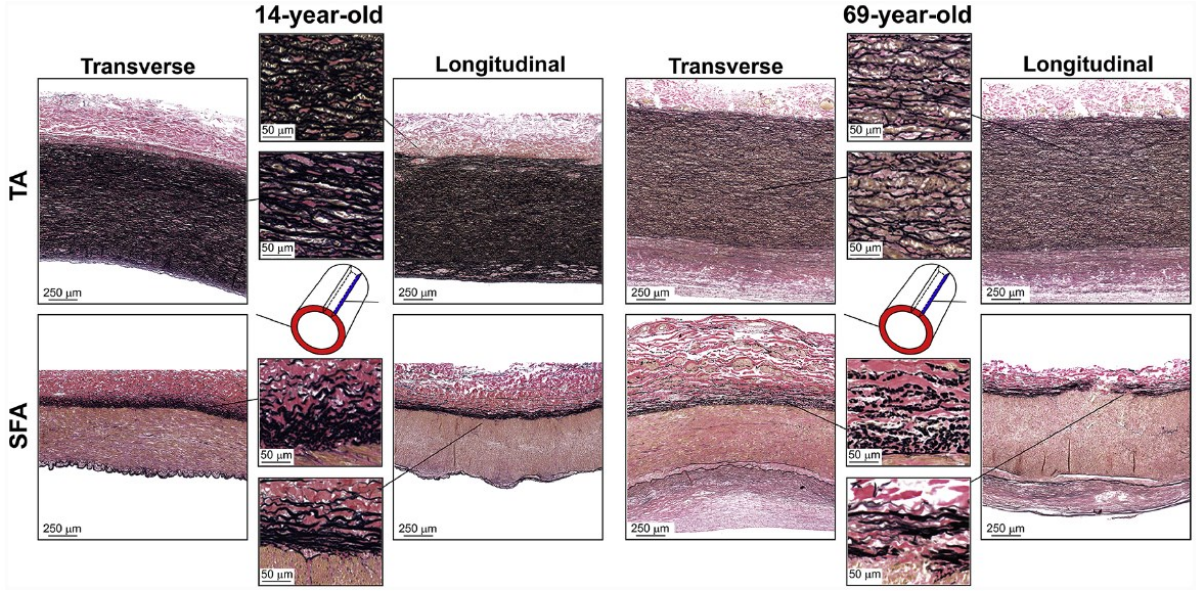

Figure 4: Representative transverse and longitudinal VVG-stained images of the descending thoracic aorta (TA, top) and the superficial femoral artery (SFA, bottom) of a 14-year-old and 69-year-old subjects, demonstrating differences in the elastin (black) [7].

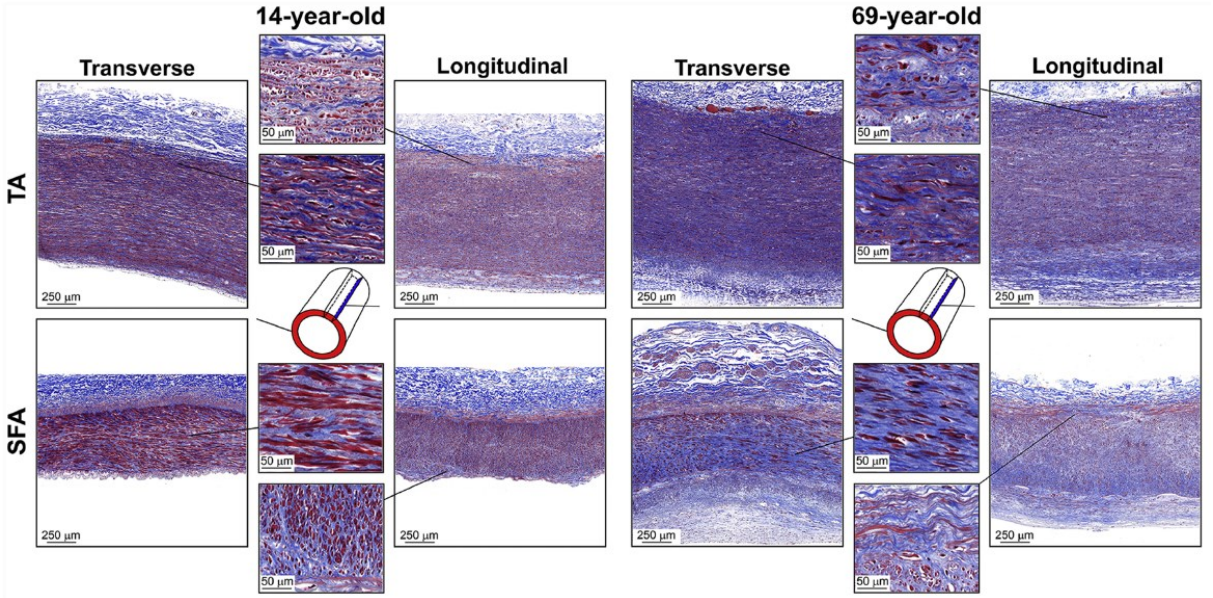

Figure 5: Representative transverse and longitudinal MTC-stained images of the descending thoracic aorta (TA, top) and the superficial femoral artery (SFA, bottom) of a 14-year-old and 69-year-old subjects, demonstrating the differences in collagen (blue) [7].

This study highlighted not only the microstructural differences between the two types of arteries, but also as the aging results in different changes to the intrinsic mechanical properties the physiologic arterial characteristics based on the types of arteries.

For example, even though both elastic and muscular arteries suffer of loss of elastin, the effect on the first one has a higher impact since during the cardiac cycle it undergoes higher pressure and so higher load. In general, with age a drop in elastic artery distensibility is registered but a relatively constant distensibility in muscular artery is observed. On the contrary, both types are subjected to progressive dilation, even though the changes are more marked in the aorta.

Additionally, natural aging is strongly related to cardiovascular risk, in particular, age-related stiffening is attributed to degeneration of the *media* and changes in the *intima* due to atherosclerosis [4].

Cardiovascular pathologies have been shown to be correlated with arteries wall mechanical characteristics; this leads to a deep investigation in order to be able to perform a prompt diagnosis and understand deeply how it impact blood vessels. For example, carotid *intima-media* thickness has been assumed as a discriminant factor for carotid atherosclerosis, and many studies also found association with CAD [8]. As mentioned in the introductive paragraph, atherosclerosis has a relevant impact on cardiocirculatory system. An unequivocal factor underlining this pathology is the presence of the atherosclerotic plaques. Another possible marker for the atherosclerosis is the arterial wall elasticity; it can be assessed evaluating the strain values analysing the changing in the thickness of arterial wall via tissue Doppler imaging or ultrasonographic 2D imaging during a cardiac cycle [8]. Karimi *et al.* [9], performing a uniaxial tensile test, were able to assess the different mechanical properties between a healthy and atherosclerotic coronary artery. Has been showed that the atherosclerotic vessel is able to experience 44,55% more stress, but 34,61% less strain compared to the healthy sample; a significative increase of the elastic modulus and a growth of the wall's stiffness were registered. Dissection of the aorta represent another pathological situation, highly deadly caused by a breach in artery wall leading to a copious blood loss. This phenomenon is triggered by a defect in the middle layer of the wall, evolving in a growing tear involving the progressive delamination of the muscolo-elastic sheets. Even though the aortic tissue is an anisotropic sample since the fibres are not homogeneously distributed, it appears to break at the same average force with the same mechanism [10].
Referring to fibre's orientation, collagen fibres are oriented circumferentially in the *tunica media* and longitudinally arranged in *adventitia*, in both veins and arteries [10]. The different distribution of fibrils has a role in the mechanical behaviour of the vessel' wall: in presence of high pulse wave velocity, in other words higher cardiac load associated to arterial stiffening, smaller diameter fibrils endorse resilience and resistance of the vessel.

Although many efforts have been made, it is important to pursue the investigation of the mechanical properties and microstructural features of the healthy blood vessels. Recognising structural changes caused by ageing or diseases can lead to a premature diagnosis of pathologies and a more efficient therapy. Moreover, a complete knowledge of their properties is fundamental for the future development of artificial arteries, the design and fabrication of

cardiovascular grafts. The advancement of the technology, in particular in the imaging field, lead to the development of numerous tools useful for this kind of investigation. MRI, CT and ultrasound have been used to perform *in vivo* test allowing accurate physiological loading, but the limited resolution does not allow to resolve the microstructure [11]. Additionally, the weak X-rays absorbing property of the soft tissue make their imaging acquisition via X-rays based technique more complicate. Therefore, the introduction of use of contrast enhanced agents and increased image resolution, allow to visualise the microstructure of the soft tissues. In the following section will be presented some techniques developed to carry out this type of investigation.

B. Contrast-enhancement techniques

Since its first introduction in the early 1980s, micro focus X-rays computed tomography (microCT) has become a gold standard for the visualisation of mineralized and hard tissues. Soft tissues have a low X-rays attenuation property resulting in an image with low contrast. With traditional microCT approach, often soft tissue requires staining and dehydration in order to be visualised, resulting in shrinkage and distortion of the sample [12]. This can impact the mechanical evaluation of the sample, since the original structure is disrupted. As a consequence of the use of radio-opaque contrast agents (CA) and high resolution microCT, about a decade ago, also nonmineralized and soft tissues can be discriminated using this X-rays imaging techniques [13]. Two are the possible approaches: phase contrast microCT (PCCT) and contrast enhanced microCT (CECT)

PCCT

As discussed before the conventional microCT is not able to output a well-defined reconstruction of low X-rays attenuating sample. PCCT approach can avoid these microCT's limitation. As alternative to the CECT, it is a CA-free technology that allow soft tissue's analysis. Using a synchrotron, the X-ray beam impact the material studied causing a phase shift that could be quantified and converted in measurable amplitude information. It allows to enhance edges of the structure where the additional phase shift is observed, where in this case absorption-based imaging is weaker [14]. Elfarnawany *et al.* [14], show how using phase contrast imaging reported improved qualities images of intracochlear soft tissue, compared to the one harvest via microCT (Figure 6). The use of PCCT allows to obtain sharpened and finer edges and allows a better classification and discrimination of the different structures, where the

use of CECT obtained weaker results. This clear visualisation led to the possibility to apply an effective semiautomatic segmentation, resulting in a realistic 3D model of the intracochlear.

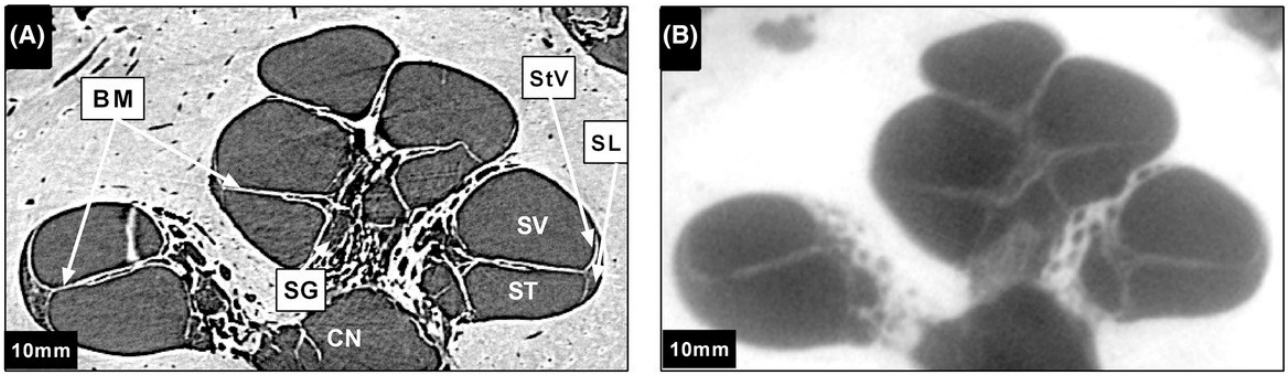

Figure 6: Intracochlear soft tissue visualization in PCCT images (A) and absorption-based micro-CT images (B). In the picture are visible Scala tympani (ST) and Scala vestibuli (SV) by the basilar membrane (BM) in the basal, middle and apical turns, spiral ligament (SL), stria vascularis (StV), cochlear nerve (CN) fibers and the spiral ganglion (SG) [14].

One of the major limitations of PCCT is the equipment: this technology requires the access to synchrotrons facilities, not always available in the researching laboratories. In the recent years many are the successful attempts made in order to use PCCT as an investigation tool to study different anatomical structure: tendon, intravertebral disc, cartilage and more [15]. Although all the features PCCT presents, CECT is more commonly used for soft tissue visualization since it requires less specific software and equipment.

CECT

Performing CECT, the tissue studied is enriched with CAs, particular chemical compounds able to increase the linear attenuation coefficient. This technique is based on the attenuation of the X-rays by the specimen and usually benchtop devices are used with a polychromatic X-rays source [16].

Is possible to refer to two different types of CA: contrast-enhancing staining agents (CECAs) and casting contrast agents (CCAs). To have a 3D reconstruction of the cardiovascular tree is more appropriate to use the CCAs, instead to assess wall's microstructure CESAs are favoured since in this case the tissue itself should be highlighted rather than the volume of the vessels. Via perfusion, CCA is injected in the biological structures, usually blood vessels and heart, filling all the cavities and making the measurement of the volume and the spatial distribution of the structure possible. Anyway, *ex vivo* characterisation of vascular network remains a challenge: once the sample are harvested some are opened up to the air causing possible leakage of the perfused CA and so distortions of the final image that is obtained [13]. Other important parameter to take under control while using CCA is the perfusion pressure: if it too low there's

the possibility that not all the cavities are filled and so some structures are missing in the 3D reconstructed image. On the contrary, if the pressure is too high can cause damage to the tissue, in particular to the vessels with small diameters.

The other possible approach is the staining of the tissue by passive diffusion: the sample is immersed in the solution containing the CESA. It is able to interact with particular molecules present in the structure of the tissue, making it more X-rays attenuating.

The development of CA is a current challenge, although all the improvement made in these years, in order to obtain the most suitable CA to the tissue studied. An optimal CA should be biocompatible, non-toxic and should not interfere with the natural metabolism of the organism; at the same time, it should be cost-effective.

During *in vivo* experimentation another factor to consider is the renal clearance: CA's particles should be of such a size that they remain in the body a useful time for analysis. Unlike, *ex vivo* experimentation does not have this limitation, but it is always necessary to remind CESA can show side effects involving the structure of the tissues such as dehydration and shrinkage [17]. Changing in volume of the specimen preclude the possibility of making consideration on its structure or how it changes following pathological events.

Buytaert *et al.* [18] evaluated the volume shrinkage effect of three popular staining solution on different type of tissue: phosphotungstic acid (PTA), iodine with potassium iodide (IKI) and iodine in absolute ethanol (I2E). reports the average percentage tissue volume shrinkage (negative values) registered performing CECT:

Table 1: Average percentage of volume shrinkage on brain, muscle, bone tissues using PTA, IKI, 12E CECAs.

	PTA	**IKI**	**I2E**
Brain	-27.3 %	-38.8 %	-66 %
Muscle	-10.4 %	-41.6 %	-55.8 %
Bone	1.3 %	-0.6 %	0.7 %

Performing evaluation like this is important to find the most suitable CESA based on the tissue analysed, to prevent the shrinkage effect and so work with the sample as intact as possible. Additionally, carrying out mechanical evaluation of tissue is important to evaluate the possible CA influence on the performance of the specimen.

Focusing on blood vessels, the components mostly investigated are elastin and collagen fibres since are the most important components of the walls. Here are briefly illustrated some CESAs used with this purpose

The use of sodium polytungstate (SPT) as CESA for the elastin sheets was assessed while performing a tensile to rupture test for the media layer of artery showing that SPT has not effects on the microscopic mechanical properties of the layer of interesting and does not need dehydration [10], [19]. Additionally, it doesn't show tissue shrinkage [16]. The other important component of blood vessel wall is collagen. In order to enhance its visualisation in a porcine vein the following stain solutions were tested and compared to no staining condition (Figure 7) [20]: iodine potassium iodide (Lugol), phosphomolybdic acid (PMA) and PTA. As outcome, PTA and PMA lead to similar and satisfactory visualisation result of *adventitia* and middle layer and quantification of the collagen volume fraction, also assessing its stability in 10 months observation, thought they require sample's dehydration and longer time to penetrate in the tissue compared to Lugol. Lugol leads to better results compared to no staining case, but still the resolution is low.

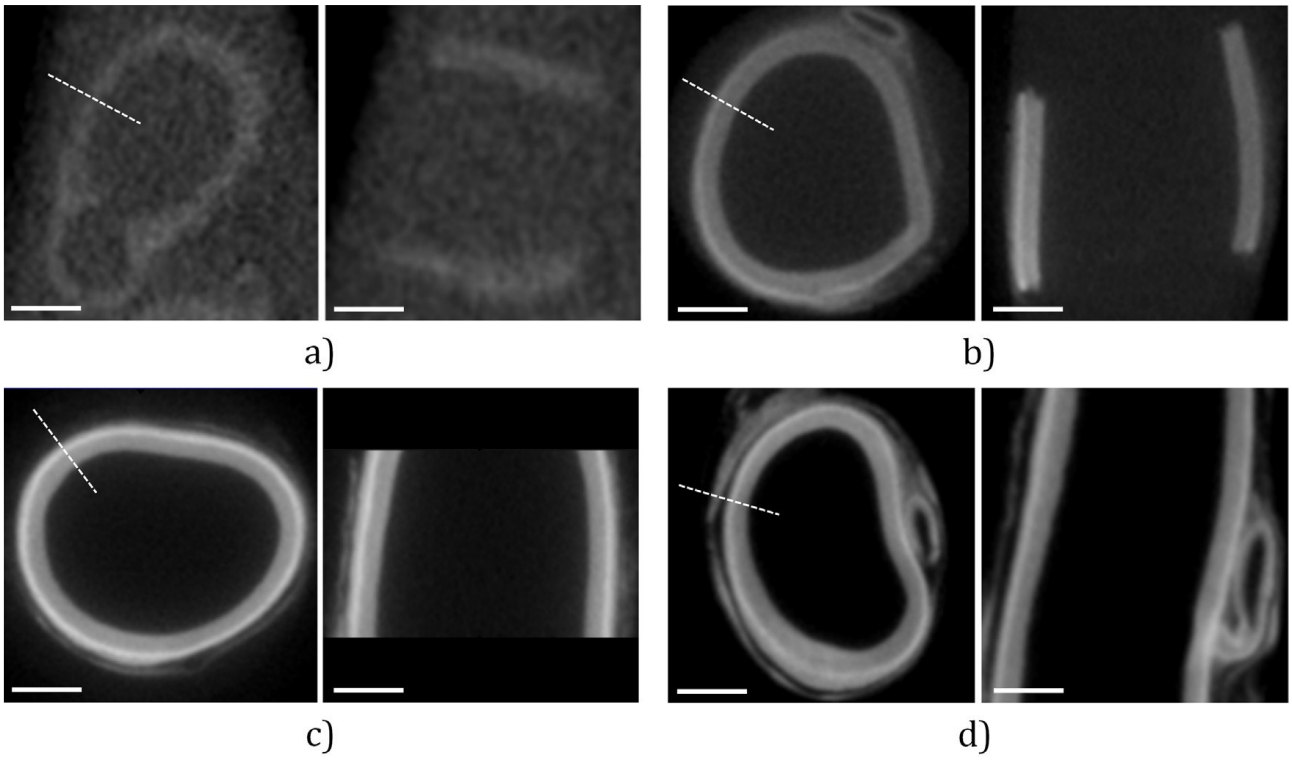

Figure 7: Comparison of the different proposed staining procedures. The voxel size for these observations is 25 mm (cubic voxels). For each sample, a circumferential (left image) and a longitudinal cut (right image) of the vessel are given. (a) Reference sample (unstained). (b) Lugol staining. (c) PMA staining. (d) PTA staining. The scale bars are 2 mm [20].

As well as for the collagen, PTA is claimed to be able to specifically stains fibrin, fibres of connective tissue and blood [16].

Investigating blood vessels, could be useful use the CESAs to highlight marker of specific CVD give their ability to bind to specific molecules. For example, OsO_4 is commonly used since it is able to binds to lipid, but on the other hand it is characterised by high toxicity. Due to his affinity,

has been used to visualize lipid-rich plaque in artery wall in case of atherosclerosis [16].
As already highlighted, mechanical evaluation of blood vessels is a subject currently of great interest and microCT is an imaging technique useful to carry out such type of investigation. Traditional microCT is an already a well-defined and investigated approach, but in the last decade more and more interested has raised 4DmicroCT and 4D-CECT. Combined with specific software they allow to evaluate the stress and strain developed within the biological structure when loaded and deformed. Following will be presented the current knowledge about this topic and the future challenges.

C. 4DmicroCT

MicroCT has shown in the decades to be a great non-destructive imaging technique able to reproduce digitally a 3D volume, and so helping our understanding of complex system not only in biological or medical fields. A remarkable improvement was the transition from static microCT to 4D microCT, introducing the temporal component. This makes the evaluation of the behaviour of materials over time possible and allows to study how their structure changes when they are subjected to loads and stresses. Using 4D microCT is possible to study dynamic biological processes, such as the deformation of heart chambers to push heart in the circulatory system or the changing volume of the lungs during the inhalation and expiration [21].
Compared to traditional microCT the acquisition of 4D microCT images is more complicate given the mechanical test performed simultaneously. Additionally, post-acquisition image processing is required to remedy at possible unintended motion of the sample from the original position. This technology is not being employed only in medical field, it has been studied in material science field for the features' analysis of different materials such as ceramic, metals and alloy [22]–[24]. It is used, for example, to study processes at high temperature such as sintering of ceramic material, reaching nanoscale spatial resolution [25]. It is widely applied for the investigation of fatigue-induced structural changes, for example track the advancing of cracking mechanism in carbon composite [26].

Mechanical testing set up

The mechanical testing can be performed following two different approaches: performing *ex situ* test the imaging process is performed at different loading step and the specimen is unloaded to be scanned; on the contrary *in situ* test allows to perform the mechanical test while the specimen is scanned [27]. Usually this second method is applied for 3D strain measurement of biostructures.

MicroCT acquisition can be carried out following two different approaches (Figure 8): with *time-lapsed* acquisition the load is applied on the specimen in discrete steps and for each of them a scan is performed; during *time-resolved* acquisition the mechanical loading is continuous and simultaneously the specimen is scanned without interruption [22]. Usually time-lapsed scanning is preferred to the time-resolved since require less time. At the same time, working with biological structure the time-dependent mechanical behaviour of some tissues, such as stress relaxation and viscoelasticity, has to be taken under account because it can influence the measured strains.

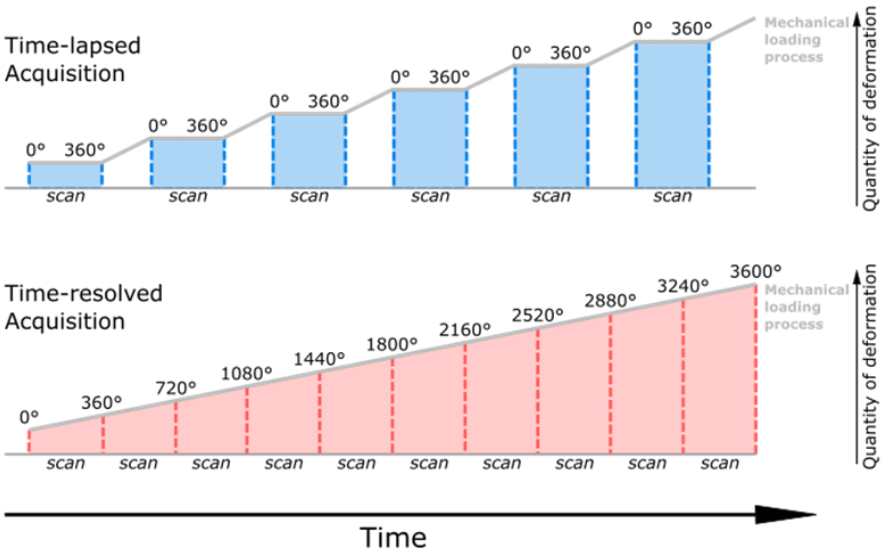

Figure 8: Comparison between images acquisition methods.

Strain measurement: DIC and DVC techniques

Full field strain measurement can be achieved via Digital Image Correlation (DIC) or Digital Volume Correlation (DVC) [11]. DVC and DIC are both technique able to compare datasets of deformed and undeformed volumes, correlate them and compute the corresponding displacement field.

DIC is based on the acquisition of sets of images of the specimen surface, both in deformed and undeformed states [28]. The surface is divided in smaller sub-images and specific patterns on the surfaces of the structure are detected and matched by an algorithm based on the optimisation of a normalised cross-correlation or sum of squared difference function. It is possible also to resolve nonplanar surfaces using stereo imaging and 3D DIC [11]. As downside this technique is able to detect only the surface of the object and the investigation of internal strain is not possible.

Coupling microCT with DVC can overcome the limitation that DIC has, exploiting material's internal structure, investigating the internal deformation and compute the displacement of a

small reference sub volume and consequently subsequent volumes generated when the specimen is loaded [29].

DVC can be performed following two approaches: local (or subset-based) or global. Performing local approach, the reference and the deformed volumes are divided into sub-volumes and correlated independently and the interpolation is used to calculate displacement of voxels limited by the nodes [30]. The local approach shows poor accuracy and high precision: high precision goes with small random errors (i.e., standard deviation of the displacement field), poor accuracy goes with high systemic error (i.e., spatial average of the determined displacement)[1]. This approach could compute reliable displacement, but results should be considered truthful in sub-volumes where the correlation is really high. In literature different correlation thresholds values has been indicated; according to Dall'Ara *et al*. [30] a threshold of 60% for musculoskeletal application indicate acceptable results, where for more optimal results a threshold value of 80% should be reached.

Global approach relies on the minimization of the differences existing between the reference and the deformed images when a continuous displacement field is applied and the registration equation are solved in the nodes [30]. In other words, to solve the computation is necessary to solve the Equation 1 or minimize the correlation residual (Equation 2)[1]:

Equation 1: Equation for the resolution of DVC global approach

$$f(x) = g(x + u(x))$$

Equation 2: Correlation residual equation

$$\eta = f - g$$

Where x is the position vector, f the reference image, g the deformed one, u the displacement field and η the residual. Finally, the problem can be linearized and converted to a matrix inversion problem.

Usually, local and global approaches are used jointly (Figure 9) and the local approach provide an initial displacement field for the global approach that shows both higher accuracy and precision.

[1] Information taken from Avizo software helper.

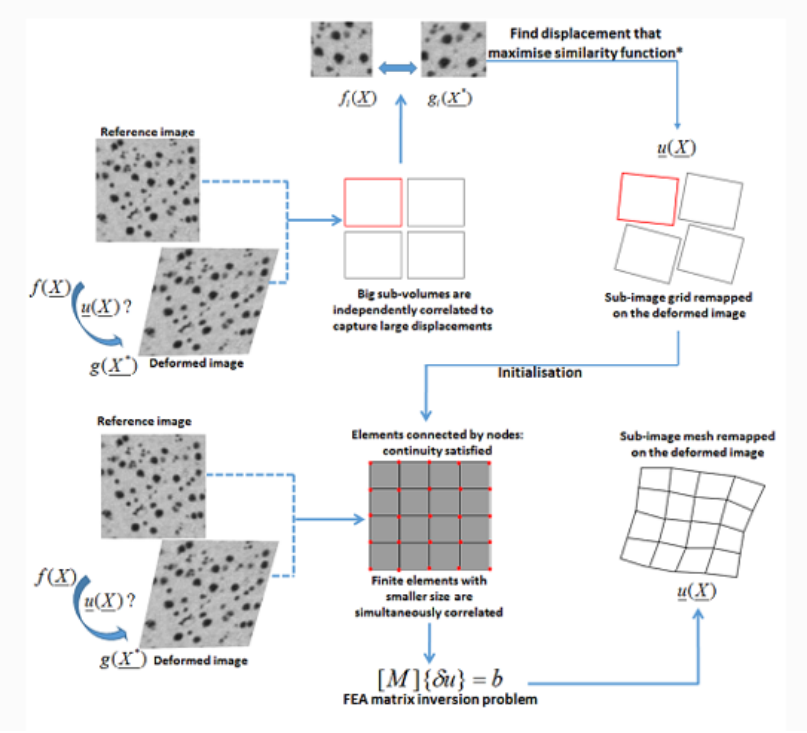

Figure 9: Schematic functioning of local ang global approaches used jointly.

4DmicroCT application and DVC parameters assessment

The precision of the DVC is strongly correlated to the input image quality: increasing the image resolution and high signal-to-noise ratio lead to an increment of the spatial resolution of the DVC [30]. At the same time, the image quality is also linked to the exposure time.

Working with biological tissue it is fundamental to pay attention to the exposure time, because of the well know harmful nature of the X-rays that could compromise the integrity of the tissue analysed. Above all, 4DmicroCT application for bone tissue has been extensively studied since its mineralized nature does not require the use of CA and its porous structure divided in distinct trabeculae creates a texture easier to resolve. Peña Fernándeza *et al.* [31], based on the work of Barth *et al.*, were able to assess the damaging effect of synchrotron radiation microCT on the elastic properties of bone tissue while performing a compression test. As a consequence of the collagen matrix degradation, they observed a reduction of the strength, the ductility and the toughness of the bone tissue. Additionally, as reported before in literature, they showed as the reduced exposure (64ms/projection) and a dose of radiation under the safety dose limit of 35 kGy, lead to the preservation of the mechanical behaviour of the tissue but decreased the quality of the images impacting the performance of the DVC. Thus, underlining the importance of define the most suitable imaging set up before the mechanical tests, in order to maintain the radiation dose in the safe range.

Many are the factors that can influence the outcome of the DVC analysis, one of this is the subvolume size. Numerous are the works in literature focused on this topic and often is underlined the necessity to find a compromise between the subvolume size, the spatial resolution[2] and the precision of the DVC. A small subvolume size, in fact, is more susceptible to noise, but its increasing could lead to an insufficient spatial resolution [32]. At the same time, larger is the subvolume size, lower are the random errors associated to the displacement computation.

Gillard *et al.* [33], evaluated four different sub volume size (24, 48, 64 and 96 voxel edge length) to assess the best one to perform a compression test on porcine trabecular bone under displacement control during microCT scanning. They assessed that doubling the voxel size, from 24 to 64 voxels, reduced of 2.5 times the strain SD computed. Also, based on the subvolume size, changes the portion of trabecula contained in it: for 48 voxel subvolume only a trabecula was contained, making it more susceptible to noise, for 64 voxels multiple portions of different trabeculae where enclosed, creating a more defined pattern for the correlation (Figure 10). In fact, DVC technique relies also on the material's internal pattern to compute the correlation between reference and deformed volume. For this reason, this last size was chosen.

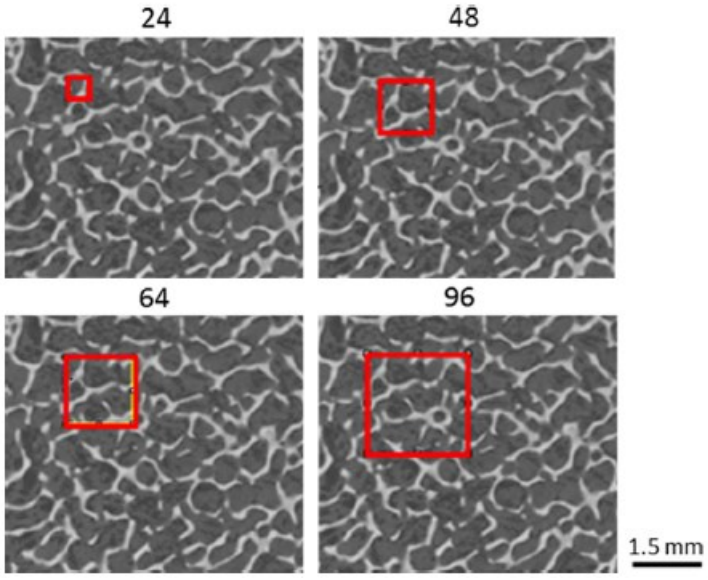

Figure 10: Different voxel edge length for subvolume (red square) compared to trabecular bone features [33].

An interesting result was reached by Trachet *et al.* [34] that combining synchrotron-based phase propagation imaging and pressure-inflation experiment reaching high resolution of 1.625 µm, were able to visualize and individually segment the carotid elastic lamellae; being able to quantify the changing of diameter, straightness and length as the pressure increase and precisely

[2] Spatial resolution defined as the smallest displacement that can be computed [32]

describe the mechanical behaviour of the elastic lamellae. This work, in combination with a layer-specific material description, can lead to the development of a computational model for the mechanical description of the artery wall.

DVC precision assessment

The precision of DVC analysis depends on the quality of the input images, the structure of the material investigated, the correlation scheme and the operational setting. It is important to estimate the precision of the DVC performed, via multiple scanning of the same undeformed specimen in "zero-strain" condition or virtually simulate known deformation on microCT datasets [35].

D. 4D-CECT

In the medical field is important not only have a complete overview of the biological structure, but also see how they respond to mechanical stimuli within the organism. Even though many studies have been performed on hard or mineralized tissues, both animal and human (for example trabecular and cortical bone or vertebral body), soft tissues are still a field not widely covered by 4DmicroCT. As already underline, many pathologies (atherosclerosis or aortic dissection) influence the mechanic behaviour of the blood vessels. Their poor absorbing property make more difficult their investigation, but the combination of CA use and 4DmicroCT can overcame this problem, leading to the possibility to study this relationship via 4D-CECT.
Despite so, *in situ* test on soft tissues like arteries are still scarce in literature [36], and application of DVC on this type of material are even more difficult to find. Moreover, soft tissues are less stable during image acquisition performing *in situ* testing resulting in blurring images, because of creep and stress relaxation [36]. For this reason, is preferable performing fast acquisition, as well as to decrease the exposure time.

Not only the general structure of vessel wall is investigated, but also its behaviour under critical conditions. For example, running tensile test on porcine aorta, the tissue can be brought to the fracture point in order to achieve a complete description of its mechanical behaviour and dissection of the aortic medial layer while collecting microCT images. Brunet *et al.*[36] stained the aortic sample with a solution of PST and performed tension-inflation test after creating a notch on a porcine carotid to initiate the dissection process, reaching a resolution of 7 μm (Figure 11). A semi-automatic method was developed to segment the notch on the X-ray images and, thus, follow its evolution with the pressure increase. They were able to assess the

mechanical behaviour of the layers and quantify the size of the notch, and underline as this data can be used to perform a DVC analysis to quantify the strain of the arterial wall.

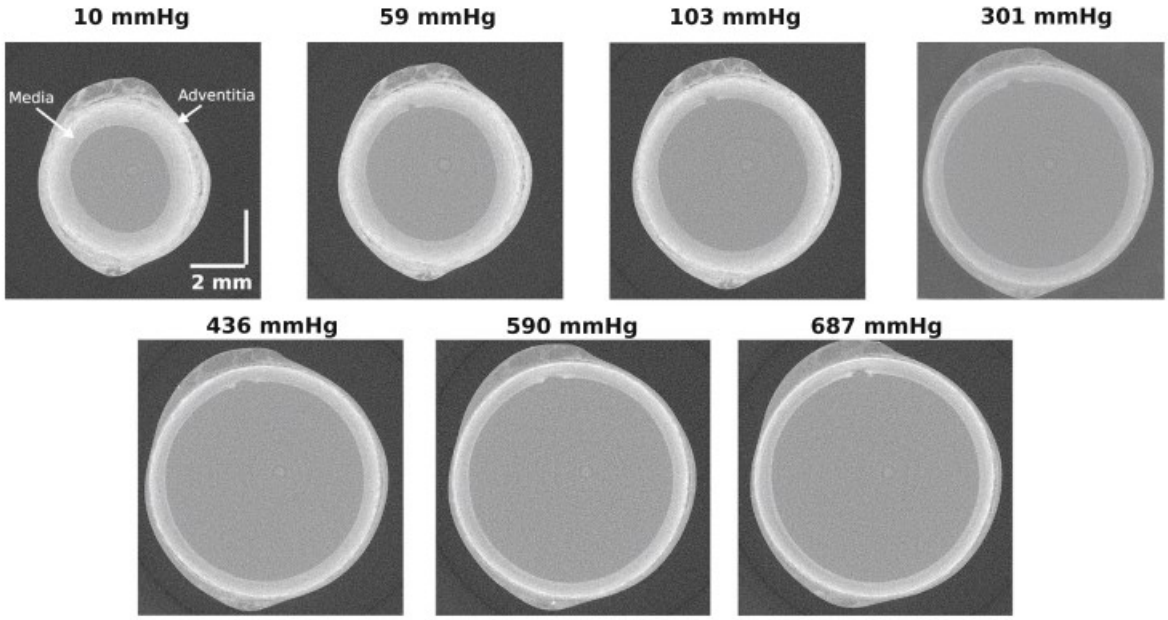

Figure 11: Cross sectional views of the carotid specimen at a stretch of 1.5 and at different pressure steps [36].

Even though 4DmicroCT is a field covered in literature for material science and hard tissue, is not possible to say the same thing about 4D-CECT; even if it represents a suitable tool to resolve microscale structure and make biomechanical evaluation. As in the research just presented, other studies [10] centred on soft tissues carry out mechanical evaluation successfully while performing image scanning, assessing for example the effect of the CESA implied or discussing the image resolution possible to reach, but the work did not lead also to the strain evaluation or the implementation of DVC analysis.

There is also wide description of different approach in order to balance time of exposure and resolution, but there is still lack of knowledge about the application of DVC for soft tissue.

This is a still going on challenge and many technology improvements are required as the definition of precise procedure to perform the strain quantification.

III. Problem statement, aim and objectives

The analysis and characterisation of the microstructure of blood vessel is an incumbent challenge, in order to be able to correlate the aging and cardiovascular pathologies to the mechanical and microstructural changes occurring in the tissue. The use of the CESA allowed to overcome the soft tissues low X-rays attenuation leading to their morphology analysis via microCT. A major step has been done combining the microCT technique with *in situ* mechanical testing and the DVC analysis, making possible the investigation of 3D full-field displacement and strain. Despite in literature 4DmicroCT has been investigated and more knowledge has been gained, not only in biomedical field but also for example in material science [23]–[25], there is still the necessity to explore more. For example, the application of 4D-CECT on soft tissue for the study of the microstructure and the difficulties that raise performing such kind of analysis, is raising more attention given the huge contribute that this type of knowledge could bring in medical and diagnosis field.

Whether this technique has been deepened for mineralised tissue, for soft tissue the challenge is still open. Above all the soft tissue, given its composite structure and its relevance in the healthcare, cardiovascular system and more specifically blood vessels have raised a relevant interest in 4D-CECT. This technique in fact could represent a tool to study the microstructure of the blood vessel and understand the relationship with CVD. At the same time, the complexity of these tissues and of the technique itself make the challenge more difficult. In combination with 4D-CECT, it is also necessary to employ a technique able to quantify the displacement of the specimen: DVC is used for this purpose.

Given the well-known damaging nature of the X-rays, balancing the time exposure, the spatial resolution and the preservation of the tissue is the first difficult faced during images acquisition while performing in 4D-CECT. Smaller sub-volume size is more susceptible to noise effect, whereas large sub-volumes may not ensure satisfactory spatial resolution. Thus, the aim is always to find a sub-volume size able to both capture the deformation and ensure good quality. This concerning is most relevant when the final purpose of the image acquisition is the DVC analysis. It is also necessary to take under account possible noise, body motion and artifacts that can raise, ruining the dataset collected and effecting the DVC computation producing incorrect results. Of equal importance of the acquisition setting is the dataset post processing analysis. Tuning the DVC parameters according to the microstructure of the tissue in analysis is necessary to ensure the higher correlation possible between reference and deformed volume. The complications raise since there are not precise protocols to follow and so is necessary to perform a priori analysis to quantify DVC uncertainties in function of the resolution.

This master thesis project is focused on the postprocessing analysis of 4D-CECT datasets of porcine aorta tissues, aiming to understand how to optimise the DVC computation and to produce accurate displacement field. The work will be divided in two principal branches: first the generation, virtual deformation and displacement analysis of synthetic sheets generated using Python script, second the acquisition of porcine aorta images via microCT, virtual deformation and displacement analysis of the dataset acquired. The synthetic sheets aim to mimic the behavior of the native elastin sheets of arteries' wall. Working with such controlled dataset allow to easily simulate virtual deformations, setting the desired parameters. This has been done with the purpose of gain a better comprehension of the impact of such factors on the DVC outcome and consequently understand how to adjust the computation to ensure a better correlation. At the same time, working with the synthetic sheets give an overview about their strengths and weakness, with the view of improve their future reliability. The comparison between synthetic sheets and real datasets acquired via microCT aims to make clearer the differences between them and so help to understand how to improve the synthetic sheets in order to better resemble the features of the native elastin sheets.

The virtual deformation of the porcine specimen aims to reproduce the procedure followed when performing *in situ* testing and the displacement computation on a volume of interest. In parallel, the simultaneous analysis of different porcine aorta datasets acquired in different condition allows to evaluate how the changes of acquisition parameter impact on the image quality and thus to the outcome of the displacement analysis.

IV. Materials and methods

A. Synthetic sheets datasets

1. Generation of the synthetic sheets and Python code

The first major aim of this master thesis work is focused on the deformation of synthetic sheets originated using *ad hoc* developed Python code. As described in the previous chapter, the wall of the arteries is made up of, among other things, a tangled network of fibres of collagen and elastin sheets, characterising the mechanical properties of the walls itself. The synthetic sheets aim to mimic the elastin component. Performing 4D-CECT, it is possible to detect only elastic sheets; thus the approach pursued intent to simulate the passage of the elastin sheets from a crimped configuration, observable in lower stress situations, to an elongated one found when the blood vessels experience high pressure or tension (Figure 12).

Consequently, the evaluation of their deformation is carried out performing a Digital Volume Correlation analysis. The virtual simulation of this process allows to replicate not only different configuration of the fibres itself or different levels of density, but also assess how the change of some factors in the grayscale images, such as noise or the level of contrast, impacts on the final displacement field that the software is able to produce.

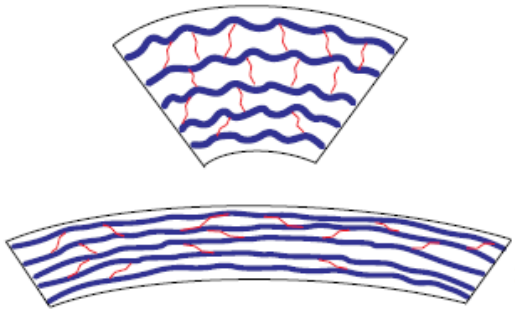

Figure 12: Schematic representation of elastin sheets (blue) and collagen (red) fibres in artery wall during workload [5].

The Python script implemented is able to generate a cubic volume in which are included the sheets representing the elastin. The user can set the dimensions of the volume and the number of sheets generated that are distributed equally spaced within the volume. Controlling these two parameters is possible to manage the packing of the sheets and their density over the volume: keeping the same volume size but incrementing the number of sheets will result in a denser organisation. The algorithm stacks a number of 2D grayscale images equal to the size of the dimension set before, creating the 3D volume. The surface of the planes is composed of numerous Gaussian distribution that develop slice after slice in the pile of images. Gaussian distribution could have both positive or negative values and so rise in both sides of the plane.

The sheets are parallel to the XZ plane (Figure 13C). Changing the sectioning orientation, it is possible to appreciate the waves representing the elastin fibres from the front view (Figure 13A) and from the lateral view the grayscale circle-shaped curves that compose the Gaussian surfaces (Figure 13B).

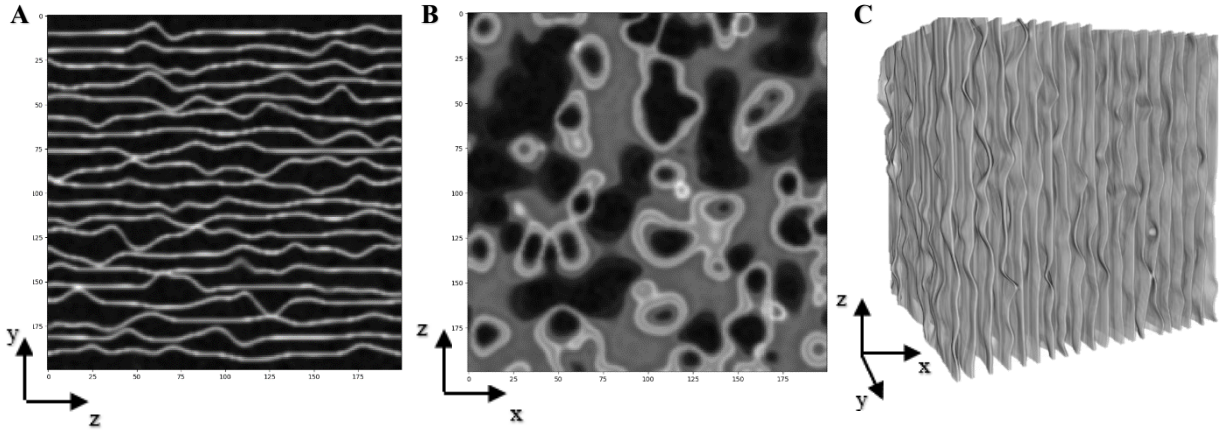

Figure 13: (A) Lateral view and (B) top view of the synthetic sheets by Python script, (C) the resulting 3D volume displayed in Avizo.

To simulate the different arrangement that the sheets could have (Figure 14), the user can increase or decrease the amplitude parameter, to amplify the effect of the plane distortions and so reproduce a more accentuate waviness. As the amplitude of the Gaussian distribution decreases the sheets appear more linear, mimicking the real workload situation. Each plane can be set at a specific amplitude and it is possible to generate region with different waviness (Figure 14C).

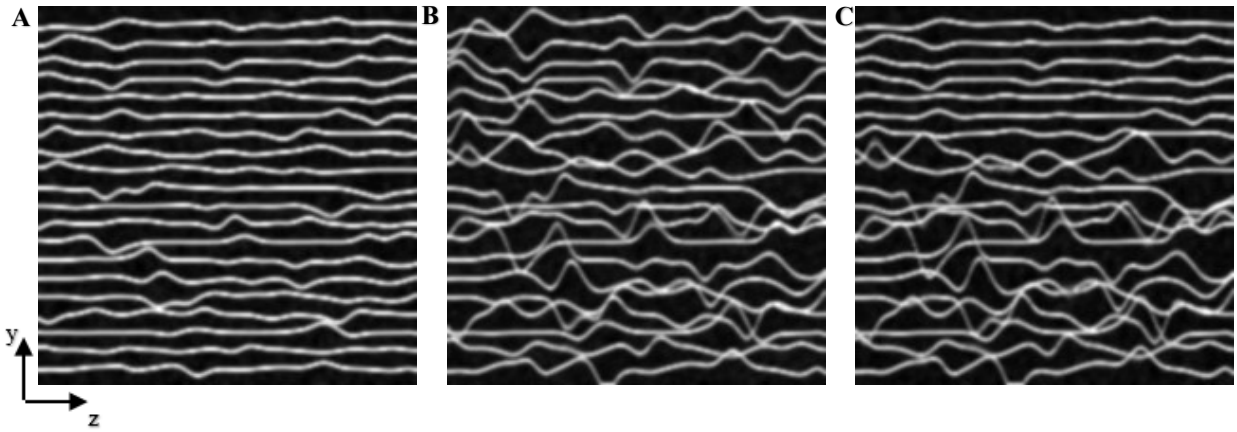

Figure 14: Different synthetic sheets configuration changing the amplitude parameter, in (A) is 1, in (B) is 3 in (C) upper part is 1 and lower part is 3.

Another parameter that is possible to control is the average radius of the Gaussian distribution composing the sheets: as the radius increase the sheets will appear brighter (Figure 15).

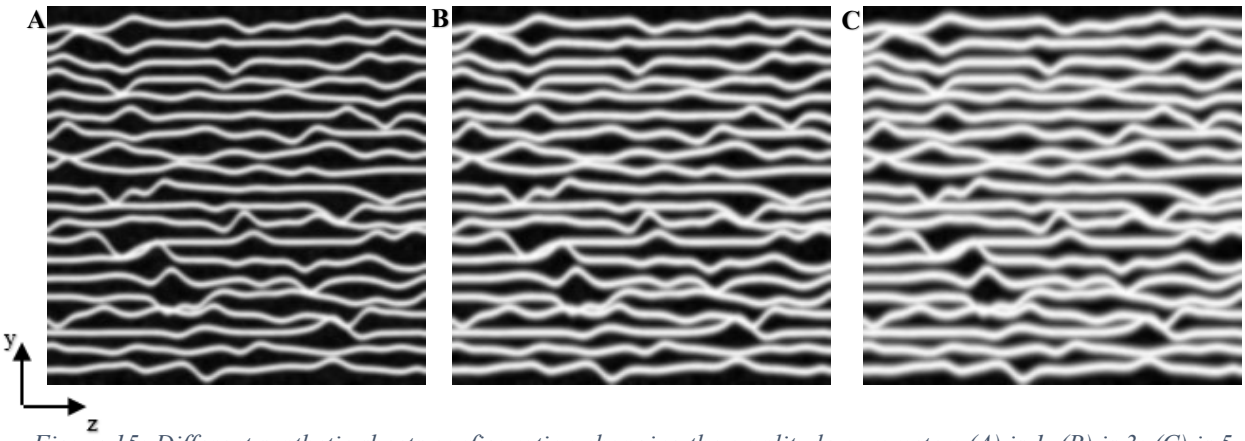

Figure 15: Different synthetic sheets configuration changing the amplitude parameter; (A) is 1, (B) is 3; (C) is 5.

The histogram is a useful tool from which is possible to obtain various information about the image being analysed. Comparing the histogram (Figure 16) of the same configuration created but with two different radius values, the average mean values of the grayscale increase as the radius value too.

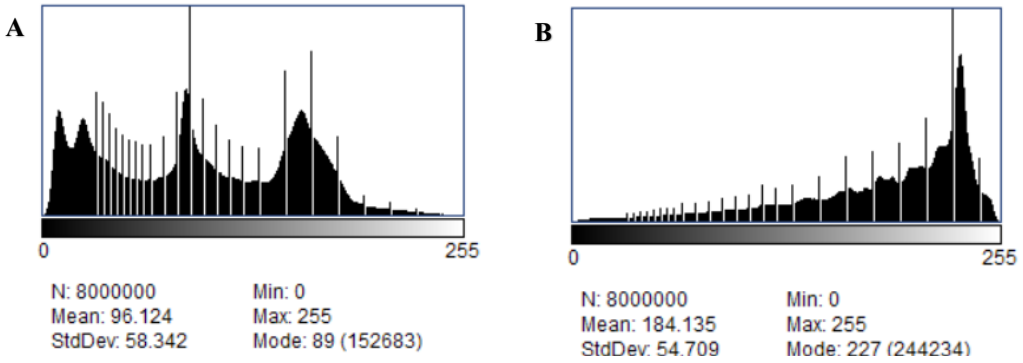

Figure 16: (A) Histogram synthetic sheets radius 1, (B) histogram synthetic sheets radius 3.

The application of the noise to the generated stack of grayscale images is an important step in order to obtain images as similar as possible to the one obtained by CT scan. In order to do so, using the software ImageJ, is possible to add salt and pepper noise or random noise. In the first case black and white pixel are sparsely distributed on all the slices of the volume, in particular replacing 2.5% of the pixels with black pixels and 2.5% with white pixels; in the second case the noise is Gaussian normal distributed that require two parameters as input: the average, set by default to 0, and the standard deviation, set by the user[3]. In order to generate two volumes that will undergo the DVC analysis, after setting the dimension of the volume, the radius and the number of the sheets the initial configuration will be generated by the Python script. Running a second time the script with the already generated volume as input, maintaining constant the radius parameter but changing the amplitude one, a different arrangement will be created to be correlate to the previous one and so simulate the deformation. Once the two

[3] The information about the noise is taken from the helper of the software ImageJ.

volumes are generated, if desired is possible to import them on ImageJ to add the noise and following perform the DVC analysis on Avizo software.

B. Porcine aortic sample

1. Harvesting of the sample

The second major section of this master thesis work is centred on the virtual deformation and analysis of porcine aorta sample. The datasets were acquired performing CECT scans of the sample at different condition, to evaluate how the change of the acquisition parameters effect the resulting images. The resulting acquisition time is affected by how the acquisition parameter are set; for example, higher number of projections will rise the time required for the scanning. Thus, it impacts the hydration level of the sample under investigation and, as result, the volume of the specimen experiences a shrinkage appreciable via the software of acquisition.

The specimen used is a portion a of porcine aorta (Figure 17A) harvested on the 2nd of February 2022, then dissected and underwent fast-freezing in isopentane for 2 minutes on the same day. Following, it has been stored in the freezer at -80 °C until the moment of the staining. As staining agent has been used Hf 1:2 WD POM (35mg/ml in PBS), the specimen has been immersed in 5 ml of staining solution for 7 days on a shaker plate at room temperature. Note that usually 10 days is a more suitable time of staining for this type of sample. After the staining period, the specimen has been collected, rinsed with PBS and stored in PBS solution before the preparation for the scanning right after the collection from the staining solution. To do so, it has been dried to remove the PBS excess and cut obtaining a small rectangle of 5x10 mm. It has been placed on a plastic support and wrapped in parafilm to keep it in place preventing possible shifting and the loss of hydration (Figure 17B).

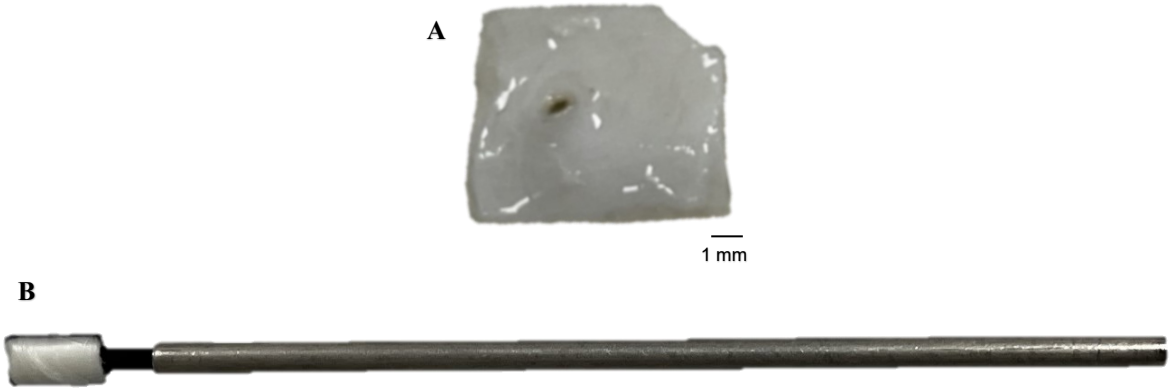

Figure 17: (A) Porcine aorta sample, small incision in the corner to distinguish the longitudinal to the radial direction, (B) specimen wrapped in parafilm and positioned on the left part of the plastic support.

2. Image acquisition protocol

Once the specimen was prepared and put on the scanning support, the scan was performed using the acquisition parameter presented in Table 2.

Table 2: Acquisition parameters

Focus-detector distance (FDD)	Focus-object distance (FOD)	Voxel size	Tube voltage	Tube current	Focal spot size	Filter
600 mm	15 mm	2.5 µm	100 kV	105 µA	2.49 µm	No

A first fast scan of the porcine aorta, denominated Porcine_Aorta_0, was performed and considered in the following steps as default scan and its parameters as reference. Following a series of other datasets were created changing for each of them one or more of these parameters: time of exposure, number of images and voxel size. The FDD, tube voltage, tube current, focal spot size and no filter have been kept the same for all the acquisitions.

In Table 3 are presented all the acquisition performed, reporting the parameters modified compared to the first scan taken as reference:

Table 3: Acquisition parameters of porcine aorta specimen

	Normal/fast scan	Voxel size [µm]	Exposure time [ms]	Number of images	Averaging	Skip
Porcine_Aorta_0	Fast scan	2.5	500	2000	1	0
Porcine_Aorta_1	Fast scan	2.5	750	2000	1	0
Porcine_Aorta_2	Fast scan	2.5	500	1500	1	0
Porcine_Aorta_3	Normal scan	2.5	500	2000	3	1
Porcine_Aorta_4	Fast scan	3	500	2000	1	0
Porcine_Aorta_5	Fast scan	3	500	1500	1	0
Porcine_Aorta_6	Fast scan	4	500	2000	1	0
Porcine_Aorta_7	Fast scan	4	500	1500	1	0
Porcine_Aorta_8	Fast scan	5	500	2000	1	0
Porcine_Aorta_9	Fast scan	2.5	500	1200	1	0
Porcine_Aorta_10	Fast scan	2.5	500	1000	1	0
Porcine_Aorta_11	Fast scan	2.5	500	800	1	0
Porcine_Aorta_12	Fast scan	2.5	500	600	1	0

For the CT reconstruction of the volume the same settings were kept for all the datasets:

Table 4: CT reconstruction settings

Scan optimizer	Filters applied	Beam hardening correction
Done	Inline median, ROI-CT, Filter volume	7

C. Dataset pre-processing analyses

1. Signal to noise ratio

The signal to noise ratio (SNR) is a useful tool used as quality indicator in imaging analysis. It gives a quick overview of the image quality, relating the amount of signal of interest versus the amount of noise present. Numerous are the formulas used to define the SNR, in this work it will be calculate as the ratio of the mean grayvalue in the region of interest, denominated *sig*, over its standard deviation (Equation 3) [37]:

$$SNR = \frac{\mu_{sig}}{SD_{sig}}$$

Equation 3: Signal to noise ratio

The average value of the grayscale in fact represents the signal and the standard deviation quantify the noise.

To define the SNR the software Dragonfly has been implemented. A sequence of the slices of the datasets, in particularly taken from the middle section, are loaded on the software. Using the line tool is possible to draw a path following the trend of a specific elastic sheet in the VOI (Figure 18A) and looking at the statistic (Figure 18B) is possible to obtain the corresponding mean value and SD of that specific segment used to calculate the SNR. For the synthetic sheets, it's applied the same procedure.

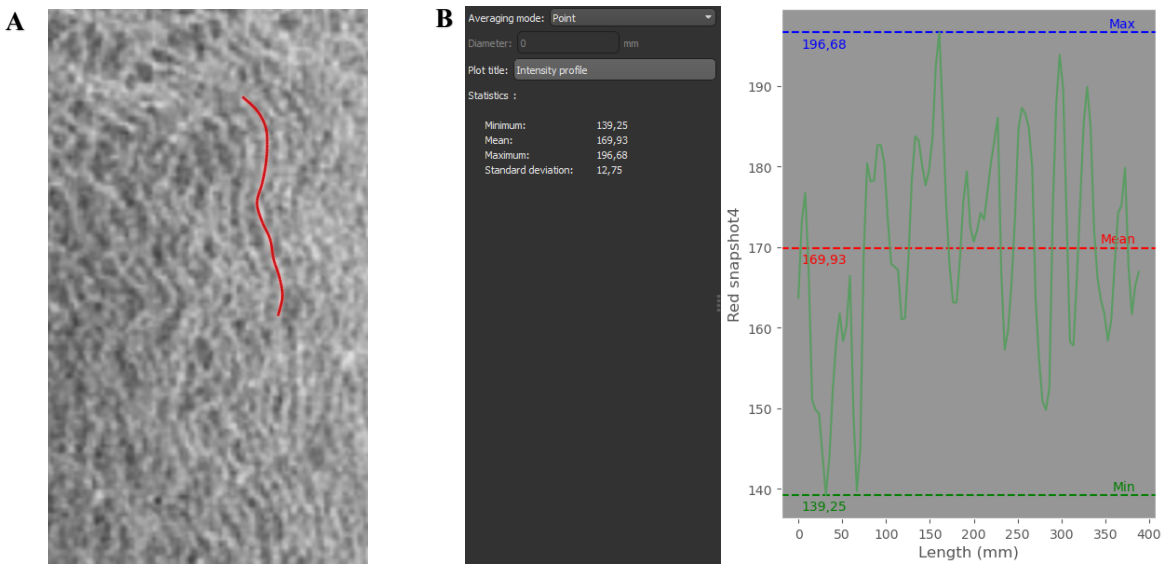

Figure 18: (A) Selected path on VOI in Porcine_Aorta_0, (B) path statistics provided by Dragonfly software.

D. Post processing analyses

In order to perform the virtual deformation of the porcine aorta datasets collected and the DVC analysis, as for the synthetic sheets generated, is necessary to use a software for the image analysis implemented to carry out these types of elaborations. Avizo software (ThermoFisher Scientific company), has been employed for this purpose. Avizo is a software for the visualization and analysis of CT and microscopy images able to quantify the displacement between a reference volume and its deformed configuration, useful to quantify the deformation induced by changes in the microstructure. The Avizo XDigitalVolumeCorrelation Extension provides Digital Volume Correlation (DVC) techniques to compute to compute the 3D full-field continuous displacement and strain maps[4]. As output, it is possible to have a visualization of the displacement and the strain field, ensuring easy understanding for the user thank to graphical representation with vectors or coloured maps.

1. Virtual deformation of porcine aorta specimen

The virtual deformation applied on the porcine aorta specimen aims to simulate the natural process happening when the blood vessels undergo high pressure. It is the counterpart of the one simulates by the synthetic sheets: from a relaxed condition in which the elastin is wrinkled, they are stretched till a linear condition. The aim is to clarify how the virtual deformation process works on a volume of interest (VOI) extracted from the original porcine aorta specimen. Will be simulated a bidirectional or monodirectional tensile test along the longitudinal direction

[4] The information about the functioning of the modules of Avizo software described following has been taken from its helper.

(following the Z axis, perpendicular to the XY slice presented in Figure 19) of the VOI extracted using Avizo software and next perform the DVC analysis. Following are presented the steps performed to virtually deform the VOI.

Once the data containing the slices of the volumes have been uploaded on the software, since each raw dataset shows different histogram range of values, it has to be equalized to a more uniform one converted to a grayscale range from 0 to 255. For example, the first fast scan performed presents a raw data range of 0-6545353 before the normalisation. This ends up in an improvement of the visualization of the images with a better contrast.

This step is crucial because the DVC compares grayvalues to compute the correlation and so it is important to normalise the different raw histogram associated to different datasets between each other, to be able to confront comparable datasets.

In Figure 19A is possible to appreciate the specimen surrounded by the parafilm and the background made of blackish pixel. Since these outer parts are not interested in the procedure, applying a segmentation based on the histogram thresholding and selecting only the grayvalues corresponding to the tissue of interest was possible to isolate the specimen from the background (Figure 19B). In this work the segmentation step was not mandatory since the analysis has been performed on a VOI, but it is useful to work with a dataset of smaller size and so improving the computational time. Following, in order to focus on a region of interest elastin fibres dense, a parallelepiped shaped sub-volume has been extracted from the original one (Figure 19C).

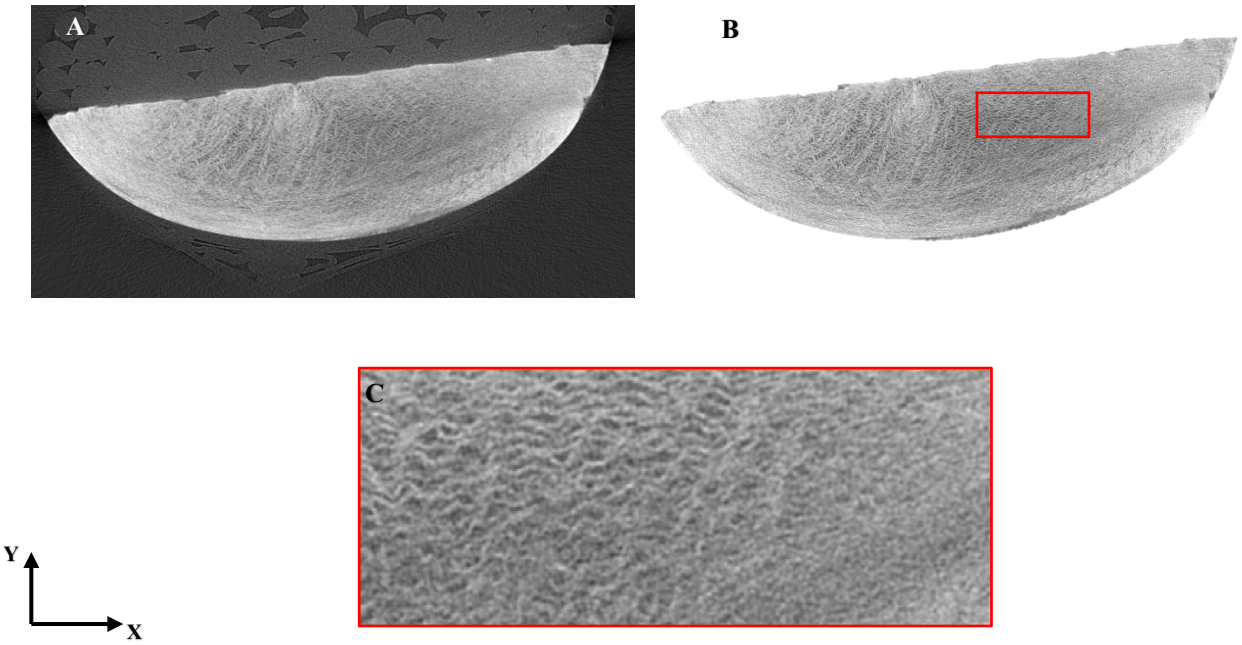

Figure 19: (A) Original porcine aorta, (B) segmented volume (physical size: 5247.5, 21225.5, 4622.5 µm), (C) 2D slice of the VOI (physical size: 1312.5, 530, 1155 µm).

Once the VOI has been extracted it can undergo the deformation desired. For the sake of ensure the highest correlation between the reference volume and the deformed one, a copy of the original dataset is created and then modified. To do so, a particular module of Avizo, *transform sequence*, has been used: it allows to apply a series of transformations to the object for example rotation, translation, application of a shear and scaling in the three dimensions. In the following analysis presented in this work, has been imposed a scaling in Z direction controlling the scaling factor: a value between 0 and 1 impose a compression, a value greater than 1 impose an elongation. Using this tool is necessary to pay attention to the reference system: when data are imported on Avizo, the software memorize the position of the local refence system of the object, so it is not automatically centred on the global reference system.

The relative position of local refence system to the global one brings to different modification of the volume, even if the same deformation is applied. For example, if the centre of gravity of the VOI is located on the origin of the global reference system the scaling leads to a symmetrical deformation respect to centre of gravity of the object (Figure 20A). This aspect will be discussed in the following chapter. For a better comprehension, in Figure 20 below is possible to see a comparison between a VOI extracted from the porcine aorta and the result of scaling in longitudinal direction in different way.

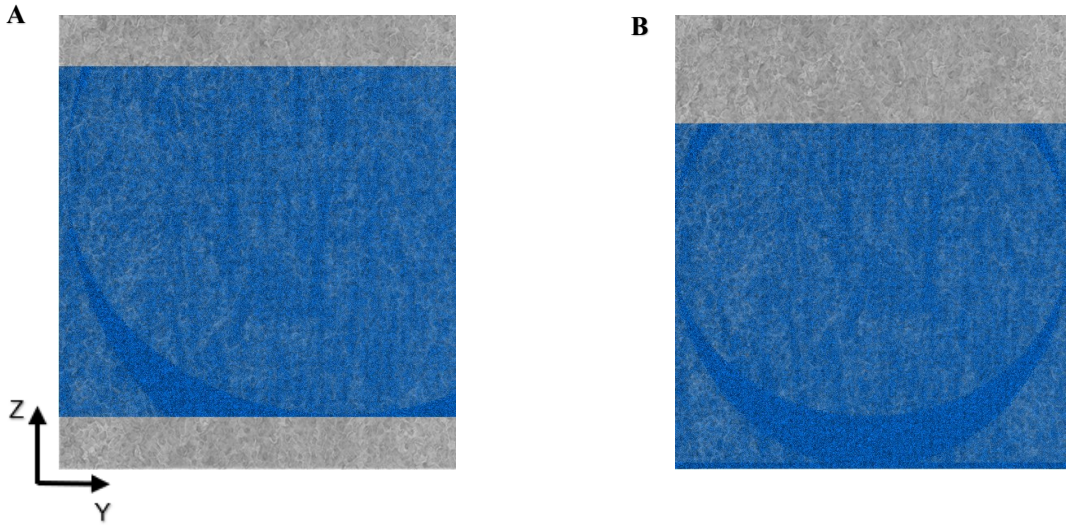

Figure 20: Comparison between reference VOI (blue) and deformed VOI (grey). (A) scaling in positive and negative Z direction, (B) scaling in positive Z direction.

After performing a transformation on a volume, its representation in memory is untouched so only the visualization of the object its changed but not the information in the dataset. To do so, the module *resample transformed image* is applied to the deformed volume to create a new field for it. Note that, since required to be able to perform the DVC, this passage will crop the original volume to fit its original dimensions; so, if it is applied scaling factor a part of the object

analysed will be lost. Once the desired deformation has been applied to the VOI, is possible to proceed with the deformation analysis.

2. DVC uncertainty measurement

Before moving forward with the DVC analysis, usually it is common to estimate in advance the uncertainty level. During *in-situ* testing, first the specimen is imaged twice without changing its position or the acquisition parameters and then correlating the two scans it is possible to calculated random and systematic errors, such as the standard deviation of the displacement field. Performing a DVC on a volume that has not been deformed allows to find the best compromise between displacement/strain uncertainties and spatial resolution, in particular is a useful tool to define the most suitable value for the subset size and the cell size, parameter required performing the local and the global approach. For the synthetic sheets, this type of evaluation has been done on the same unchanged dataset. Alternatively, is possible to compare the reference volume to a its copy which data range has been slightly modified (for example 10-255) to simulate two different acquisitions.

Using the *DVC uncertainty measurement* tool, the software can perform this kind of analysis automatically. The user set an initial cell size, the increment value and the number of steps; the module runs many DVC computation as the number of sets every time incrementing the cell size. As output are produced: spatial average displacement and strain and corresponding standard deviation, the mean average and standard deviation of the correlation residual useful to check the correlation. Plotting for example the SD of the spatial displacement against the cell size can help the user finding the compromise between resolution and uncertainty.

3. DVC protocol

Before carrying out the DVC analysis is necessary to follow specific steps: registration, radial autocorrelation, measurement of maximum displacement and mesh generation. This protocol is valid both for synthetic sheets and porcine specimen.

Registration

Once the desired deformation has been reached, is necessary to co-register the reference volume with the deformed one. The module *register images* computes an affine transformation using an interactive optimization algorithm; the approach involves applying a hierarchical strategy, initially resampling the dataset at a coarse level and then progressing to finer resolutions.

Specifically, the method utilizes a reference histogram to calculate an energy-entropy ratio. The goal is to minimize entropy and maximize mutual information between the two datasets.
Note that if the deformed volume has been moved from its original position, before performing the registration, is necessary to bring it back according to the local system of the reference volume. To achieve this is possible to perform an automatic re-alignment based on the overlap of the centres of the volumes via *register images* module, or alternatively the user can move it back manually (manual registration). The registration step is useful to align the two volumes and avoid errors due to large rigid body motion.

Radial autocorrelation

It is necessary to identify the length scale of the microstructure: applying the module *radial autocorrelation* to the reference volume it calculates the two-point correlation function of the tomographic image. Plotting the autocorrelation versus the distance, is possible to note the voxel size corresponding to the microstructure range because it is located at the asymptote point of the curve (Figure 21). This value has to noted, since it will be required during DVC to calculate the subvolume size and the cell size.

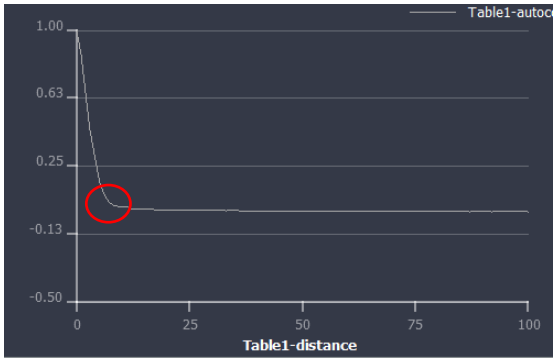

Figure 21: Example of autocorrelation plot, the red circle highlights the asymptote point.

Measurement of maximum displacement

Looking at the region of the VOI where the deformation is more visible, must be noted the maximum displacement of a specific point.
This could be done comparing the same slice of the reference and deformed volume and measuring, using the Measure tool, the displacement of a specific point. Alternatively, using the module *Subtract images*, is possible to perform a subtraction between the images of the two datasets. This will originate a new dataset in which images the maximum displacement is marked by white area; using the *measure tool* is possible to quantify it. Again, this information will be required to run the local approach.

Mesh generation

Lastly, before running the DVC, is necessary to generate a mesh on the reference volume. To do so, is possible to follow three different approaches.

After transform the grayscale images into a binary image selecting all the volume using the *interactive threshold* module, to ensure that all the material between the sheets is selected it is performed also a closing operation. Using the *generate surface* module the surface is generated; but before creating the tetra grid mesh is necessary to reduce the number of its nodes otherwise the computational work will be too heavy. Via an edge collapsing algorithm, setting as minimum edge length 3-4 times the macrostructure length noted before, a tetragonal mesh is created with a reduced number of triangles of not regular shape composing the surfaces (Figure 23A). The following illustration (Figure 22) shows as the blue edge is reduced to a single point and the pre-exciting triangle become degenerate and so deleted.

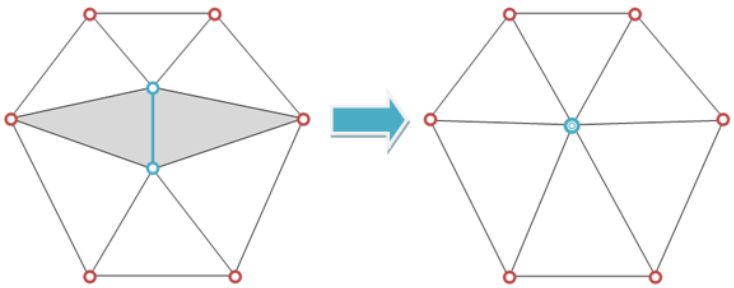

Figure 22: Edge collapsing for mesh simplification [Avizo helper].

Following the same procedure but imposing a thresholding that will select only the sheets, is possible to generate a mesh following the shape of the planes (Figure 23B) (this approach has been tested only on synthetic sheets).

Alternatively, is possible to produce a cubic mesh using a specific tool of the DVC module, indicating as input for the cell size of the mesh, 3-4 times the macrostructure length noted before. This will generate a tetragonal mesh and the triangles composing the surfaces will have all the same shape (Figure 23C).

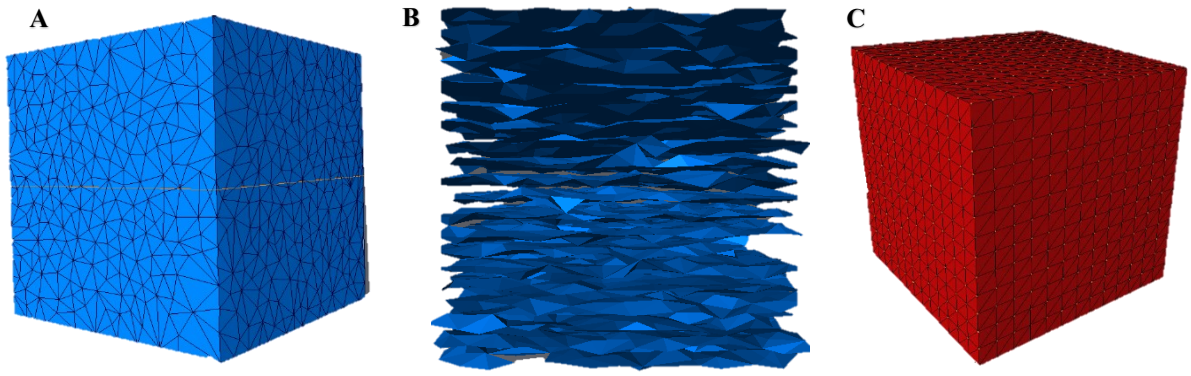

Figure 23: (A) cubic mesh generate via generate surface tool, (B) sheets-shaped mesh, (C) cubic mesh generated via DVC tool.

DVC analysis

Finally, is possible to perform first the local DVC and after the global approach. In the first case is necessary to pay attention to the sub-volume size and the max displacement parameter to ensure the best correlation and a good trade-off between spatial resolution and measurement accuracy; for example, a small sub-volume assure a more precise measurement but it is more susceptible to noise and image quality. As subvolume size is advised to set 3-4 times the macrostructure length noted before. To check the quality of the correlation is possible to check the statistics of the metric map contained in the metric output, verifying that the average is close as possible to 1. Local DVC will compute the displacement field, and it will be used as input for the global DVC with the tetra mesh previously created.

In the global approach, the displacement field is obtained by minimizing the correlation residuals; therefore, the histogram average value of the residual image should be as close as possible to 0. Additionally, is possible to display the residual image in where the weak correlation areas are marked by voxel with highest and lower intensity. Another way to assess the quality of the global approach is looking at the log output that contains the convergence value for each iteration of the algorithm. The user can set the number of iterations that have to been done to try to reach the convergence criterion set to 0.001. If after the number of iterations set the critical values is not reached is possible to try to increase the number of iterations, but if the algorithm continues to float around higher values than the criterion it means that the algorithm is not able to converge. Once the analysis has been carried out, is possible to visualize the displacement vector field and extract the corresponding X,Y and Z scalar component. For each of it is possible to display a gradient colormap in which darker colour correspond to smaller displacement and brighter colour to larger displacement.

V. Result and discussion

A. Porcine aorta

In this section will be discussed the behaviour of the porcine aorta when it is subjected to a virtual deformation. The aim is to clarify how the virtual deformation process works and investigate how the image quality effects the DVC. First will be compared the different datasets acquired applying different acquisition parameters, secondly will be discussed the results of different analysis performed.

A first attempt was an elongation both in positive and negative Z direction on a volume of interest (VOI) extracted from the reference porcine aorta dataset (Porcine_Aorta_0, Table 3 section IV.B.2), However, the result was inconsistent showing an unwanted shift in Y direction. In order to perform the bidirectional scaling is necessary to move the centre of gravity of the VOI on the origin of the global reference system. Thus, after the deformation is necessary to perform a manual registration. The DVC is not able to show the displacement caused by the scaling, but instead reports the displacement caused by the manual registration step. The results are presented in the appendix section.

A second attempt was done performing the scaling of the same VOI only in one direction, obtaining good correlation quality and consistent results. Though, the deformation process also caused an unpredicted translation of the VOI caused by the misalignment of the local and global reference system. In order to overcome this issue, the same scaling was applied after centring the VOI in the origin of the global reference system. Given the good DVC outcome this analysis has been performed in all the datasets acquired.

As last attempt, to simulate what usually is performed during a *in situ* 4D-CECT analysis, the original volume of the porcine aorta has been performed and following the DVC has been carried out on the VOI extracted. Despite so, the results in this case are inconsistent.

1. Porcine aorta specimen datasets comparison

In this section are presented the datasets acquired and for each of them the corresponding signal to noise ratio (SNR) value.

In Figure 24 are reported the different datasets acquired of the porcine aorta specimen, after the normalization of the histogram (refer to Table 3 to see the acquisition parameters). The XY slices are presented, selected in the middle of the volume, in order to appreciate the elastin fibres. The collagen fibres are not visible because the microCT is not able to detect them; this is caused by the low resolution and because the CESA used in the protocol binds only the elastin. Close to the upper border of the specimen the fibres are more wrinkled, whereas in the lower part they are more stretched because of the parafilm that tensions them.

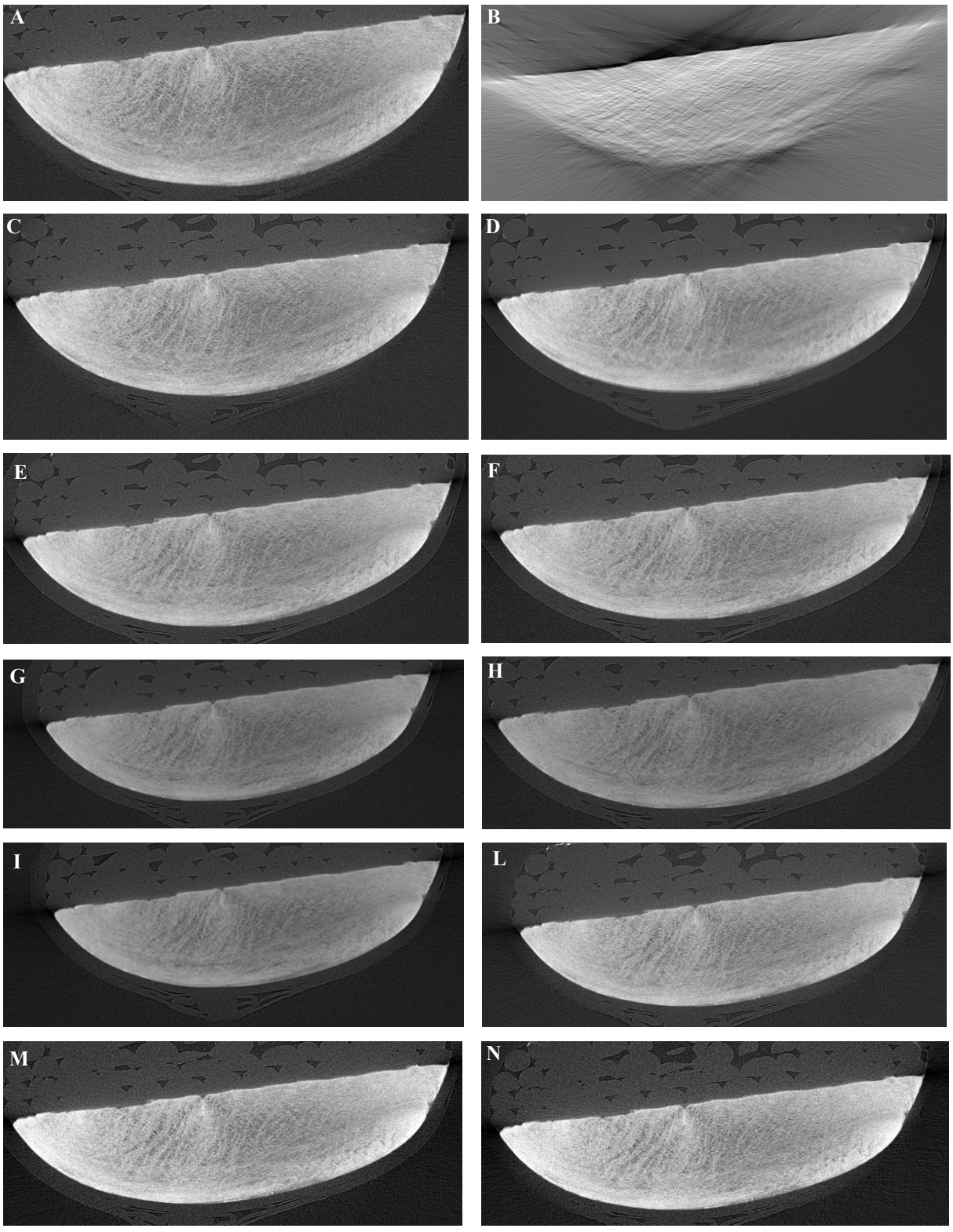
A
B
C
D
E
F
G
H
I
L
M
N

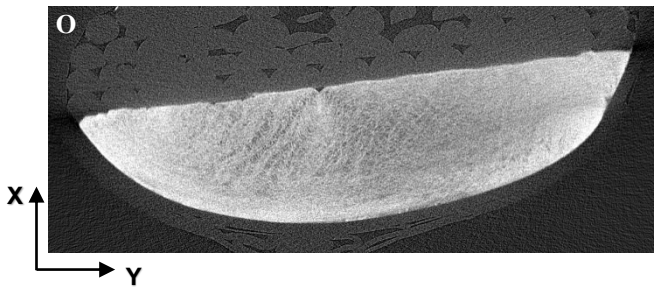

Figure 24:Datasets of porcine aorta specimen at different acquisition parameters (A) Porcine_aorta_0, (B) Porcine_aorta_1, (C) Porcine_aorta_2, (D) Porcine_aorta_3, (E) Porcine_aorta_4, (F) Porcine_aorta_5, (G) Porcine_aorta_6, (H) Porcine_aorta_7, (I) Porcine_aorta_8, (L) Porcine_aorta_9, (M) Porcine_aorta_10, (N) Porcine_aorta_11, (O) Porcine_aorta_12,

The first databased acquired shows already a good quality. Also decreasing the number of images to 1500 allow to obtain good visualization of the elastin sheets (Figure 24C). In Figure 24B, performed with exposure time increased to 750 ms, the edges of the specimen are less clear and are present artifacts visible as parallels lines all over the sample, making the fibres anymore clear. This shows that 500 ms is an adequate exposure time. Comparing the long scan (Figure 24D) to the fast scan (Figure 24A) is possible to see that the edges in the lower part of the specimen are not well define and appear blurred. In Figures 24 from G to I is possible to see the acquisition performed at bigger voxel size and for different number of images, a decreased contrast is visible. This fact is caused by shrinkage of the samples because of its dehydration. Comparing Figure 24 from M to O, corresponding to a decreasing number of images, is possible to notice an increasing of noise, making less defined the elastin fibres because their pattern is mixed with the noise pattern.

To better appreciate the quality of the images, in Figure 25

Figure 25 are reported the slice of the VOI used in the virtual deformation analysis extracted from the same position in the different datasets. In Figure 25B is possible to appreciate the artifact that does not allow to clearly see the pattern of the elastin. In Figure 25G to I is visible the lower contrast due to the increment of the voxel size. In Figure 25M to O is more appreciable the presence of the noise that makes the elastin almost not visible associated to the decrement of the number of images. From these images seems that the incrementation of the voxel size and the decreasing of the number of images make worse the quality of the resulting images.

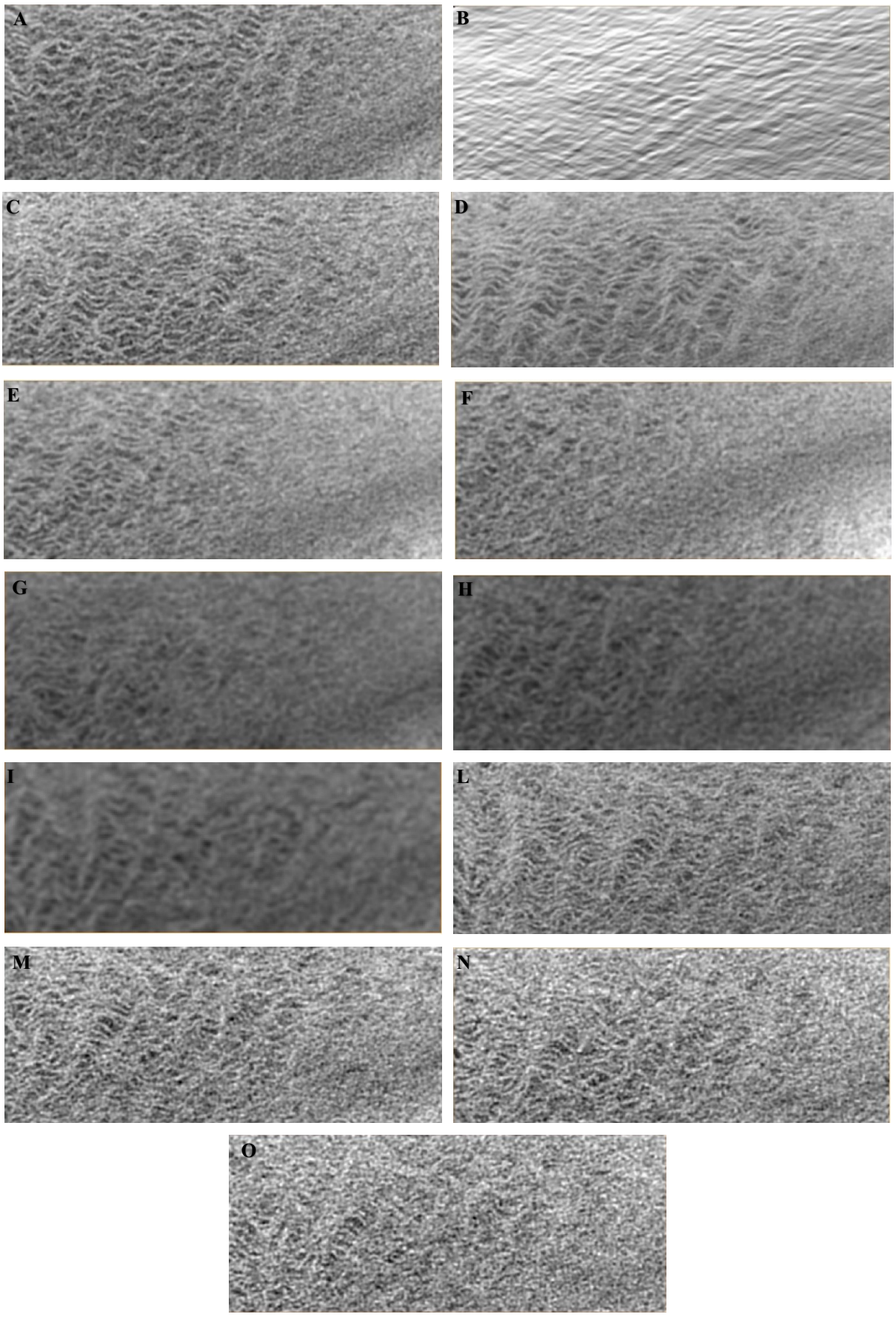

Figure 25: VOI extracted from datasets of porcine aorta specimen at different acquisition parameters (A) Porcine_aorta_0, (B) Porcine_aorta_1, (C) Porcine_aorta_2, (D) Porcine_aorta_3, (E) Porcine_aorta_4, (F) Porcine_aorta_5, (G) Porcine_aorta_6, (H) Porcine_aorta_7, (I) Porcine_aorta_8, (L) Porcine_aorta_9, (M) Porcine_aorta_10, (N) Porcine_aorta_11, (O) Porcine_aorta_12.

Signal to noise ratio

In Table 5 are presented for the signal to noise ratio calculated for each dataset[5]. These values have been calculated on the aorta specimen datasets, following the procedure described in section IV.C.1.

Table 5: SNR porcine aorta specimen dataset acquired

	Mean intensity grayscale value	**SD**	**SNR**
Porcine_aorta_0	159.39	15.39	10.35
Porcine_aorta_1	198.33	68.99	2.87
Porcine_aorta_2	151.71	17.35	8.75
Porcine_aorta_3	154.39	10.05	15.36
Porcine_aorta_4	142.88	10.61	13.46
Porcine_aorta_5	158.29	14.66	11.01
Porcine_aorta_6	124.17	8.08	15.36
Porcine_aorta_7	122.91	8.84	13.90
Porcine_aorta_8	122.91	8.38	14.65
Porcine_aorta_9	150.37	17.19	8.74
Porcine_aorta_10	167.90	17.77	9.44
Porcine_aorta_11	180.29	20.28	8.89
Porcine_aorta_12	168.38	28.15	5.98

The Porcine_aorta_1 shows the lowest SNR confirming, with the high SD value, the low quality of the dataset, indeed it presents artifacts due to the probably too high exposure time. The increasing SD and the decreasing SRN of the Porcine_aorta_10,11,12 confirms the increasing noise in the datasets due to the downscaling of the number of images. The lower contrast in Porcine_aorta_6,7,8 seems to be confirmed by the lowest intensity average; at the same time the low SD values lead to the highest SNR values. This fact is counter intuitive since the lower contrast should be linked to a lower SNR.

[5] The SNR values presented are calculated as the average of 5 measurement.

2. Scaling in Z direction of the VOI

To avoid the bias caused by the shifting along the Y axis in the displacement field performing the bidirectional elongation of the volume (see appendix section B), a scaling only in positive Z direction has been applied with a factor of 1.03. In this way the VOI does not have to be moved in the centre of the global reference system. In this section will be evaluated the results of the DVC analysis after applying the deformation; will be paid particular attention to the registration step to see how it effects the performance of the DVC. The VOI used was extracted by the Porcine_aorta_0 dataset. Once applied the scaling to the VOI, it's observed a translation (around 66 μm) following the same direction respect the global reference system; probably, this is caused by the fact that the local reference system of the VOI does not have the same origin of the global reference system. To better understand how this will influence the outcome of the DVC, in this section will be examined three distinct attempts performed on the same VOI, applying the registration in different way after the deformation, in particular:

1. Registration not effectuated
2. Registration effectuated without manual realignment
3. Manual registration

1. Registration not effectuated

Even though already showed the importance of the registration step, in this first attempt after applying the scale of the volume in Z direction, the deformed volumed has been resampled but the registration module has not been used. Performing the local DVC and looking at the metric output a mean value of 1.2 was registered. This marks an error in the procedure since, usually, the maximum value obtainable in case if perfect correlation is 1. Consequently, it is possible to assume that the registration step cannot be skipped because it guarantees the correlation between the deformed volume and the reference one.

2. Registration effectuated without manual realignment

As explained in section IV.D.3, if the deformed volume has been translated from its original position is necessary to re-align it to the reference volume before performing the registration. In this test are presented the result of not performing the re-alignment step.
After the deformation and the resampling of the modified volume, the registration has been applied without the realignment with the reference volume. Looking at the metric output of the local DVC (mean value 0.32) is possible to state that the correlation is not good. Talking about the global approach, the convergence wasn't reach since, even incrementing the number of

iterations (convergence residual value computed was 4000, when the threshold was set to 0.001. Moreover, the displacement range is between 64 and 4655 µm, emphasizing how the results are not reliable. This inconsistent result can be due to the registration step: since the missing alignment between the two configurations, the algorithm is not able to correlate them. The two datasets implied in the registration step, should be positioned fairly close, otherwise the algorithm could require longer time since there is lack of information and larger parameter space have to be determined cause of the longer distance between the two volumes.

3. Manual registration

For a better understanding of the processes of deformation, resampling and registering, the images corresponding to each step are presented (Figure 26), applying a scaling on the VOI. Is possible to see the changes that occur on the deformed volume (in blue), compared to the reference volume visible in grey.

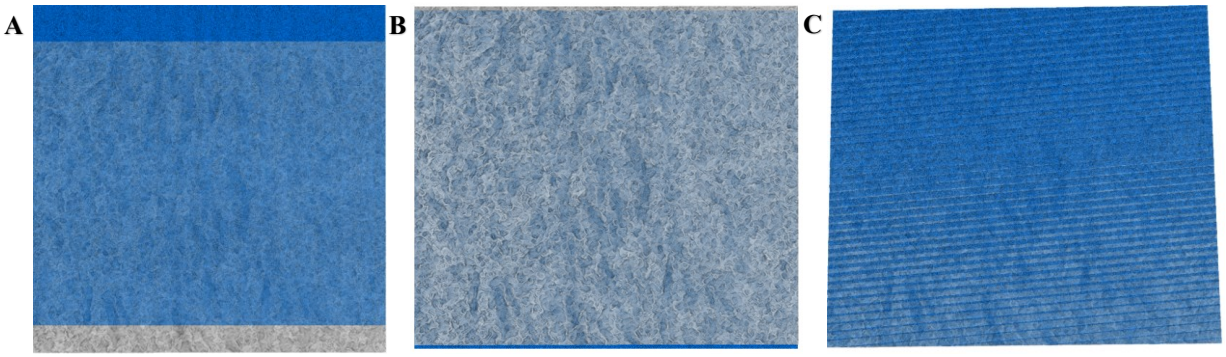

Figure 26: Comparison between (A) scaling, (B) resampling, (C) registration of porcine aorta. In gray the reference volume, in blue the deformed one.

In Figure 26A, at the bottom part of the volume, is it possible to see the rigid translation of the volume caused by the scaling transformation. The resample module (Figure 26B) cuts the deformed volume in order to have the same dimension as the original one. Also, apparently, even though the deformed volume has been moved to be aligned to the local reference system of the original volume, the resampling change its position. Finally, the registration (Figure 26C) aligns the centres of gravity of the two volumes.

Another aspect that is possible to analyse is the subtract images (Figure 27) between the reference volume and the deformed one, after applying the registration. This allows to appreciate the differences between the two stages of the deformation: is possible to notice that the central part show no difference, on the contrary the extremities of the volume are more deformed. This is consistent with what is shown in Figure 26C, where the centres of gravity of the reference and deformed volume are aligned.

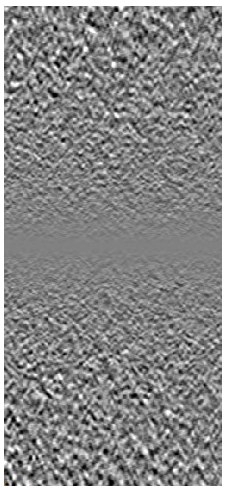

Figure 27: Subtract images between reference and deformed volume after the registration.

Returning to the analysis in hand, after the pre-alignment and the registration the local and global DVC were performed. Comparing the metrics with the one showed in case 2 "Registration effectuated without manual realignment" of this section, the quality of local and global approach is improved, as proved by the metric output (average value: 0.85) of the local approach and the correlation output (0.004) of the global approach. Even though this last result is not under the convergence criteria set (0.001), it could be considered acceptable.

In Figure 28 is shown the displacement vector field and the displacement in Z direction (Uz).

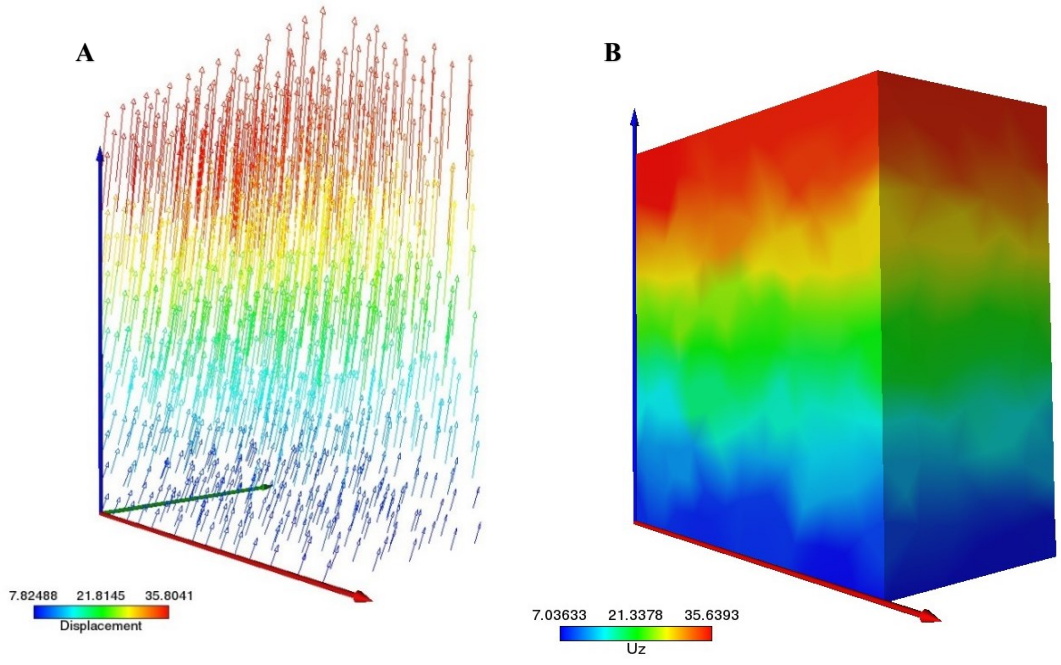

Figure 28: (A) Vector field and (B) Uz of porcine specimen VOI scaled in Z direction [µm].

The vectors in the displacement field point correctly in positive longitudinal direction but they deflect in Y direction. The deformation appears to be gradient and not uniform along the volume, so the upper part of the volume is stretched more than the lower part. Comparing this

result with the Figure 27 there is a discrepancy: above, after the registration step, seems that the deformation occurs only in the extremities of the VOI following positive and negative direction; here, as testify by the displacement map, the deformation is gradient in positive direction. Probably, the registering step take as reference point the middle of the volume and so in this portion no deformation is displayed, but the DVC can anyway compute correctly the deformation applied.

The displacement in X direction (range: -0.0012 – 0.013 μm), it is almost null as it should be for the type of deformation applied; on the other hand, in Y direction is observable a displacement around 3.2 μm that could be related to imprecision of manual registration process linked to the user intervention since it has not performed in an automatic way.

To validate the result shown, is possible to compare the expected displacement and the one produced by the computation. Known the spatial dimensions of the original volume (1312.5x530x1155 μm), multiplying the third values corresponding to the Z size for the scaling factor and then performing the subtraction with the initial dimension, is possible to calculate the expected displacement: 34.65 μm. It is within the displacement in Z direction range (Figure 28B) and correspond to the deformation in the upper part of the volume.

In order to obtain a more accurate displacement field it is important to pay attention to the manual registration step in order to align in the best way the reference and the deformed volume and so avoid unwanted shift in X a Y direction. It is important to underline that this simulation is simplistic and does not mimic perfectly what happened in nature: during a tensile test the specimen not only it's stretched in longitudinal direction, but also shows a shrinkage in the transverse plane.

3. Scaling in Z direction of VOI centred in global reference system

The analysis presented in the previous section still suffer of the unwanted rigid translation of the volume during the scaling. In order to avoid it, the local reference system of the reference volume has been moved and aligned to the origin of the global reference system and then resampled. It is important to underline that this action is not recommend since it is more recommendable to do not modify the original reference dataset to not change information that could influence the DVC and the correlation algorithm. A priori analysis to understand which was the most suitable cell size for the DVC computation was performed. Note that this procedure is usually performed on real dataset acquired by *in situ* test; in this case no penalization is expected. A VOI, extracted from the Porcine_aorta_0 dataset, has been used. As predicted, once the volume has been scaled no translation has been observed, then following the protocol the volume has been registered.

DVC uncertainties measurement

The DVC uncertainties measurement has been made between the VOI used and its identical copy after performing the registration. The module performed consequently 4 global DVC, increasing at each step the cell size within a range set by the user considered suitable for the structure in analysis. The cell size tested were 80, 100, 120, 140 µm.

Table 6: DVC Uncertainty measurement results for VOI extracted from Porcine_aorta_0 dataset

	<Ux>	SD (ux)	<Uy>	SD (uy)	<Uz>	SD (uz)
80	5,26E-16	1,67E-15	-5,57E-17	1,22E-15	-1,07E-17	1,05E-15
100	0	0	0	0	0	0
120	-4,32E-15	2,18E-15	1,89E-15	1,54E-15	1,61E-15	1,79E-15
140	-8,45E-16	1,65E-15	1,36E-15	1,80E-15	8,76E-16	1,82E-15

In the table above are presented the average spatial displacement and its uncertainties. The values are in the range of $10^{-15} - 10^{-17}$, except for the first increment, testifying how no body motion is recorded and that the level of correlation is good for the cell size value given as input. The null output in the first increment could be due to a rounding of the values calculated really close to 0. After all, it is an expected outcome as the uncertainty analysis has been performed on the same object. Since for all the cell size tested the result were comparable, 140 µm was selected as cell size in order to diminish the computational weight. The same value was used as subvolume size for the local approach.

DVC analysis

Moving to the evaluation of the DVC quality, the local approach produced as metric average value 0,92 and for the global approach the algorithm was able to reach the convergence of critic value of 0,001. These values ensure excellent correlation between the two volumes. Following (Figure 29) are presented the resulting displacement vector field and the displacement map in Z direction (Uz), where the higher deformation is concentrated.

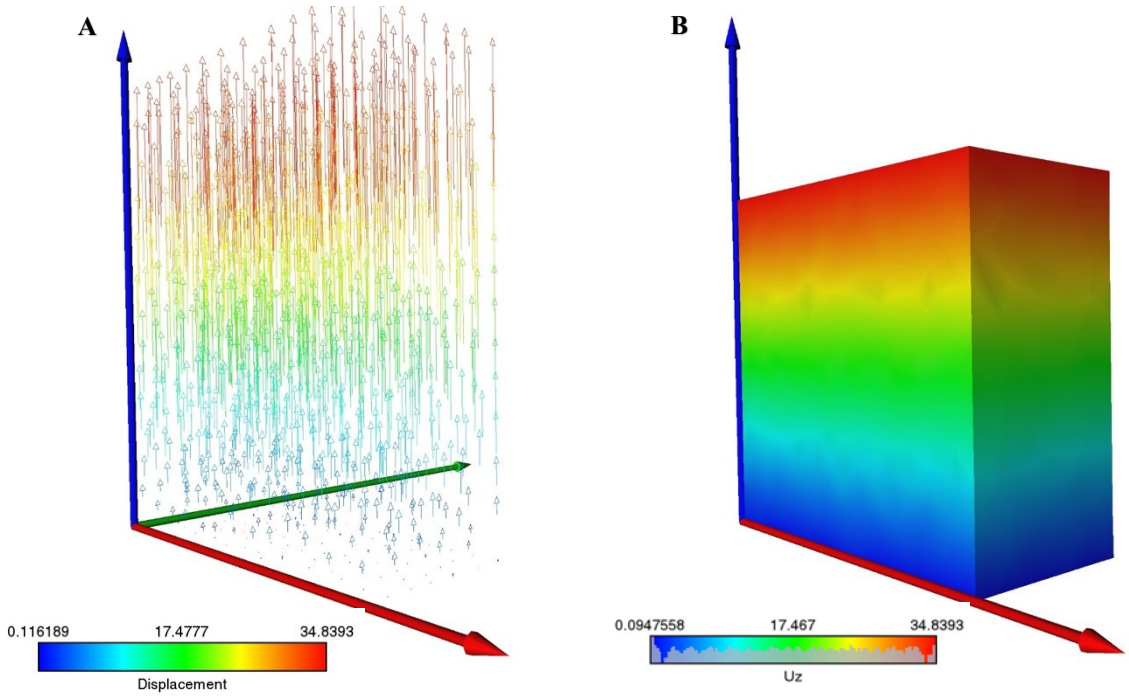

Figure 29: (A) displacement vector field, (B) Uz of the VOI centred in global reference system before the scaling of Porcine_aorta_0 dataset.

The result displayed are what is expected from this deformation: the vector field is composed of parallel vectors pointing in positive Z direction and are not observed outlier values. The deformation is gradient, as in the previous test showed in the *manual registration* section (V.A.2), and the maximum value registered on the top of the volume correspond to the predicted displacement calculated previously (34,65 µm). The displacement in X and Y directions show ranges[6] really close to 0, except for some uncertainties considered acceptable referred to the computation. In this case, compared to the result showed in the manual registration section, the displacement in X a Y direction is lower maybe because the re-alignment has been performed with more precision, underlining the importance of this step in order to get more accurate results. Additionally, the translation and the resampling of the reference volume before the deformation seems to not affect the performance of the DVC. Given the consistent results and the good convergence of the algorithm, this procedure could be a valid alternative in order to avoid undesired and not truthful shift during the scaling. Hence, the same procedure just presented has been applied also to the other datasets collected after performing again the DVC uncertainties analysis. Following will be presented the results to try to establish is the different acquisition parameter lead to different results.

[6] Ux: -0.12 – 0.06 µm
Uy: -0.12 – 0.11 µm

For each dataset acquired, a VOI of the same physical size (1312.5x530x1155 µm) has been extracted from the same position, and for the acquisition performed at different voxel size has been paid particularly attention to extract a subvolume with the same physical size as the others, in order to apply in all the cases the same deformation.

DVC uncertainties measurement

A priori DVC uncertainties measurement has been performed a second time in order to evaluate which was the best cell size to set for the Porcine_aorta_2 dataset (Table 3). Recalling the procedure for the selection of the subvolume size (section IV.D.3), firstly as microstructure scale has been individuated 35 µm secondly as suitable cell size 80,100,120,140 µm were hypothesized. For these values has been performed the DVC uncertainties measurement and in Figure 30 are plotted the average value and SD of the displacement in Z direction in function of the cell size. For 140 µm it's visible the smallest value for the displacement and its SD, so this value has been used as cell size.

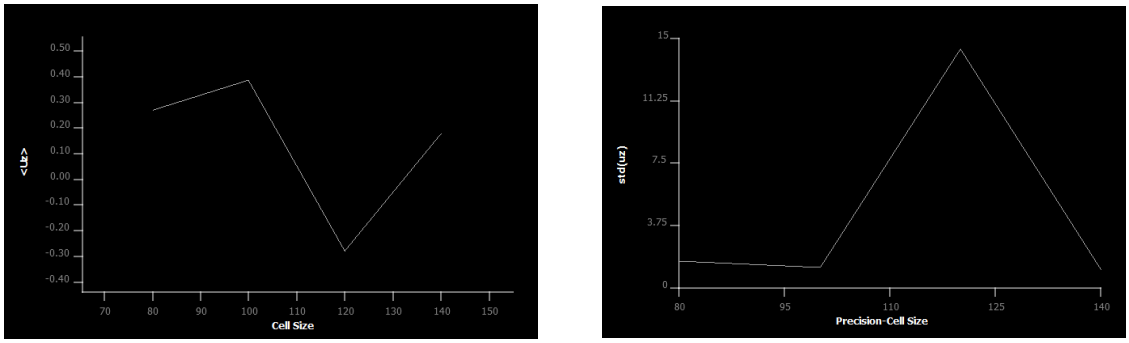

Figure 30: (A) Uz uncertainties in function of Cell size, (B) SD of Uz in function of Cell size.

Should be noted that the uncertainties measurements analysis should performed also for all the other datasets and define in each case the best cell size. In this work, to make the process easier, has been decided to use the same cell size for all the datasets.

DVC analysis

All the VOI extracted from the different acquisition underwent the same deformation: after having cantered the VOI in the global reference system a scaling factor of 1.03 has been applied. For the local approach of the DVC as subvolume size has been set 140 µm and the same values has been used as cell size for the generation of the mesh.

In general, all the analysis performed showed good correlation level for the local approach (metric average value >92) and also the global approach reached the convergence in almost all the cases. In almost all the cases, the displacement vector field produced was coherent and composed of parallel arrows pointing in Z positive direction, as expected given the deformation

applied. The deformation is gradient increasing from the bottom of the volume to the top. Recalling the expected displacement of 34.65 µm, calculate multiplying height of the VOI for the scaling factor and then performing the subtraction with the initial dimension, it is possible to see that this value is within the range computed. As reference, is reported the displacement vector field and the Uz map of Porcine_aorta_2 (Figure 31), underlining that almost all the other cases produced a comparable result. Comparing the displacement of this dataset with the Porcine _aorta_0 (Figure 29) the results are similar.

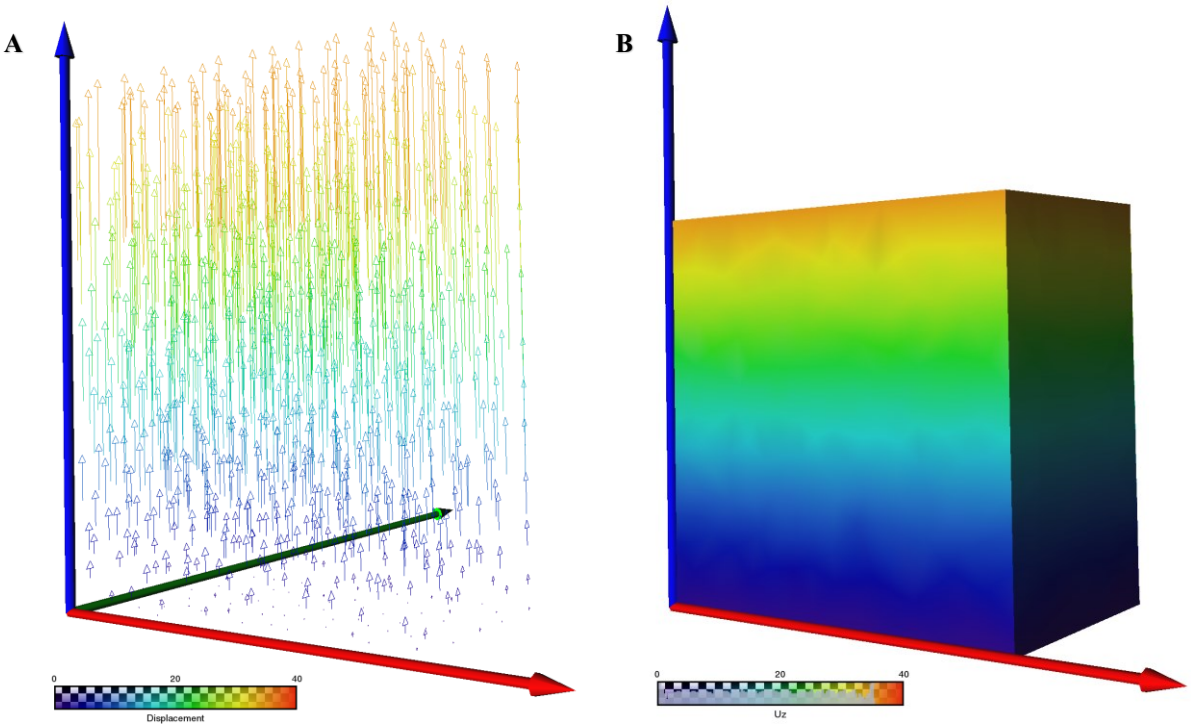

Figure 31: Displacement vector field (A) and Uz (B) of Porcine_aorta_2 (range values normalized [µm]).

To have a complete overview, in Table 7 in the following page are reported all the displacement computed for each dataset.

Table 7: Displacement ranges computed for the porcine dataset

Dataset	Displacement X direction [µm]	Displacement Y direction [µm]	Displacement Z direction [µm]
Porcine_aorta_0	-0.12 – 0.06	-0.12 – 0.11	0.009-34.83
Porcine_aorta_1	-0.77 – 0.38	-0.09 – 0.29	0.03 – 34.96
Porcine_aorta_2	-0.04 – 0.15	-0.027 – 0.14	0.14 – 35.17
Porcine_aorta_3	-0.57 – 0.84	0.08 – 0.17	0.56 – 34.87
Porcine_aorta_4	-0.19 – 0.21	-0.36 – 0.16	0.54 – 36.82
Porcine_aorta_5	-0.09 – 0.12	-0.10 – 0.12	0.69 – 35.39
Porcine_aorta_6	-5.20 – 12.29	-6.67 – 9.31	-20.85 – 32.28
Porcine_aorta_7	0.14 – 0.21	0.25 – 0.29	0.16 – 35.91
Porcine_aorta_8	-0.83 – 0.44	-0.33 – 0.61	-2.12 – 34.16
Porcine_aorta_9	-0.11 – 0.30	-0.22 – 0.11	0.12 – 35.02
Porcine_aorta_10	-0.13 – 0.06	-0.31 – 0.15	0.10 – 34.79
Porcine_aorta_11	-0.45 – 2.18	-4.98 – 0.33	0.64 – 48.68
Porcine_aorta_12	-0.36 – 1.15	0.98 –1.37	-34.55 – 34.03

The Porcine_aorta_6 did not produce result according to what just presented. Despite the local approach showed a good correlation, the global approach algorithm did not converge. In the upper part of the volume is shown an incorrect displacement (Figure 32A) in contrast with the deformation applied. Maybe this is due to an area in which the correlation is weaker. This hypothesis seems to be proved by the residual image, in which is possible to define the weaker correlation areas because they are the darkest and brightest in the image. Looking at the slice of the residual image (Figure 32B) corresponding at the area of the volume in which the displacement is incorrect is possible to notice this effect.

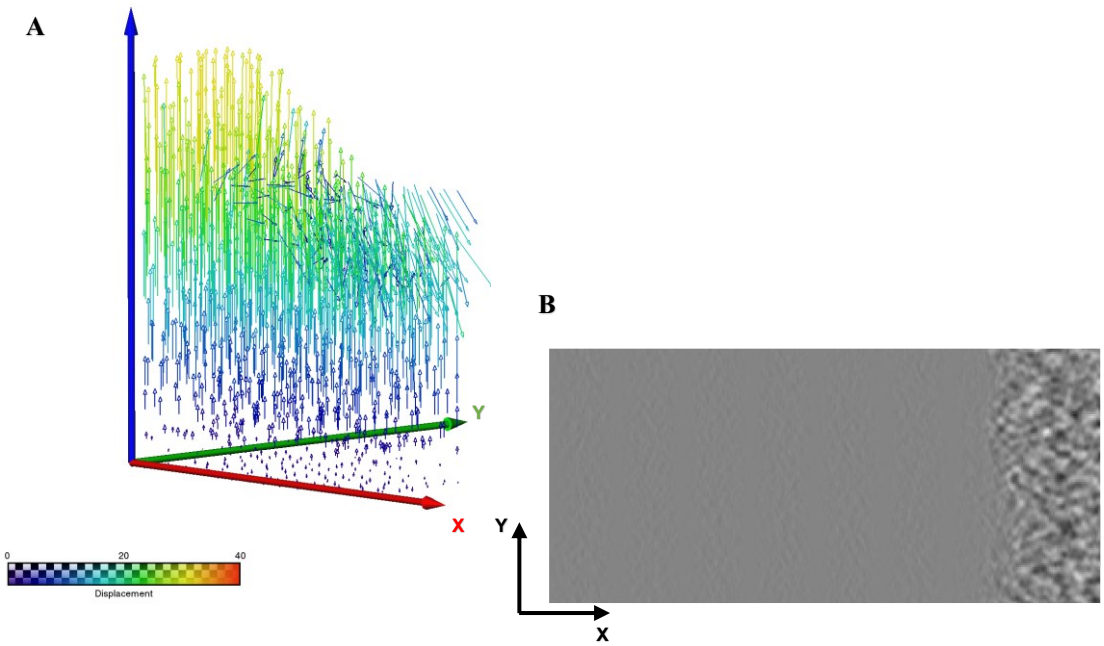

Figure 32: Result of Porcine_aorta_6 (A) displacement vector field, (B) residual image.

The low quality of the computation could also be linked to inappropriate quality of this datasets. This dataset shows low contrast, but the SNR, compared to the values of the other dataset, is higher highlighting a better quality. On the contrary, also Porcine_aorta_7 and 8 have similar SNR values to Porcine_aorta_6 dataset but the displacement computation in these cases is correct. Hence, in this case, the error in the computation seems to not be linked to the image quality, but the issue is still an open question.

Also the Porcine_aorta_11 and 12 show outlier values in the ranges, but the convergence was reached and their vector field have the same pattern as the one showed in Figure 31 except for a random vector.

In conclusion, the acquisition parameter adopted in this thesis work seems to be suitable for the image acquisition of the porcine aorta specimen and to not have an important impact on the performance of the DVC, except in the case of Porcine_aorta_6 dataset, in fact also in the case in which the visual image quality was not good (Porcine_aorta_1 dataset) the convergence was reached. For Porcine_aorta_11 and 12 datasets, even though the convergence is reached, the outlier values showed in the displacement ranges could be linked to the low image quality. The presence of the noise and the low sharpness can cause the increment of the DVC uncertainties; a priori uncertainties measurement perform on these datasets could confirm this hypothesis. Despite all, the reason why in one case the computation was erroneous remain unknown.

4. Scaling in Z direction of aorta specimen and DVC on VOI

In this section will be presented the results obtained applying a different approach on the porcine aorta specimen. The idea was to perform on the original volume of the Porcine_aorta_0 dataset the deformation, the manual registration and then extract the subvolumes (Figure 33). The scaling caused a rigid translation of the whole volume smaller (around 16 µm) than the in the case examined before (around 60 µm) where the VOI was scaled. Nevertheless, this smaller shift maybe could affect less the DVC outcome and presenting the outcome of this approach can be useful since it better copies what is performed in real experimentation: the extraction of a VOI after having performed the mechanical test and the scanning on the specimen analysed.

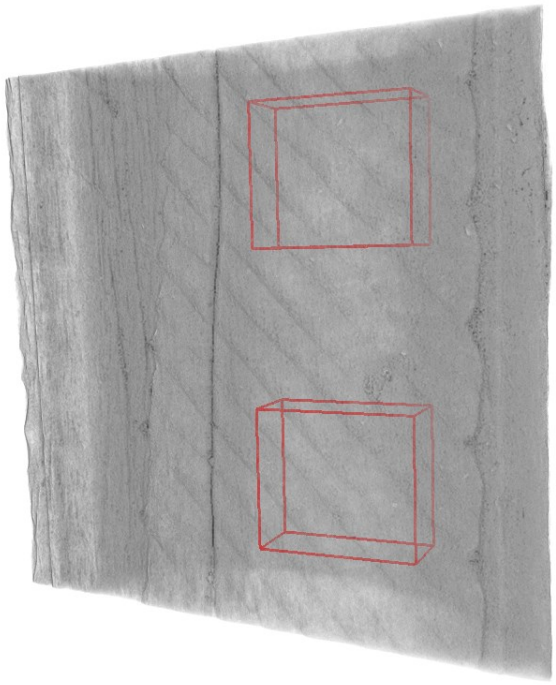

Figure 33: VOI of porcine aorta analysed.

The deformation has been applied on the upper volume (Figure 33). The outcome was not what was expected: both the local approach and the global approach didn't perform well (metric average value: 0.14; residual average value: 10^38) and the convergence output testify the algorithm was not able to converge. It is important to underline that given the weak performance of the DVC the outcome cannot be considered reliable and it is not possible to make accurate conclusions; despite so to have a complete overview the result are reported.

Although the weak correlation, the displacement vector field (Figure 34A) is composed of parallels vectors pointing in Z positive direction, as expected. No deflection of the vectors in X and Y direction is observed, maybe because the manual registration was performed more precisely. The displacement range is concentrated around a value of 92 µm, but the expected deformation value calculated multiplying the Z dimension of the aorta specimen's original

volume (dimension: 5247.5x 2122.5x4622.5 µm) to the scaling factor and subtracting the original size is 138 µm. The displacement in Z direction (Figure 34B) shows a range from 92.4 to 92.6 µm.

Comparing this approach, in which the whole specimen was deformed, and previous one, in which only the VOI after the extraction was deformed, is possible to notice two differences. Comparing the displacement vector field (Figure 28A with the Figure 34A), is possible to see two different deformation: in the case of deformation applied on the VOI the displacement map is gradient, increasing from the bottom to the top part, in the case of deformation of the whole specimen, the deformation is homogeneous in the entire VOI.

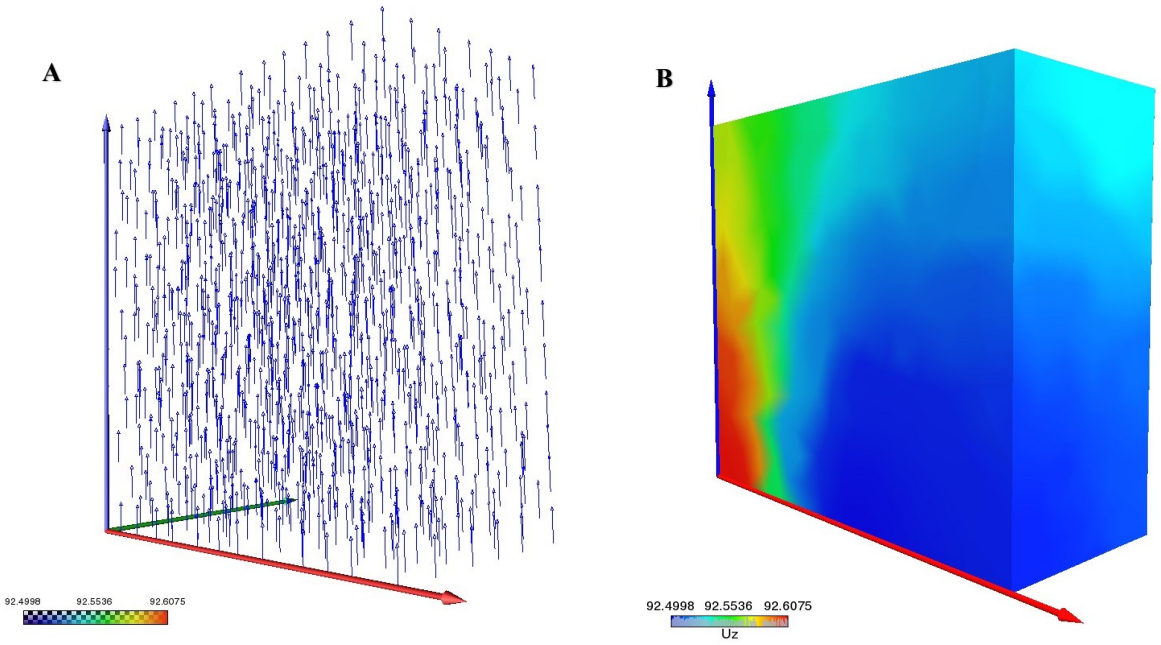

Figure 34: (A) displacement vector field, (B) Uz of VOI of specimen aorta deformed [µm].

The second comparison that is possible to do is looking at the subtract images of the VOI (Figure 27 and Figure 35), the first one refers to the deformation directly on the VOI, the second to the deformation of entire specimen. In the first case the difference between the deformed and the reference volume was evident only in the ends of the volume, in the second case it is homogenous in all the slice.

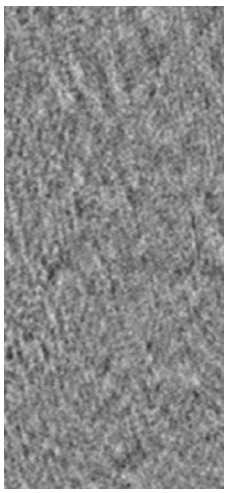

Figure 35: Subtract images between reference and deformed configuration of the VOI extracted from the upper part of the aorta specimen.

This difference could be linked to the different way of performing the registration. In this case, since the whole specimen volume undergoes registration and VOI is taken in the upper part far from the middle area, the centre bandage showing no-deformation is not showed in the VOI extracted after the registration.

For the sake of a complete evaluation and see if the deformation is homogeneous through the entire porcine aorta volume, the same procedure was applied on the lower VOI (Figure 33). Also, in this case the algorithm did not reach the convergence, so the result cannot be considered truthful. (See appendix section D).

In order to understand why the DVC did not work properly, another attempt has been made: after the deformation of the original volume and the resampling, the VOI are extracted from the lower part and the registration step has been performed on the VOI and not on the whole original volume as before. The outcome is comparable with the approach just presented: the quality of the correlation is weak and also the displacement field shows the same values. Thus, applying the registration to the entire volume or to the VOI doesn't change the outcome.

Is not easy to make a hypothesis about the reason why the application of the scaling on the whole aorta volume computes a solution so different compared to the previous method in which the deformation was applied directly on the VOI. The problem could be linked to the scaling factor applied: the deformation applied on the aorta specimen volume maybe is too high to allow the algorithm to correctly correlate the deformed and the reference configuration. The deformed VOI is too different from the original one and are missing too much information in order to be able to match the two configurations.

Investigate this issue is still a going on for this master thesis and performing the same evaluation but applying a smaller scaling factor could lead to an answer. Additionally, also the size of the VOI could influence the outcome of the correlation algorithm: try to change the edge dimension of the VOI could lead to a better overview of all the factor that can influence this procedure. Explore more this analysis could be important, since it resample the most what happened during 4D-CECT mechanical tests.

5. Conclusion

This section was focused on the analysis of the porcine aorta specimen applying on it a virtual deformation, in particular a scaling in longitudinal direction.

A first attempt, performing a bidirectional elongation, was performed, but the result led to no useful information since the algorithm did not compute the correct displacement despite the good correlation value.
A second attempt was made scaling the VOI only in one direction; but the deformation applied also caused a translation of the whole volume in the same direction. This is because the local refer system is not aligned to the global reference system. Particularly attention has be given to the registration step: it has been noted that the registration is a fundamental operation and it is also important, if the deformed volume has been translated during the deformation, to manually re-align it to the reference volume before performing the registration.
In general, performing the DVC, the algorithm was able to converge and a coherent displacement with what predicted has been computed even though a slight shift in Y direction was highlighted but maybe because of an imprecision in the re-alignment step. Also, the predicted displacement is coherent with what displayed in the displacement map. From this analysis, even it is simplistic, is possible to say that the DVC works correctly, but is important to set the correct subvolume size and pay attention to the registration step. Since other subvolume size has not been tested, would be interesting test a denser mesh with smaller cell size to see if the precision improves.

Following, has been performed the same scaling in longitudinal direction as in the previous analysis. In this case, in order to avoid the translation effect, the reference volume before the deformation has been moved according to the global reference system. This operation is not advised since the dataset of the reference system should not be changed. Despite so, the DVC algorithm was able to converge correctly and produce the displacement predict. For this reason, the very same procedure has been applied on the other datasets acquired, extracting the VOI from the same lower part of the aorta specimen.

All the dataset analyzed performing the DVC showed good correlation value and the algorithm, converged computing in average the same displacement field according to the previous result. All of them except for Porcine_aorta_6 scan that produces and incorrect computation. The reason why in this case the analysis was not successful is still an open question since the SNR value was high and other dataset with a comparable value produced coherent results.

The last evaluation performed in this chapter aim to mimic what usually is done performing a 4D-CECT test: the specimen is deformed and following the displacement computation is performed on a VOI. In this case, the global reference system of the specimen was expected to be aligned to the global one and so avoid the unwanted shift of the volume while scaling it. But this was not the case. Despite so, the scaling has been performed on the aorta specimen, registered and two VOI have been extracted from the upper and the lower part. In both cases the global DVC algorithm did not converge and two different displacement field were produced. Given this information, is not possible to state if the outcome produced are totally truthful. Maybe the problem is linked to the too high scaling factor, causing a deformation too high that the algorithm was not able to track. Or, as alternative, some errors were performed in the VOI extraction step from the reference and the deformed volume, so the displacement computed was different from the one expected.

The work performed in this master thesis project here illustrated can be considered a first approach to the porcine aorta specimen, since, from my point of view, this topic has not deepened enough. Starting from the DVC uncertainty measurement, it helped to find a suitable subvolume size. Despite so, no other subvolume size were tested, further development can concentrate on this parameter and try to define a precise procedure in order to be able to set the best parameter for the DVC. Additionally, here the DVC uncertainty measurement has been done only on two datasets so it would be interesting to try it also on others.
Even though the registration step has been in part disclose, the deformation process remains an open question since has not been clarified clearly the reason why the VOI extracted from the porcine aorta specimen after its deformation, showed different displacement field and why the algorithm was not able to converge.
For a future development of the worked presented in this master thesis, a crucial point is understanding the mechanism of the virtual deformation because is fundamental to operate on the dataset acquired and produce reliable results. Should be considered to test different scaling factor to determine the range of deformation that is possible to apply to make DVC works. Furthermore, another possible improvement of this technique is simulating a deformation more realistic, not only elongating the sample in longitudinal direction, but also simulating the

changes in the microstructure in the perpendicular plane. It would be useful implement this aspect in the virtual deformation to have a better representation of the real behaviour of the blood vessels.

B. Synthetic sheets

In this section will be presented the analyses performed on the synthetic sheets generated via Python script, following two different approaches. In the first case has been performed the DVC correlating two volumes with different amplitude parameter, evaluating the effect of the mesh, noise and radius parameter. Given the unreliable result because of the poor correlation, has been performed a different approach. The volume generated has been virtually deformed performing a scaling. This is the same deformation performed on the porcine aorta VOI in the previous section (V.A.2.).

1. Mesh

The mesh generation is a fundamental part in the in the global DVC analysis; it allows to divide the surface of the object under investigation in smaller sections in order to discretize it. As described in the section IV.D.3 in the description of the DVC protocol, in this master thesis have been exploited three different way of generating the mesh, using the tool on the DVC module or manually generating the tetrahedral mesh. In this section will be presented different tests performed to evaluate which approach for mesh generation would be the best. This evaluation has been performed on the synthetic sheets, but the same evaluation could be effectuated also on the porcine specimen. To evaluate the different possible meshes, the DVC analysis has been performed on a volume of 200 µm containing 20 sheets, simulating a deformation from a reference volume with amplitude of 2 to a deformed volume with an amplitude of 1. In this section will not be evaluated in the specific the performance of the DVC since was not possible get reliable information about the deformation. Indeed, the resulting displacement field was very chaotic and inconsistent, and the displacement range produced changed from test to test presenting outlier values. Despite so, will be discussed the pro and cons of each approach for the mesh generation.

1.Plane-shaped mesh

The first mesh tempted was generated using the *generate surface tool* and consequently the *generate tetra mesh* tool as described in material and methods section. The idea was to create a mesh that follows the pattern of the synthetic sheets. The first problem faced was define an adequate size for the mesh cell. By choosing a very small dimension, it is possible to adequately follow the pattern of the sheet, but the computational load will increase. On the other hand,

increasing the cell size the mesh does not resemble the shape of the planes (Figure 36).

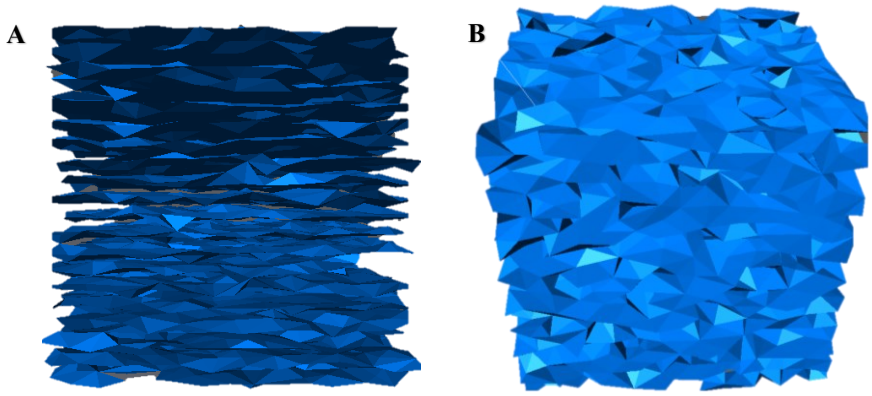

Figure 36: Comparison different mesh generated via surface generator tool.

It is necessary to find a balance between computational time and accuracy, following at the same time the indication reported in the procedure explanation for the generation of the mesh based on the scale length of the microstructure.

Performing the DVC with this type of analysis the algorithm did not converge. This approach is not considered good for this kind of analysis since the DVC takes under account only the sheets and not the background presents between them. In the reality, the blood vessel wall is composed not only by the elastin fibres, but also by other biological structures (collagen fibres, smooth muscle cells) that give a contribute in the mechanical response. So, in order to have a realistic representation of the displacement produced, is necessary to take under account not only the sheets, but also the background that with this approach is ignored.

2.Cubic mesh

Hence, has been decided to use a cubic mesh in order to include the entire volume in the computation, both the synthetic sheets and the background.
As previously mentioned two approaches are possible. The first one (Figure 37A), here referred as automatic generated mesh, is based on the tool in the DVC module in which is necessary to indicate the cell size. As rule of thumb, it should be 3-4 time the scale length of the microstructure, but there is no precise indication, so it depends on the user decision. The grid should be dense enough in order to appreciate the features of the structure in analysis, but at the same time not too dense in order to save computational time.
The second approach (Figure 37B), here referred as manually generated mesh, is based again on the *generate surface tool* and one the *generate tetra mesh* tool. The manually generated mesh is not composed of tetrahedrons all with the same shape, and maybe this could impact the DVC. Both approaches were attempted performing the virtual deformation above explained, creating

two meshes with a similar number of tetrahedrons in order to be able to compare the DVC computation. In both cases the DVC did not show good correlation quality and very different displacement ranges were computed. Given these inconclusive results, was not possible to clearly establish which approach was better, for this reason this aspect has to deepen more. The automatic generated mesh seems to be more suitable for simpler volume, such as cubic and parallelepiped since it is easier to divide them in triangles with the same shape. For complex shaped volume, showing for example cavities, the manual generated mesh is more suitable because operating with binarization and closing ensure to catch all the features of the volume. For the following analysis, both on synthetic and real datasets, has been decided to pursue the manual mesh generation, via generate tetra mesh tool, in order to follow the same procedure for all the analysis.

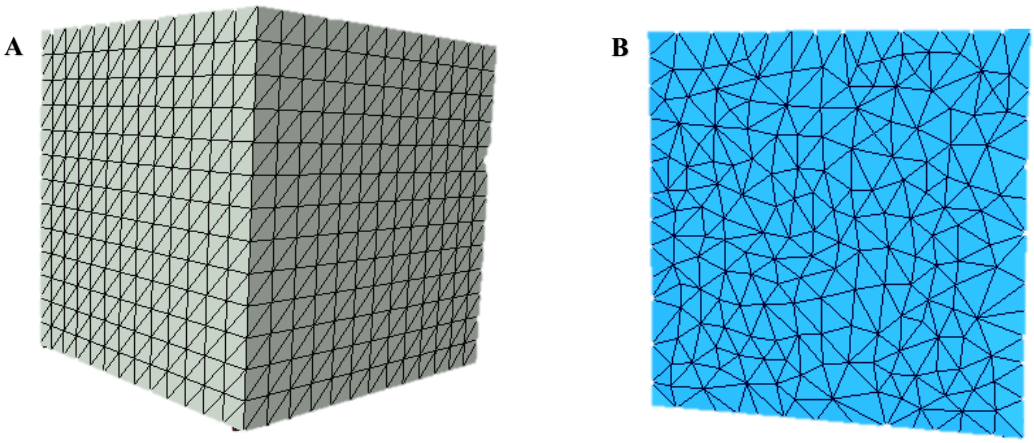

Figure 37:(A) Automatic cubic generated mesh showing homogeneous faces, (B) manually cubic generated mesh showing nonhomogeneous faces.

2. Noise

In this section will be evaluated the impact of the noise on the grayscale images composing the synthetic sheets volumes and discuss how it can affect the DVC analysis performance.

Noise is a component always present in CT images and can be visible in different ways such as dark strips or ring artifact (see section appendix A to refer to artifact in CT). Generally, noise can make the displacement computation more complex, since makes more difficult for the DVC algorithm to precisely correlate the reference volume and the deformed one [11].

Here will be compared two different situations. In the first one, first using the Python script is created the reference volume of a size of 200 µm containing 20 sheets and the amplitude parameter set to 1; second the deformed volume is generated with the original amplitude parameter tripled (Figure 38A,B). In the second situation the same volumes have been generated, but Gaussian normal distributed noise is added (Figure 38C,D). Following, the first

configuration will be referred as no-noise the second one as noisy. The DVC analysis were computed and the outcome compered.

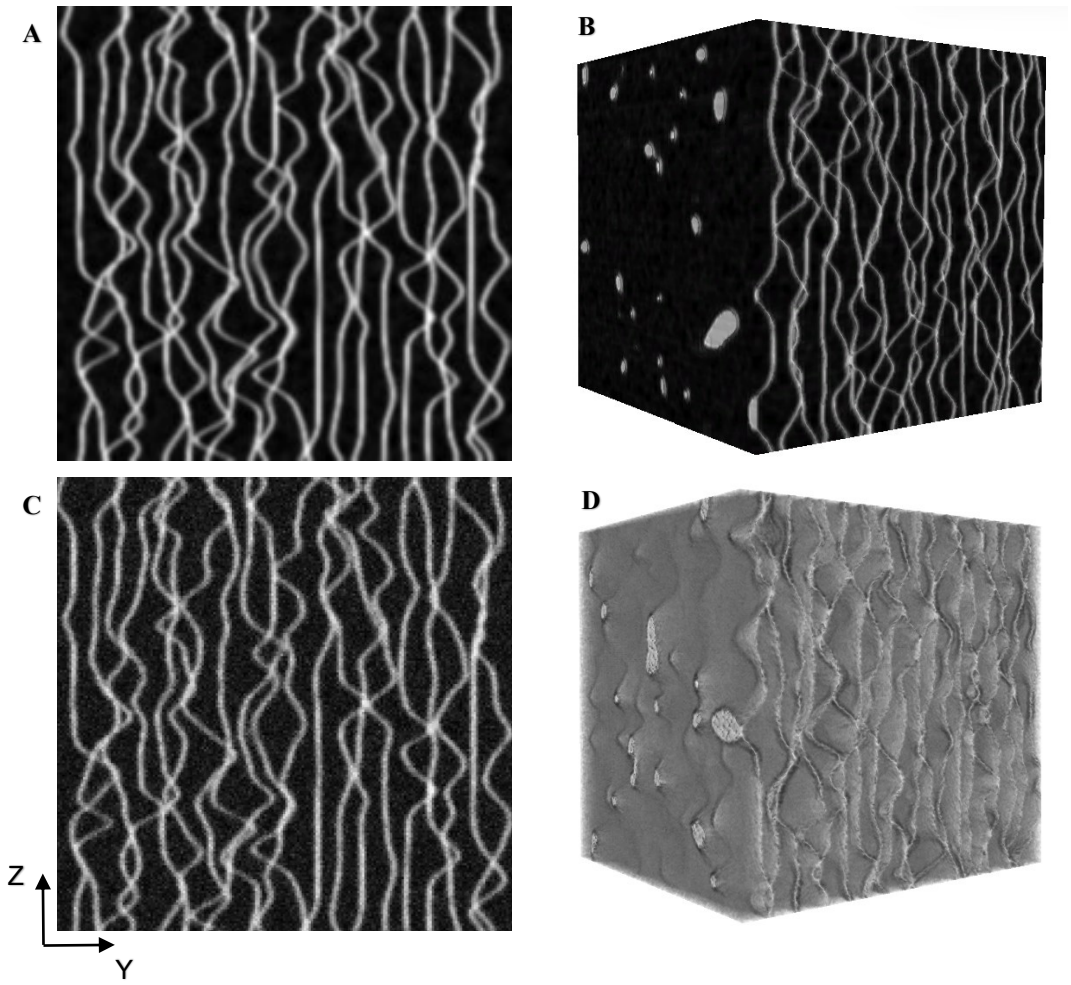

Figure 38: (A) synthetic sheets no-noise configuration, (B) 3D volume no-noise configuration, (C) synthetic sheets noisy configuration, (D) 3D volume noisy configuration.

The addition of the noise allows to have a better refiguration of the reality: in artery tissue scan images the background of the elastin fibres is composed of other biological structures present in the wall so it does not appear as homogenously black. In the synthetic images, on the contrary, this the background between the planes appears more homogenous and blacker. This is observable also in the 3D volume rendering: in the noise-free images the sheets are more divided and distinguishable from each other, where in the noise configuration the background is composed of a random distribution of not black voxel filling the gaps between the planes.

In order to evaluate and compare the two different configurations will be considered the grayscale histogram and signal to noise ratio.

Grayscale histogram and signal to noise ratio

The histogram of an image is an important tool since it can give more information about the distribution of the voxel intensity on the grayscale. Working with aorta images obtained by microCT scan, an ideal histogram of this type of images (Figure 39C) should present two peaks equally distributed on the grayscale. The first peak, more concentrated on black grayvalues, correspond to what is considered the background of the image (collagen fibers, GAGs…); the second peak, more concentrated in the whiter area of the grayscale, corresponds to the structure of interest: the elastin fibre. Not always this ideal result is obtained in the reality and the histogram can present an intermediate area where the two peaks overlap. Looking at the histogram of the generated sheets (Figure 39A,B) is useful to have an indication of how much they can resemble a CT scan of blood vessel wall. The first histogram presents a narrow-based peak in correspondence of black grayvalues associated to the background; the application of the noise makes it wider, but it is still concentrated in the left side of the histogram and its whiter part show a low frequency of voxels. In general, seems that the application of the noise makes more realistic the histogram.

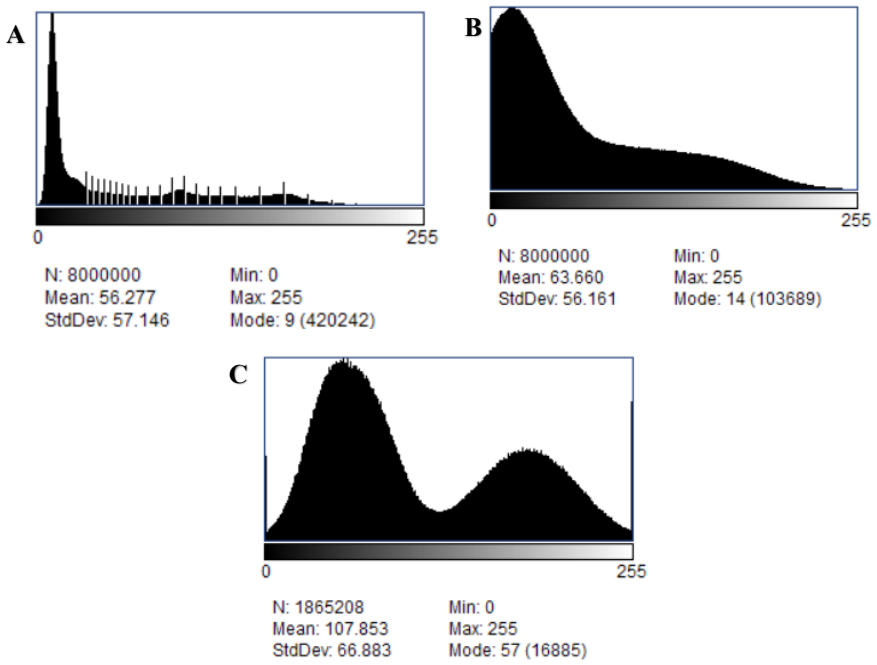

Figure 39: (A) histogram of no-noise configuration, (B) histogram of noisy configuration, (C) typical histogram of aorta; ImageJ software.

Comparing the mean and the SD metrics in situation A and B, the difference is not remarkable, but the mean average is increased, underling a higher frequency of whiter voxels. Since the noise has been added the SD value should have raised, but this is not what is shown comparing the histogram in situation A and B. The ideal situation depicted in picture C is still far and the application of the noise does not allow to reach it. To have a more complete overview, the SNR

values[7] of the original dataset (no-noise configuration) and its noise-added version (noisy configuration) are presented and compared to the SNR of the refence scan of the porcine aorta (Table 8) (see IV.B.2 to recall the reference scan), focusing specifically on the sheets.

Table 8: SNR of porcine aorta and no-noise and noisy configuration of synthetic sheets.

	No noise configuration	Noisy configuration	Porcine aorta
Mean value	162.99	148.95	160.75
SD	20.63	33.164	13.76
SNR	8.87	4.042	11.68

These results are in contrast with the histogram just presented and are more realistic. In fact, comparing no-noise and noisy configuration the SD increases, underlining the noise added, and the SNR decreases underlining the worse quality image. Probably ImageJ, the software used to compute the noise addition, is not able to correctly quantify the SD difference on the whole image between the no-noise and noisy configuration, but focusing specifically on the sheet pattern the difference is more evident. Another hypothesis that is possible to make is that this is not the most suitable procedure to apply the noise, and maybe implementing this option in the Python script during the synthetic sheets' generation would be a better approach.

Local and Global DVC

Despite the not clear quantification of the noise, has been decided to perform anyway the DVC to see if it is able to perform correctly with this kind of datasets.

The local and global approaches have been carried out following the identical passages in both analyses, no-noise and noisy configuration, and the parameters are tuned according to the image's specifics. Specifically, as measure of the length of the microscale has been noted 15 µm, so as subvolume size have been selected 49 µm. Different subvolume size (22,33,39,55,60 µm) has been tempted but not such difference was observed in the DVC quality. At the same time was not possible to find a direct connection between the subvolume size and the statistic of the metric map. The same value used as subvolume size has been used as maximum edge length for the edge collapsing algorithm during the generation of the mesh following used to the global approach.

For the local approach it is important to evaluate the reliability of the DVC checking the statistic

[7] The SNR values presented are calculated as the average of 5 measurement.

of the metric map (Table 9) for the local approach and the residual correlation for the global one.

Table 9: statistic of the metric map and residual correlation (mean average, dimensionless)

	Statistic of metric map	Residual correlation
No noise configuration	0.51	11.8
Noisy configuration	0.44	8.9

These results indicate in both cases a weak correlation between the undeformed and deformed volume, with a slight improvement for the global approach. Looking at the residual image (Figure 40) is possible to individuate the areas in which the correlation is weaker since are highlighted by the presence of the darkest and brightest strings areas. They are in correspondence of the points where the distance between one sheet and its deformed configuration is higher. It is possible that the algorithm is not able to follow the movement of the sheets, in particular where the displacement is more pronounced. Probably performing a lower deformation, the result will increase in quality. Investigating this aspect could lead to a better comprehension on the capability of Avizo software of working with these synthetic sheets.

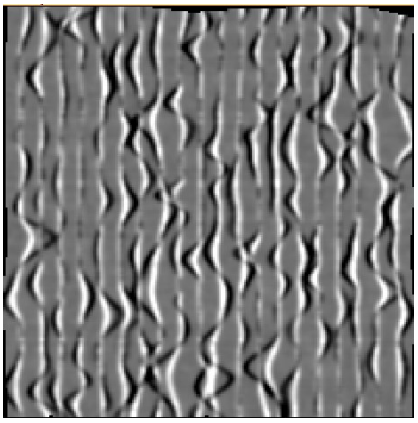

Figure 40: Residual image of noise configuration; low correlation areas are in correspondence of brighter and darker strings.

At the same time, the synthetic sheets are not able to perfectly mimic the behaviour of the elastin fibres. In the residual image, and in the explaining scheme below, is possible to observe that the gaussian curves composing the planes develop within the same two points in both conditions (Figure 41A), relaxed and stressed; whereas in reality elastin fibres in stretched condition show a lower slope spread in a wider segment (Figure 41B). The Python script should be able to better reproduce the peculiarity of the fibres in order to create better images reproducing the unique features of the native tissue.

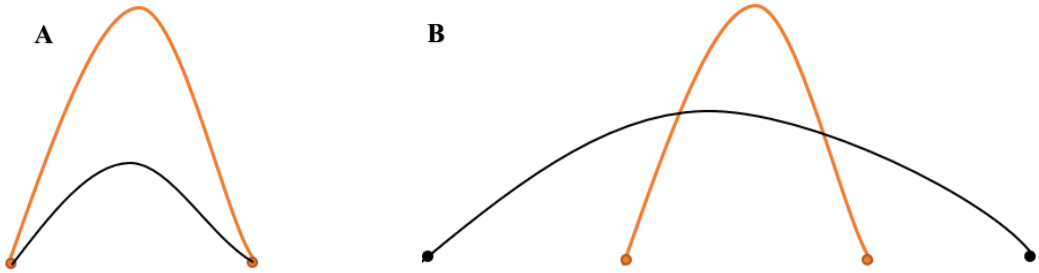

Figure 41: schematic representation of elastin fibres behaviour during deformation in synthetic sheets (A) and in reality (B). In orange the relaxed condition, in black the stretched condition.

Since the weak correlation quality, the outcome of the DVC is not reliable and so the displacement computed in not truthful. In both configurations, no-noise and noisy, the displacement vector field computed is a random pattern of vectors pointing in all direction, so it does not give a realistic depiction of the deformation process. The Uz and Uy ranges computed, where the maximum displacement should be registered, in the noisy configuration does not show outlier values as in the no-noise configuration. Despite so, there is not a method to precisely confirm the ranges computed and, since the poor quality of the DVC is not possible to state if this observation is true or is just the result of a bias given by the impression that the noisy configuration produced better results. To give a better depiction of the analysis, the result are reported in the appendix section C.

From this analysis is difficult to get precise results since the DVC, in both configurations tested, shows inadequate performance. What is possible to evince is that, probably, the deformation applied in these cases is too high and the algorithm is not able to correlate the reference and the deformed volume because there too few features in common between them. Additionally, the quality of the input dataset is not adequate and so, as consequence, nonsense output is computed.

3. Radius parameter

In this paragraph will be evaluate the influence of the radius parameter in the generation of the synthetic sheets. The reference and deformed volumes were generate simulating the same deformation as in the noise section seen before and following have been applied the same type of noise. Has been decided to apply the noise since it gives a better representation of a real artery dataset. The radius parameter has been increased moving from a value of 1 to 3, creating synthetic sheets that appear brighter (Figure 42). Following, to differentiate them, this configuration will be referred as brighter configuration. This test aim to understand if increasing the mean average value of the grayscale of the volume also the performance of the DVC analysis will be better.

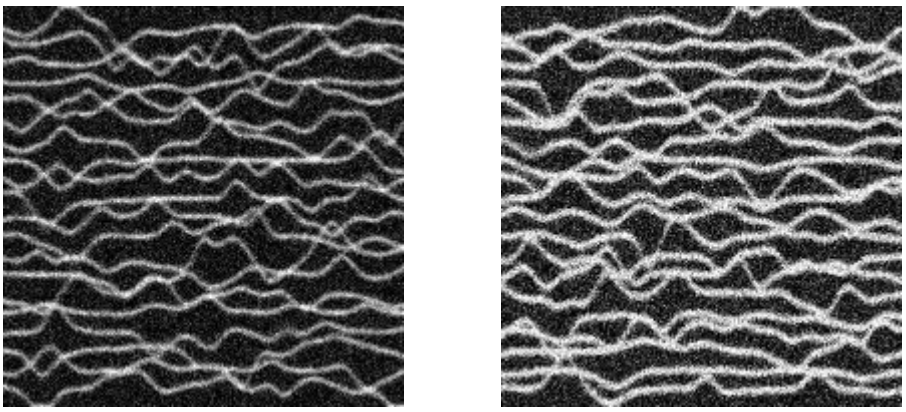

Figure 42: Comparison between synthetic sheets (A) radius 1 and (B) radius 3.

Histogram and SNR

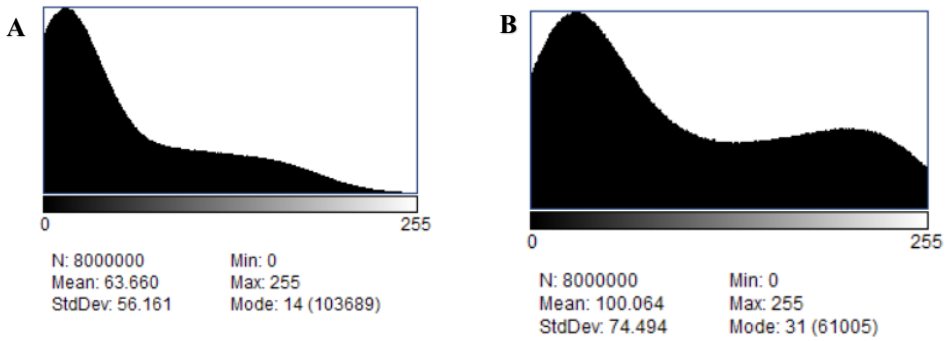

Figure 43: Comparison between histogram of (A) noise configuration and (B) brighter configuration.

Compared to the noise configuration histogram, in the brighter configuration the mean value is increased and the SD too (Figure 43). The incremented radius parameter makes stronger both the signal and the noise component. The peak in the whiter part of the histogram increased in height and the peak in the darker area shift slightly to the right. At the same time in correspondence of the medium part of the histogram the frequency of voxels increases too, making the two picks closer and overlapping. The SNR of the brighter configuration has a value of 8.5. Compared to the others values presented in Table 8, this result shows that the incrementing the radius parameter makes this configuration closer to the situation depicted in the aorta image histogram (Figure 39C).

Local and global DVC and analysis of the displacement

The DVC analysis were performed trying to maintain the same parameters adopted for the noisy configuration. Moving to the DVC quality assessment, the local approach didn't show an improvement compared to the previous analysis presented in Table 9 (metric average value: 0.48); on the other hand the residual value for the global approach was 2.5 showing a significant improvement. The displacement vector field shows the same chaotic pattern of the no-noise configuration (Figure 48A), but the range of the displacement is closer to the one of the noisy configuration reported here for easier comparison.

Table 10: Comparison between displacement range of brighter and noisy configuration

	Displacement [µm]	**Uz [µm]**	**Uy [µm]**
Brighter configuration	0.38 – 3.37	-1.21 – 2.31	-2.10 – 3.21
Noisy configuration	0.41 – 3.97	-0.97 – 2.97	-3.35 – 3.68

Even though this result seems to confirm the values computed in the noisy configuration, the poor correlation quality makes the outcome not reliable. As in the previous configurations, from the displacement vector field is not possible to have a clear overview of the deformation that the volume undergoes to, since it is chaotic, and the DVC shows a low quality. Hence the result above reported are not surely truthful but want to give to the reader a complete overview.
From this analysis is not possible to claim whether increasing the radius parameter brings an improvement to the DVC performance but can show the effect on the dataset.

4. Scaling in Z direction

Since the poor correlation obtained between two synthetic datasets, is useful to see if the DVC is able to perform better on the synthetic sheets but changing approach. In this paragraph will be applied an elongation in Z direction on the synthetic sheets volume enriched with the noise. A volume of 497.5x497.5x497.5 µm with a voxel size of 2.5 µm, has been used and applied a scaling factor of 1.03. Multiplying it by the size of the volume and then subtract the initial length is possible to calculate the predicted displacement in Z direction: 14.925 µm.

The local system of the synthetic volume is in correspondence of the global system, therefore a translation of the volume in Z direction during the scaling is not observed as it is in the case of the porcine specimen seen in the previous section (V.A.2). The same protocol as for the porcine specimen was applied but manual realignment was not necessary. Consequently, the DVC was performed: the local approach produced a metric average value of 0.98 and for the global approach the residual value was of 0.0001. These results testify a good correlation between the reference volume and the deformed one.

The displacement vector field (Figure 44A) shows a consistent result: the group of vectors is pointing homogenously in positive Z direction, according to the deformation imposed. Some outliers are present, for example the green vector in correspondence of the origin of reference system, showing an unpredicted displacement. These values are considered as error, probably caused by area where the correlation is weaker.

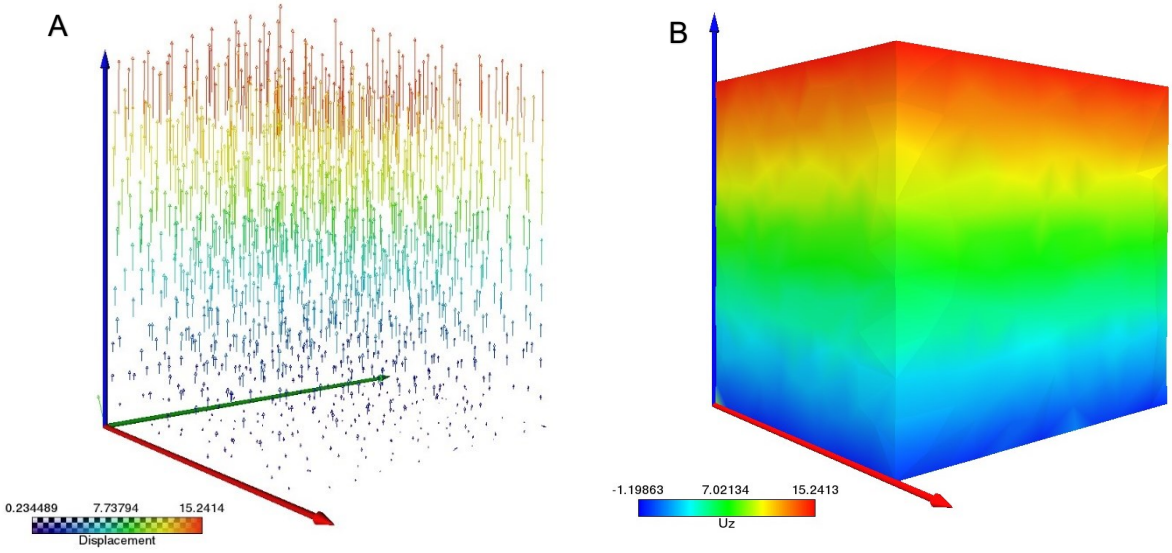

Figure 44: (A) Displacement vector field and (B) Uz computed after scaling the synthetic sheets [µm].

Looking at Uz (Figure 44B), the displacement map shows a gradient deformation and the predicted displacement is within the range produced by the computation. Despite so, it is possible to see at the base of the volume some negative values, testifying a displacement in the

opposite direction. This unpredicted result is probably due to uncertainties of the DVC. In order to validate this hypothesis should be performed a priori DVC uncertainty measurement.

Comparing these results to the same analysis performed on the porcine dataset the outcome are comparable: in both cases the convergence has been reached, the deformation is gradient and the computed displacement is aligned to the predicted one. Since the synthetic sheets volume and the VOI used in porcine aorta analysis does not have the same dimension, is not possible to make a quantitative comparison. The same analysis should be repeated but comparing two volumes of the same size.

From this test is possible to state that this approach works correctly with this type of dataset, and its able to correlate the deformed volume with the reference one. On the contrary, as shown before, working with two different datasets generated by the Python script does not produce the same good result. This, probably, has to refer to the Python code that is not able to generate two different configurations of the same volume with enough similarities to allow them to be correctly correlate.

Given the good results obtained by this approach, it should be more investigated. A priori analysis of the DVC uncertainties measurement should be performed and it would be interesting to apply the same procedure on different synthetic sheets configuration, for example changing some parameters such as the radius or the number of sheets.

5. Conclusion

In this section has been disclosed the work performed with the synthetic sheets generated by a specific Python script. The aim was to work with a controlled dataset in order to perform different virtual deformation tuning different parameters to validate this approach as possible tool able to mimic the real deformation that elastin fibres experience in blood vessel wall. Particularly important is the post-processing analyses. Central role is played by the DVC analysis, as tool to compute the displacement and quantify the deformation applied on the sheets. Has been tempted the comprehension of the factors that the most influence the outcome of the analysis and how to better set them.

The python code allows to control the amplitude and the radius parameter of the Gaussian distribution composing the synthetic sheets, moreover the dimension of the volume and the packing of the sheets within. Using an additional software was possible to add Gaussian distributed noise to the volumes generated. In this works the mesh type and the subvolume size used for the displacement computation, the radius factor and the noise were the main parameters focused on.

The creation of the mesh was the first aspect investigated. A first attempt was done isolating the synthetic sheets from the background in order to create a mesh shaped on the pattern of the Gaussian distributions. Afterwards, the idea at the base of this method was considered incorrect because the computed displacement takes into account only the contribution of the synthetic sheets. Compared to the native tissue this fact is not correct since the other components of the artery wall contribute to the mechanical behaviour of vessel. In addition to that, the poor results in term of displacement computation and correlation quality and the difficulties faced in order to create a mesh that could balance computational time and precision led to the use of another approach.
A cubic-shaped mesh, build on the surface of the entire volume containing the sheets was considered a better approach, since in this way also the background was included in the displacement computation. Finally, the manually generated mesh has been selected to be used in the further analysis, even if the volumes used have a regular shaped and the cubic mesh automatic generated is suitable.

The analysis of the histogram was a useful tool to compare the grayscale of the synthetic sheets with the specimen aorta, in order to understand which parameter was better to set to make them more similar. The addition of the Gaussian distributed noise and the increment of the radius parameter were observed. Unfortunately, from these analyses was not possible to obtain reliable information since the DVC was not able to correctly correlate the deformed and the reference volume. The displacement vector field and the strain map does not give a clear overview of the deformation of the volume. Hence was not possible to state whether the noise and the radius parameter impact on the DVC performance. The weak correlation could be due to the intensity of deformation applied, so more investigation tempting smaller intensity should be pursued.
On the other hand, applying the scaling factor on the volume has demonstrate to be a successful approach, which should be investigate more since, at the moment, it represents a valid tool.

To sum up from the work presented here is possible to say that the DVC is able to perform on this type of dataset, but still the results that are computed are not able to quantify in a reliable way the displacement of the sheets. It is possible to evince that the Python script is a powerful tool, since allows to recreate different configuration, but it has to be improved. First of all, should be implemented the possibility of adding the noise to the volume, without having to resort to another software, and tune its intensity. Secondly, as schematically explained in Figure 41, the resulting volume should better reproduce the behaviour of the sheets during the elongation to better reproduce the features of the real elastin sheets. Another features that could

be interest to examine is the possibility to control the thickness of the sheets, to be able to compare if different diameters influence the displacement. In order to validate the displacement computed by the algorithm, a priori is important to know the displacement impose. Only changing the amplitude parameter is not possible to get this information and the method used in this work, where the displacement was measured compared the same slice of the two configurations of the volume, is not really a reliable approach.

In my opinion, above all the aspects discussed, the setting of the parameters for the DVC should be more deepen, since was not possible to deeply understand how the different setting influence the analysis. Particular attention has to be given to the subvolume size running the local approach, in fact despite the different attempt performed, was not possible to see fundamental differences. As already underline, it is the fundamental parameter to balance precision of the DVC and the sensibility to noise, but still in this work has not been explained how it is possible to define the most suitable value. At the same time also the mesh generation should be more analyzed because, as the subvolume size, is the key parameter for the correct functioning of the global approach.
A useful tool is the Measurement uncertainty DVC tool because running the module with two different synthetic sheets configuration, for example one showing noise and the second one noise-free, can simulate two different scan acquisition and, using the data in output, allow to see how the uncertainties changes in function of the mesh cell size or the subvolume.

Others are the aspects than can be investigated to see how they impact the success of the analysis, such as the dimension of the volume and the number of planes. A previous attempt, for example, has been made using a volume of 200 μm in the cases discussed above, but with 40 planes, twice the number used in this work. The registration step failed in fact the reference volume and the deformed showed a motion of the body and resulted not aligned at the end of the process. This maybe because the planes were too close one to the other and the algorithm was not able to correlate the two dispositions. It would be interesting to investigate whether the density of the sheets is related to the success or the failure of the registration process.
Also, larger edge size of the volume should be investigated, similar for example to the dimension of the specimen scanned. In this work in fact has been used for all the analysis the same length but, to have a more realistic representation and be able to compare the result of the virtual deformation on the synthetic sheets with the one produced by the virtual deformation on the porcine specimen, bigger volume should be employed.

VI. Conclusion

The cardiovascular system and the pathologies that could damage it are nowadays a central topic in modern research and the knowledge about it are still in development. A particular attention is raised around the blood vessels and the investigation of its microstructure and biomechanical behaviour. One on the main goal in this research field is delineate the relationship between the blood vessel morphological features and the damaging effect of cardiovascular pathologies. The technological progress led to the development of many imaging investigation tool; above all 4DmicroCT and 4D-CECT could represent ad adequate tool to carry out this mission because they allow to conjugate to the mechanical tests the simultaneous image acquisition of the sample enriched with contrast agent and, coupling with DVC technique, compute the deformation field. Thus, the application of this technique on soft tissue is still a challenge given the low absorbance property and in literature this topic is not widely covered. A major difficult is also represented by the necessity of find a balance between image resolution, time of exposure and preservation of the tissue integrity.

The principal objective of this master thesis was to get a better knowledge of this field, focusing principally on the post processing analysis and the DVC technique and trying to understand how is possible to improve this tool for the artery microstructure investigation. Many are the factor that can impact on the DVC performance and affecting the correlation between the reference and the deformed volume: image quality, subvolume size, type of mesh.

The attention was focused on two type of datasets, synthetic sheets virtually generated and porcine aorta specimen acquisition. In the case of the synthetic sheets, working on a controlled dataset gives the chance to tune different parameters and see how these influence the outcome of the DVC. In the end the first approach tempted did not give satisfactory results, on the other hands the second one gave the possibility to successfully apply the DVC on this type of dataset. Despite so, this master thesis project represents a starting point for the investigation of these procedure that need to be deepen more. Many are the aspect that should be studied, for example: the size of the volume, the number of sheets and the intensity of the deformation imposed. This because are all factors that can influence the correlation process.

Is remarked also the importance of the selection of an adequate subvolume size for the local approach and mesh size for the global approach. A priori analysis of the DVC uncertainty is important to find an acceptable balance between precision of the computation and cell size.

From the work performed on the synthetic sheet was also possible to individuate some weaknesses and strengths of the Python script. Some features should be added such as the

possibility of adding the noise or precisely determine the deformation that the user want to impose in order to be able to quantify it and validate the result computed by the DVC. Additionally, the code should reproduce better the deformation process of the fibres.

The scanning process allow to better understand the impact of the scanning parameter on the resulting images and the application of the signal to noise ratio remarked its utility in qualitatively describe the image quality. Was possible to perform a realistic DVC uncertainty analysis which again helped to find the most suitable subvolume size. The DVC analysis performed after the scaling in Z direction computes coherent result, in accordance with the predicted displacement. Despite so, performing the deformation on the entire specimen and the following DVC on two VOI extracted in different position the results computed gave contrasting information, thought this type of procedure has to deepen more in order to understand better hot to perform it. This step, in my opinion, is relevant since this type of deformation reproduce better what happened during real experimentation in which the specimen is deformed and then consequently the DVC is performed on a specific VOI. As future developments of this work should de perform a more precise investigation of the subvolume size, in particular to find a possible link with the correlation process.

To conclude, 4D-CECT represents an important imaging tool and has the potential to become the *gold standard* in the microstructure analysis of soft tissue. Structural characterization is essential to fully understand the functioning of healthy and pathological tissues, as well as the impact of possible treatments. Many are the difficulties that still must be overcome given by the particular morphology of the soft tissue and in particular of the blood vessel. Despite so, it is important to pursue the research in this field to reach the final goal: correlate the changes in microstructure and mechanical behaviour of the blood vessels to the damaging effects of the pathologies.

Bibliography

[1] A. Mathur, V. Mohan, D. Ameta, B. Gaurav, and P. Haranahalli, “Aortic aneurysm,” *J Transl Int Med*, vol. 4, no. 1, pp. 35–41, Apr. 2016, doi: 10.1515/jtim-2016-0008.

[2] S. J. Ng *et al.*, “Atherosclerosis Imaging,” *PET Clin*, vol. 18, no. 1, pp. 71–80, Jan. 2023, doi: 10.1016/j.cpet.2022.09.004.

[3] K. Keklikoglou *et al.*, “Micro-ct for biological and biomedical studies: A comparison of imaging techniques,” *Journal of Imaging*, vol. 7, no. 9. MDPI, Sep. 01, 2021. doi: 10.3390/jimaging7090172.

[4] J. C. Kohn, M. C. Lampi, and C. A. Reinhart-King, “Age-related vascular stiffening: Causes and consequences,” *Frontiers in Genetics*, vol. 6, no. MAR. Frontiers Media S.A., 2015. doi: 10.3389/fgene.2015.00112.

[5] Z. Chang *et al.*, “Nanomechanics and ultrastructure of the internal mammary artery adventitia in patients with low and high pulse wave velocity,” *Acta Biomater*, vol. 73, pp. 437–448, Jun. 2018, doi: 10.1016/j.actbio.2018.04.036.

[6] R. E. Shadwick, “Mechanical design in arteries,” 1999.

[7] M. Jadidi, S. Ahmadreza Razian, M. Habibnezhad, E. Anttila, and A. Kamenskiy, “Mechanical, structural, and physiologic differences in human elastic and muscular arteries of different ages: comparison of the descending thoracic aorta to the superficial femoral artery,” 2020. [Online]. Available: https://www.elsevier.com/open-access/userlicense/1.0/

[8] S. A. Kim *et al.*, “The relationship between mechanical properties of carotid artery and coronary artery disease,” *Eur Heart J Cardiovasc Imaging*, vol. 13, no. 7, pp. 568–573, Jul. 2012, doi: 10.1093/ejechocard/jer259.

[9] A. Karimi, M. Navidbakhsh, A. Shojaei, and S. Faghihi, “Measurement of the uniaxial mechanical properties of healthy and atherosclerotic human coronary arteries,” *Materials Science and Engineering C*, vol. 33, no. 5, pp. 2550–2554, Jul. 2013, doi: 10.1016/j.msec.2013.02.016.

[10] C. Helfenstein-Didier, D. Taïnoff, J. Viville, J. Adrien, É. Maire, and P. Badel, “Tensile rupture of medial arterial tissue studied by X-ray micro-tomography on stained samples,” *J Mech Behav Biomed Mater*, vol. 78, pp. 362–368, Feb. 2018, doi: 10.1016/j.jmbbm.2017.11.032.

[11] C. M. Disney, P. D. Lee, J. A. Hoyland, M. J. Sherratt, and B. K. Bay, “A review of techniques for visualising soft tissue microstructure deformation and quantifying strain Ex Vivo,” *Journal of Microscopy*, vol. 272, no. 3. Blackwell Publishing Ltd, pp. 165–179, Dec. 01, 2018. doi: 10.1111/jmi.12701.

[12] K. Keklikoglou *et al.*, “Micro-ct for biological and biomedical studies: A comparison of imaging techniques,” *Journal of Imaging*, vol. 7, no. 9. MDPI, Sep. 01, 2021. doi: 10.3390/jimaging7090172.

[13] S. De Bournonville, S. Vangrunderbeeck, and G. Kerckhofs, “Contrast-enhanced microCT for virtual 3D anatomical pathology of biological tissues: A literature review,” *Contrast Media and Molecular Imaging*, vol. 2019. Hindawi Limited, 2019. doi: 10.1155/2019/8617406.

[14] M. Elfarnawany, S. R. Alam, S. A. Rohani, N. Zhu, S. K. Agrawal, and H. M. Ladak, “Micro-CT versus synchrotron radiation phase contrast imaging of human cochlea,” *J Microsc*, vol. 265, no. 3, pp. 349–357, Mar. 2017, doi: 10.1111/jmi.12507.

[15] L. A. Walton *et al.*, “Morphological characterisation of unstained and intact tissue micro-architecture by X-ray computed micro- and nano-tomography,” *Sci Rep*, vol. 5, May 2015, doi: 10.1038/srep10074.

[16] L. Leyssens, C. Pestiaux, and G. Kerckhofs, “A review of ex vivo x-ray microfocus computed tomography-based characterization of the cardiovascular system,” *International Journal of Molecular Sciences*, vol. 22, no. 6. MDPI AG, Mar. 02, 2021. doi: 10.3390/ijms22063263.

[17] S. De Bournonville, S. Vangrunderbeeck, and G. Kerckhofs, “Contrast-enhanced microCT for virtual 3D anatomical pathology of biological tissues: A literature review,” *Contrast Media and Molecular Imaging*, vol. 2019. Hindawi Limited, 2019. doi: 10.1155/2019/8617406.

[18] J. Buytaert, J. Goyens, D. De Greef, P. Aerts, and J. Dirckx, “Volume shrinkage of bone, brain and muscle tissue in sample preparation for micro-CT and light sheet fluorescence microscopy (LSFM),” *Microscopy and Microanalysis*, vol. 20, no. 4, pp. 1208–1217, 2014, doi: 10.1017/S1431927614001329.

[19] C. Helfenstein-Didier, D. Taïnoff, J. Viville, J. Adrien, É. Maire, and P. Badel, “Tensile rupture of medial arterial tissue studied by X-ray micro-tomography on stained samples,” *J Mech Behav Biomed Mater*, vol. 78, pp. 362–368, Feb. 2018, doi: 10.1016/j.jmbbm.2017.11.032.

[20] M. Nierenberger, Y. Rémond, S. Ahzi, and P. Choquet, “Assessing the three-dimensional collagen network in soft tissues using contrast agents and high resolution micro-CT: Application to porcine iliac veins,” *C R Biol*, vol. 338, no. 7, pp. 425–433, Jul. 2015, doi: 10.1016/j.crvi.2015.04.009.

[21] C. T. Badea, S. M. Johnston, Y. Qi, and G. A. Johnson, “4D micro-CT for cardiac and perfusion applications with view under sampling,” *Phys Med Biol*, vol. 56, no. 11, pp. 3351–3369, Jun. 2011, doi: 10.1088/0031-9155/56/11/011.

[22] M. Peña Fernández *et al.*, “Time-resolved in situ synchrotron-microCT: 4D deformation of bone and bone analogues using digital volume correlation,” *Acta Biomater*, vol. 131, pp. 424–439, Sep. 2021, doi: 10.1016/j.actbio.2021.06.014.

[23] N. Dahdah *et al.*, “Damage Investigation in A319 Aluminium Alloy by X-ray Tomography and Digital Volume Correlation during In Situ High-Temperature Fatigue Tests,” in *Strain*, Blackwell Publishing Ltd, Aug. 2016, pp. 324–335. doi: 10.1111/str.12193.

[24] S. C. Garcea, I. Sinclair, and S. M. Spearing, “Fibre failure assessment in carbon fibre reinforced polymers under fatigue loading by synchrotron X-ray computed tomography,” *Compos Sci Technol*, vol. 133, pp. 157–164, Sep. 2016, doi: 10.1016/j.compscitech.2016.07.030.

[25] J. Villanova *et al.*, “Fast in situ 3D nanoimaging: a new tool for dynamic characterization in materials science,” *Materials Today*, vol. 20, no. 7, pp. 354–359, Sep. 2017, doi: 10.1016/j.mattod.2017.06.001.

[26] P. Chowdhury, H. Sehitoglu, and R. Rateick, “Damage tolerance of carbon-carbon composites in aerospace application,” *Carbon N Y*, vol. 126, pp. 382–393, Jan. 2018, doi: 10.1016/j.carbon.2017.10.019.

[27] A. Buljac *et al.*, “Digital Volume Correlation: Review of Progress and Challenges,” *Exp Mech*, vol. 58, no. 5, pp. 661–708, 2018, doi: 10.1007/s11340-018-0390-7ï.

[28] M. Palanca, G. Tozzi, and L. Cristofolini, “The use of digital image correlation in the biomechanical area: A review,” *International Biomechanics*, vol. 3, no. 1. Taylor and Francis Ltd., pp. 1–21, 2016. doi: 10.1080/23335432.2015.1117395.

[29] F. Gillard *et al.*, “The application of digital volume correlation (DVC) to study the microstructural behaviour of trabecular bone during compression,” *J Mech Behav Biomed Mater*, vol. 29, pp. 480–499, Jan. 2014, doi: 10.1016/j.jmbbm.2013.09.014.

[30] E. Dall’Ara and G. Tozzi, “Digital volume correlation for the characterization of musculoskeletal tissues: Current challenges and future developments,” *Frontiers in*

Bioengineering and Biotechnology, vol. 10. Frontiers Media S.A., Oct. 04, 2022. doi: 10.3389/fbioe.2022.1010056.

[31] M. Peña Fernández *et al.*, “Effect of SR-microCT radiation on the mechanical integrity of trabecular bone using in situ mechanical testing and digital volume correlation,” *J Mech Behav Biomed Mater*, vol. 88, pp. 109–119, Dec. 2018, doi: 10.1016/j.jmbbm.2018.08.012.

[32] M. Peña Fernández, A. H. Barber, G. W. Blunn, and G. Tozzi, “Optimization of digital volume correlation computation in SR-microCT images of trabecular bone and bone-biomaterial systems,” *J Microsc*, vol. 272, no. 3, pp. 213–228, Dec. 2018, doi: 10.1111/jmi.12745.

[33] F. Gillard *et al.*, “The application of digital volume correlation (DVC) to study the microstructural behaviour of trabecular bone during compression,” *J Mech Behav Biomed Mater*, vol. 29, pp. 480–499, Jan. 2014, doi: 10.1016/j.jmbbm.2013.09.014.

[34] B. Trachet *et al.*, “Synchrotron-based visualization and segmentation of elastic lamellae in the mouse carotid artery during quasi-static pressure inflation,” *J R Soc Interface*, vol. 16, no. 155, Jun. 2019, doi: 10.1098/rsif.2019.0179.

[35] E. Dall’Ara, M. Peña-Fernández, M. Palanca, M. Giorgi, L. Cristofolini, and G. Tozzi, “Precision of digital volume correlation approaches for strain analysis in bone imaged with micro-computed tomography at different dimensional levels,” *Front Mater*, vol. 4, Nov. 2017, doi: 10.3389/fmats.2017.00031.

[36] J. Brunet, B. Pierrat, J. Adrien, E. Maire, N. Curt, and P. Badel, “A Novel Method for In Vitro 3D Imaging of Dissecting Pressurized Arterial Segments Using X-Ray Microtomography,” *Exp Mech*, vol. 61, no. 1, pp. 147–157, Jan. 2021, doi: 10.1007/s11340-020-00645-x.

[37] James R. Janesick., “Photon transfer : DN --> [lambda],” 2007.

[38] J. D. Boerckel, D. E. Mason, A. M. Mcdermott, and E. Alsberg, “Microcomputed tomography: approaches and applications in bioengineering.” [Online]. Available: http://stemcellres.com/content/5/6/144

[39] R. Schulze *et al.*, “Artefacts in CBCT: A review,” *Dentomaxillofacial Radiology*, vol. 40, no. 5. pp. 265–273, Jul. 2011. doi: 10.1259/dmfr/30642039.

[40] F. E. Boas and D. Fleischmann, “CT artifacts: Causes and reduction techniques,” 2012. [Online]. Available: http://www.edboas.com/science/CT/0012.pdf

Web references

[A] https://www.who.int/news-room/fact-sheets/detail/cardiovascular-diseases-(cvds)

[B] https://www.britannica.com/science/cardiovascular-disease/Diseases-of-the-arteries

[C] Bailey, Regina. "Artery Structure, Function, and Disease." ThoughtCo, Apr. 5, 2023, thoughtco.com/artery-anatomy-373235

[D] “Arteries”, The Histology Guide, Faculty of Biological Sciences, University of Leeds. https://www.histology.leeds.ac.uk/circulatory/arteries.php

[E] William D. Tucker; Yingyot Arora; Kunal Mahajan, “Anatomy, Blood Vessel”, National Library of Medicine, 8 August 2022 https://www.ncbi.nlm.nih.gov/books/NBK470401/

[F] https://www.ctlab.geo.utexas.edu/about-ct/artifacts-and-partial-volume-effects/

Appendix

A. Introduction to micro focus X-rays computed tomography

Cardiovascular diseases have a huge impact on worldwide population health and nowadays is a still ongoing challenge for the medicine finding effective therapies accessible to the majority. Another crucial point is the prevention and the early diagnosis of these pathologies in order to make more incisive the therapies and avoid more serious compliance. Many are the imaging technique developed able to detect CVD, for example, positron emission tomography (PET) imaging is able to detect atherosclerosis at the early stages thanks to the identification of

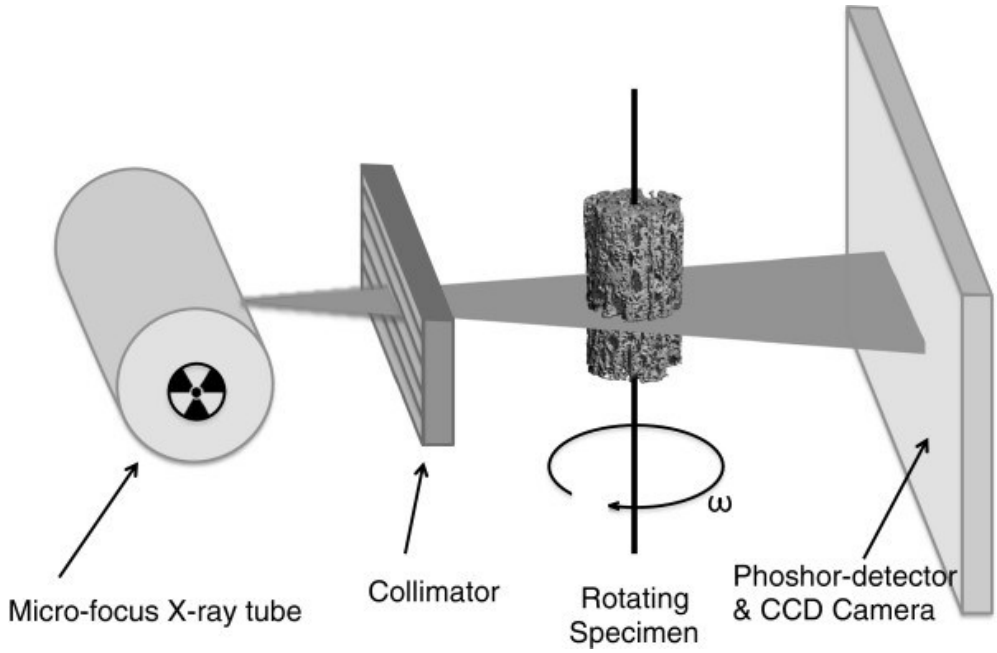

Figure 45: Schematic set up for MicroCT scan.

particular process related to the pathology such ad microcalcification marked by the F-sodium fluoride (NaF) [2]. Above all, here will focus on Micro focus X-rays computed tomography (microCT).

MicroCT is an X-rays based imaging techniques that can return a 3D structural analysis of biological structures, visualising both the interior and exterior characteristics of the sample. The three-dimensional final images are the result of the composition of two-dimensional trans-axial projection images of the sample, combined together using a reconstruction algorithm. The devices (Figure 45) developed to run a microCT analysis are composed of a micro-focus X-ray tube, a rotating stand or platform for the specimen, phosphor-detector or a charge-coupled device (CCD) camera and usually a collimator [38].

The radiation is generated by the micro-focus X-ray tube and then collimated and directed to the object that is kept rotating in order to capture several 2D radiographs from different angles.

X-rays are partially absorbed or deflected (i.e., attenuation) by the object positioned between the collimator and the detector, based on its density, its atomic number and the source energy. The attenuation of the radiation follows the equation $I_x=I_0e^{-\mu x}$ (the intensity of the radiation at a distance x from the source is the product between the intensity of the emitted beam and e to the power of the linear attenuation coefficient times the distance from the source considered the thickness of the sample [38]. Finally, the attenuation is measured by the CCD camera. Once the images acquisition is completed, specific algorithms will reconstruct horizontal slices according.

During the reconstruction of the volumes starting from the projection acquired, some factors can lead to errors in this process. Artefacts are caused by discrepancies between the physical conditions of scanning and the mathematical assumption used for 3D reconstructions and are appreciable as visual structure in the reconstructed data that are not real in object analysed [39]. Many are the artifacts that is possible to face during CT scanning, here briefly will be presented some of these.

Beam hardening artefact

The name of this artifacts is related to the fact that a polychromatic beam, when pass through an object, register an incrementation of its average energy: as the photon energy increase the linear attenuation coefficient decreases, consequently high energy photon cross the matter easier compared to low energy photons since the interaction with the matter is negligible; in other words the lower energy X-rays are more attenuated by the object scanned. This phenomenon, on the reconstructed volume, is marked by a darker area at the centre of the images and a brighter one in correspondence of the edges, even though the object is composed of the same matter [F]. It also causes the presence of dark streaks in correspondence of two high attenuation materials.

Ring artefact

This artefact is caused by the misalignment of the detector or if it is out of place, consequently while rotating around the object it will create an incorrect projection of the object. This artefact can be recognized by the presence of a cercles cantered in the rotational axe [39].

Aliasing artefact

To obtain a complete reconstruction it is needed that the sampling frequency is at least twice the frequency contained in the signal; if this condition is not respect it leads to the aliasing artefact. The sampling frequency is represented by the number of pixels per area, in this case of the detector, and so the under-sampling of its elements causes the aliasing artefact. It is appreciable as divergent lines from the center to the periphery of the reconstructed volume [39].

Cone beam artefact

It is found when multi x-rays detector are implemented. So that, the reconstruction alternately take measurement from a single detector row or interpolating data coming from two detectors rows and its result may be not accurate if there is high contrast edge between two rows. This creates smooth periodic dark and light streaks originating from high contrast edges, which are called windmill artifacts [40]

MicroCT allows to obtain high resolution scans (1µm voxel size [13]) and high field of view to voxel size ratio, not to mention that gives the chance to investigate the density, the porosity and the structure of the material [12]. Unlike other methodology used for the visual analysis and characterisation of biological structure, for example the histological slicing, microCT is a non-destructive approach: the specimen doesn't have to be treat (decalcification, slicing…) before the investigation. Hence, is possible to study it in its entirety without disrupting its structure since slicing has as possible consequences distortions and glitches. Additionally, microCT is cost saving and faster technology since these pre-process steps are skipped and a single scanning requires from minutes to hours depending on the parameters, compared to more traditional approach that could last days or weeks. MicroCT also has limitations. In order to obtain a greater magnification and resolution is necessary to increase the time of imaging and the intensity of the X-rays beam, leading to a greater exposure of the sample to the radiation. Planning a microCT studies is important to find a balance between desired image quality and radiation exposure. Another limitation is the size of the specimen that can undergo this procedure: under a certain size other imaging techniques are more indicated, for example the scanning electron microscopy (SEM) that is able to reach greater resolution.

B. Bidirectional scaling on porcine aorta VOI

Extracted a subvolume from the original porcine aorta volume, has been applied a scaling in longitudinal direction applying a factor of 1.03 to deform it symmetrically respect the centre of the VOI. From this deformation is expected to obtain a displacement vector field composed of group of arrows parallels to the Z axis both in positive and negative direction; on the contrary in the resulting displacement vector field (Figure 46) is possible to see a deformation in Y direction (green axis) and in the lower part of the volume in negative Z direction too (blue axis). This could be owed to the registration step; in fact, to be able to symmetrically deform the volume, it is necessary to previously translate it to the origin of the global system. This required a rigid translation of the VOI from its original position (at a certain height and positive Y coordinate from the origin) explaining the shift in Y and Z directions. Despite the manual registration before the resampling, the registration module takes into account the previous movement, producing a wrong representation of the displacement. Despite the good correlation between the deformed volume and the reference one, from this analysis is not possible to get information about the real deformation that the sample underwent. The reason why this type of deformation produced inconclusive results and on the contrary the monodirectional deformation produced robust results hasn't been investigate, but it could be a possible future development.

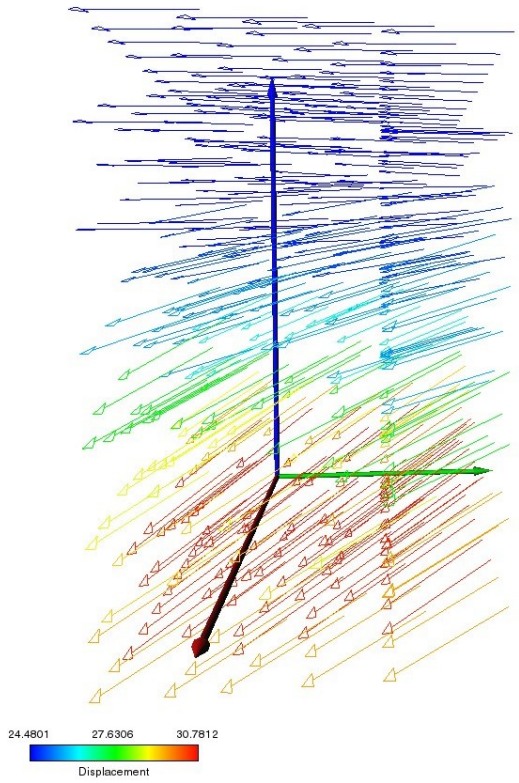

Figure 46: Displacement vector field of VOI bidirectional scaling.

C. Result of DVC analysis on synthetic sheets

In this section are reported the results of the DVC analysis performed on reference and deformed volumes generated by the Python script in no-noise and noisy configuration. Again, is underlined that the quality of the DVC is not adequate and the results cannot be totally trusted. In the following page is possible to see a comparison (Figure 48) between the displacement vector field, the relative scalar component in Y (Uy) and Z (Uz) direction where the higher deformation should be registered, of no-noise and noisy configurations. In the picture the data in the legends are normalized in order to help the reader to have a clear visualization of the deformation; in the table below (Table 11) are presented the displacement range values produced by the global DVC analysis.

Table 11: Displacement ranges for no-noise and noisy configuration of the synthetic sheets

	No-noise configuration	**Noisy configuration**
Displacement [µm]	0.16 – 19.54	0.41 – 3.97
Uz [µm]	-12.70 – 14.00	-0.97 – 2.97
Uy [µm]	-2.77 – 2.93	-3.35 – 3.68

In both cases the displacement field is a chaotic pattern of arrows pointing in all the direction, even though in the noise added case is slightly possible to observe a preferential orientation in Z and Y positive direction and so reflecting what is expected to happen. Some vectors with highest magnitude are present, corresponding at points in the volume where the displacement is the highest, however these are outlier values far from more realistic data and is where, probably, the correlation is weakest. Looking at the noisy configuration metrics, the displacement ranges appear better since they don't show outliers values. It is important to underline that from these images (Figure 48) is not possible to get clear results and have an idea of the deformation of the volumes.

It is possible to compare the Uy and Uz ranges computed to the average displacement of some points measured using the Measure tool on the slices of the synthetic sheets volume to see if they are similar. In the picture below (Figure 47) is possible to see the reference volume slice, more in blue colour, overlap to the deformed volume slice, more in red-green colour. In 5 different point both where the deformation was more evident and were less accentuate, the measurements have been done and then calculated the mean value and the SD. In the picture is reported the view (YZ plane) used for the calculation of Uy; for the Uz is possible applied the same procedure but applied on the plane XZ.

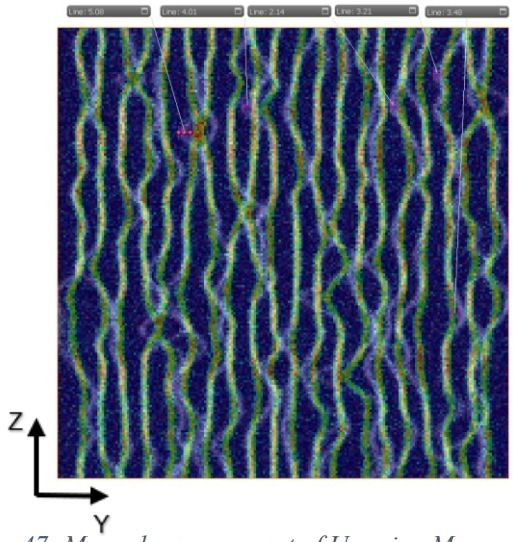

Figure 47: Manual measurement of Uy using Measurement tool

Despite so, these measurements cannot be considered totally truthfully since is necessary to contemplate possible error in the measurement given by the user operation and by the fact that using the ruler tool is difficult to determine with precision the movement of the points selected.

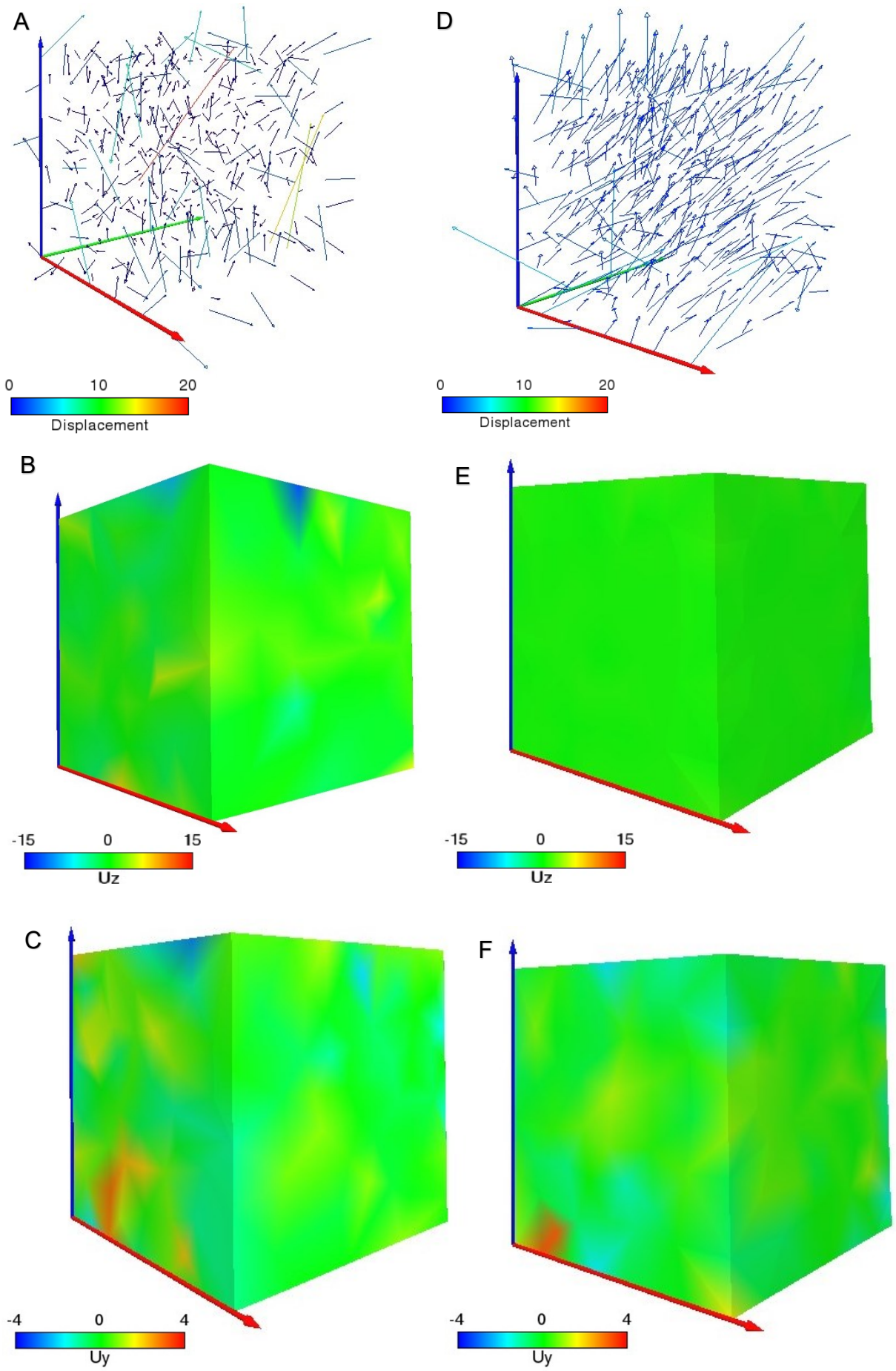

Figure 48: (A,B,C) Vector field, Uz, Uy no-noise configuration and (D,E,F) noise configuration [µm]

D. Analysis of the lower VOI after porcine aorta volume deformation

Differently from the analysis effectuated on the upper VOI, in this case the local approach shows a better correlation level (metric average value: 0,66) but for the global approach the situation doesn't change (residual output in the order of 10^38) and so the convergence wasn't reached. Following (Figure 49) is presented a comparison between the displacement vector field and the displacement in Z direction of the upper VOI and the lower VOI, normalizing the ranges.

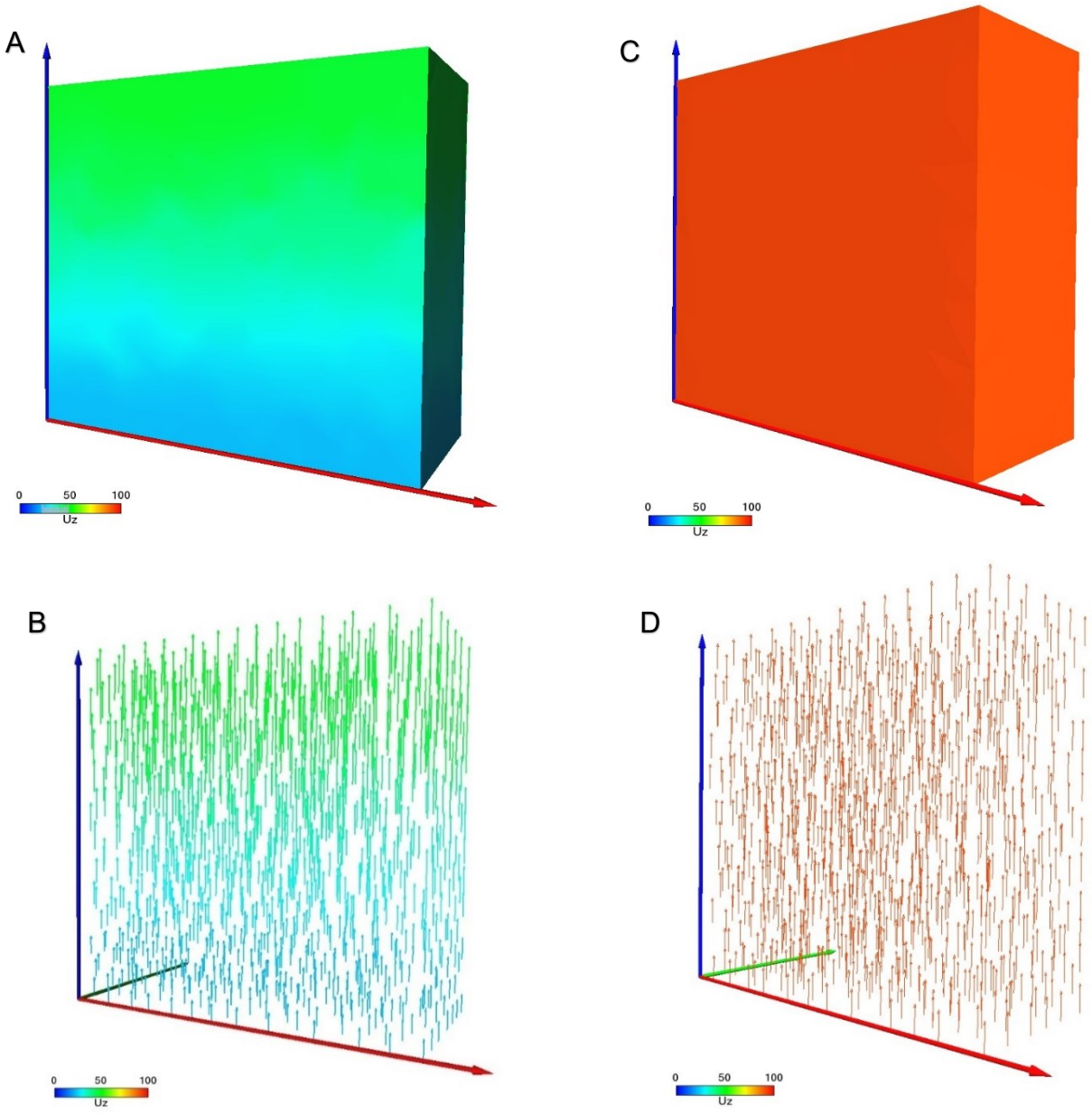

Figure 49: Comparison between displacement vector field and Uz for lower (A,B) VOI and upper (C,D) VOI [μm]

Looking at the displacement map above, it is clear that the two volumes undergo different deformation, the lower one a gradient deformation the upper one uniform. Also, the ranges are different, in particular the upper VOI shows a displacement more or less twice the lower one; in the end both cases are far from the expected displacement.

These results are in contrast and both cannot be considered reliable. To make a hypothesis, is possible that the deformation of the entire specimen is gradient, but the lower VOI was extracted in a portion in which the change of the displacement magnitude is not appreciable and so the VOI deformation appears homogeneous. Anyway, the DVC didn't reach the convergence so is not possible to state with certainty that the displacement range computed is truthful.